IOPscience iopscience.iop.org

Home Search Collections Journals About Contact us My IOPscience

Future perspectives for spintronic devices

This content has been downloaded from IOPscience. Please scroll down to see the full text.

2014 J. Phys. D: Appl. Phys. 47 193001

(http://iopscience.iop.org/0022-3727/47/19/193001)

View the table of contents for this issue, or go to the journal homepage for more

Download details:

IP Address: 83.29.228.126
This content was downloaded on 07/04/2015 at 16:25

Please note that terms and conditions apply.

IOP Publishing

Journal of Physics D: Applied Physics

J. Phys. D: Appl. Phys. 47 (2014) 193001 (40pp)

doi:10.1088/0022-3727/47/19/193001

## Topical Review

# Future perspectives for spintronic devices

**Atsufumi Hirohata[1,2] and Koki Takanashi[3]**

[1] Department of Electronics, University of York, York YO10 5DD, UK
[2] PRESTO, Japan Science and Technology Agency (JST), 4-1-8 Honcho Kawaguchi, Saitama 332-0012, Japan
[3] Institute for Materials Research, Tohoku University, Sendai 980-8577, Japan

E-mail: atsufumi.hirohata@york.ac.uk

Received 3 October 2013, revised 9 January 2014
Accepted for publication 10 January 2014
Published 25 April 2014

**Abstract**
Spintronics is one of the emerging research fields in nanotechnology and has been growing very rapidly. Studies of spintronics were started after the discovery of giant magnetoresistance in 1988, which utilized spin-polarized electron transport across a non-magnetic metallic layer. Within 10 years, this discovery had been implemented into hard disk drives, the most common storage media, followed by recognition through the award of the Nobel Prize for Physics 19 years later. We have never experienced such fast development in any scientific field. Spintronics research is now moving into second-generation spin dynamics and beyond. In this review, we first examine the historical advances in spintronics together with the background physics, and then describe major device applications.

Keywords: spintronics, devices, GMR, TMR, spin injection

(Some figures may appear in colour only in the online journal)

## 1. Introduction

### 1.1. Concepts of spintronics

Spintronics is a new emerging field based on a combination of three conventional information carriers: an electron charge, an electron spin and a photon, as shown schematically in figure 1 [1–12]. These carriers represent three major fields in information technology (IT); data processing with electron transport, data storage with an assembly of spins and data transfer via optical connections.

Recent dramatic developments in IT require both larger capacity data storage and faster data processing. Surprisingly, the performance of both data storage and processing devices has been improving at the very high rate of approximately 30% per year in data storage, and by 100% in 18 months for Si-based processors—a trend known as Moore's law (see figure 2). Since the possibilities of reaching the limits have been announced in both ferromagnet-based memories and conventional semiconductor-based electronic processors, so-called magnetoelectronics, based on spin-polarized electron transport, was born, and has been providing a much faster progress of about 60% per year in data storage [8]. Furthermore, the electron spin can be connected to optics via photon helicity, which is expected to enable a much faster transfer of data.

The breakthrough in this field was the discovery of giant magnetoresistance (GMR) observed in metallic multilayers via spin-dependent electron transport [13–16]. The GMR effect has already been used practically in hard disk drive (HDD) heads. The discovery of the tunnelling magnetoresistance (TMR) effect was also a milestone. It was discovered earlier than the GMR effect but was not realized at room temperature (RT) until recently [17–22].

Simultaneously, from the semiconductor community, dilute magnetic semiconductors (DMS) have been the subjects of a large number of studies [23–27]. After the discovery of giant $g$-factors, many important novel characteristics were found, such as carrier-induced ferromagnetism [23] and photo-induced ferromagnetism [24].

Future IT will require Gbps data transfer rates via optical fibres. An essential part of such data transfer is the fast operation of the diode laser, which depends on the efficiency of the optical isolator. An optical isolator consisting of a DMS is the first practical use of spintronics based on large magneto-optical effects [26].

 © 2014 IOP Publishing Ltd Printed in the UK

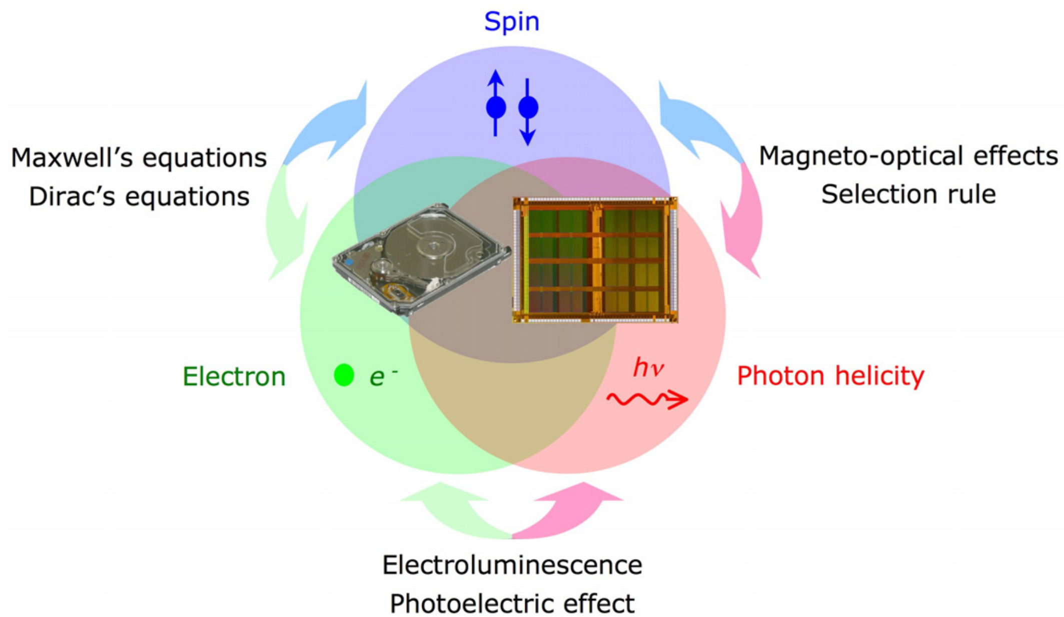


**Figure 1.** Concept of spintronic device applications.

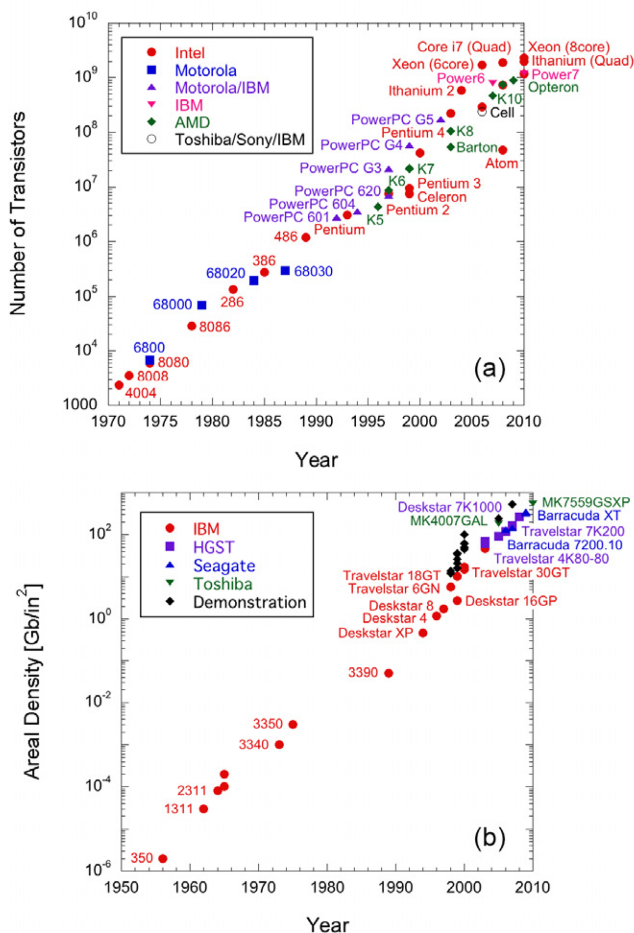


**Figure 2.** (*a*) Moore's law in Si-based processors. Closed circles, triangles, squares and rhombuses stand for microchip processors produced by Intel, AMD, IBM and Motorola, respectively. (*b*) Areal density growth of HDD. Closed circles and triangles correspond to demonstration and commercial products, respectively.

### *1.2. Advancement in spintronics*

Both GMR and TMR are based on the $s$–$d$ interaction between a local magnetic moment and the conduction electron to be spin-polarized. This is a combination of magnetism and electronics and primarily uses spin-polarized electron transport leading to magnetoelectronics.

By further investigating spin precession in the transport process, especially at higher frequencies in the GHz regime, spin dynamics has been studied for second-generation spintronics. Spin dynamics is predominantly induced by spin-transfer torque (STT) from a spin-polarized conduction electron onto a local magnetic moment. Future devices are expected to be three-dimensional (3D), and quantum spintronics will require further miniaturization and precise nano-patterning.

In this review, we first give an overview of the fundamental length scales that define spintronic devices and behaviours, and then give methods to generate spin-polarized carriers in such devices. In section 2, we categorize theses spintronic device structures into four types: all metals, tunnel junctions, ferromagnet/semiconductor hybrids and organic devices. Each structure is discussed from the viewpoint of fundamental properties. Section 3 details device operation and their recent developments. Namely, two- and three-terminal devices as well as spectroscopic applications are explained. Future perspectives of these devices are presented in section 4 by identifying seven major issues to be overcome in order to advance the specifications of the current spintronic devices and to design new devices. This progress is summarized in the concluding section 5.

### *1.3. Spintronic length scales*

The typical length scale of spintronic devices is shown in figure 3. Spin polarization is transferred either by spin-polarized conduction electrons in a conductor or spin-wave

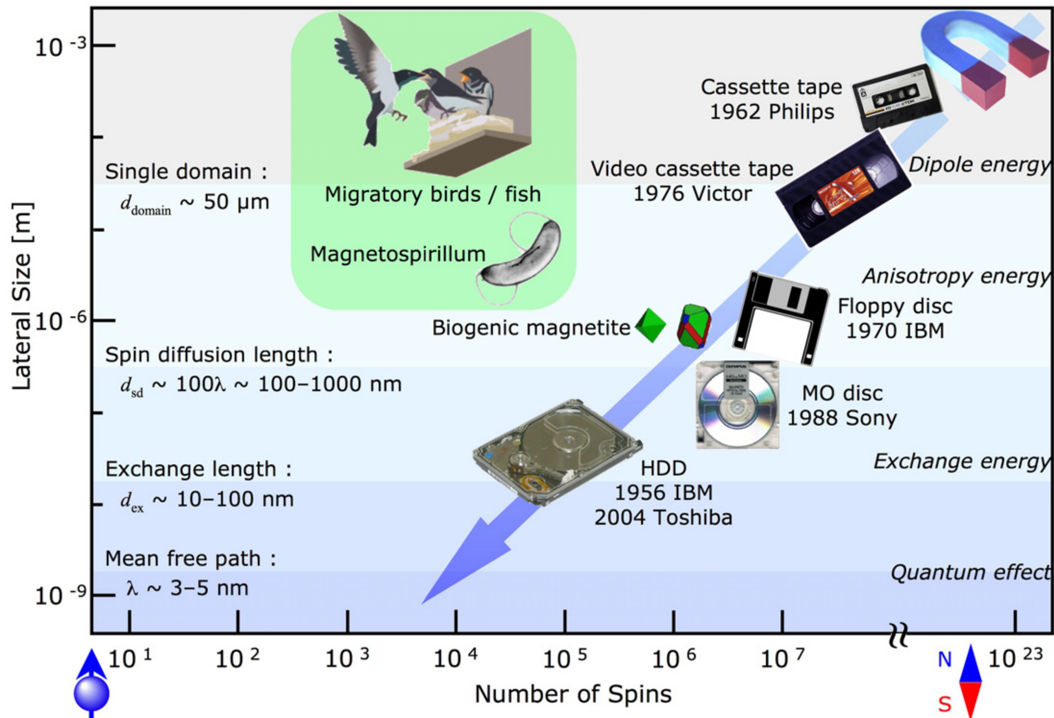


**Figure 3.** Typical magnetic length scales and development of magnetic recording devices.

propagation across local magnetic moments in a insulator. In bulk magnets consisting of local moments of 0.1 mm in lateral size, the average magnetization vector and its distribution hold the key to macroscopic behaviour [28]. Reducing the ferromagnet size, a dipole field from the edge of the sample becomes important, which may, for example, cause the splitting of a single-domain state. However, when the size is further reduced, the exchange interaction plays a dominant role and results in a single-domain state of size $d_{\mathrm{domain}}$. All of the spins are aligned along the global easy axis defined by the magnetic anisotropy, including the shape anisotropy. Each unit of magnetization consists of a certain number of spins, within which a spin is preserved in terms of its orientation. This is called the spin diffusion length $d_{\mathrm{sd}}$ for spin-polarized conduction electrons. Below this length, the exchange length $d_{\mathrm{ex}}$ between the spin-polarized electrons or moments controls the variation of the spin orientation such as the domain-wall (DW) width. With further reduction from $d_{\mathrm{ex}}$, spins can move without scattering within the mean free path $\lambda$ for conduction electrons. By choosing a certain lateral size, a specific magnetic property can be achieved.

Dipole energy is dominant over a few tens of micrometres as in conventional magnetic materials such as tapes. By reducing the length into the sub-micrometre regime, the anisotropy energy becomes dominant, as in a high-density data tape. With further reductions in scale, the exchange energy controls the magnetic properties, resulting in a magneto-optical disk and an HDD. Such passive devices are the most common memories in current technology. In the regime where the device size is much smaller than the mean free path of the electrons (in mesoscopic systems), the spin is known to be preserved during transport (scattering free). One of the ultimate goals of spintronics is to realize a quantum computer using the long spin coherence length in a semiconductor [29]. For the first step, spin-polarized three-terminal devices, which eventually lead to a single electron transistor (SET) [30], providing fundamental data processing with a single electron, have also been widely studied.

In theory, ohmic contacts using a highly doped semiconductor are applicable for spin injection, however the spin lifetime in semiconductors has a peak at a certain doping density, at least in the case of GaAs, which is around $10^{24}\,\mathrm{m}^{-3}$ [29]. The lateral separation of the ferromagnetic contacts has to be below the spin diffusion length and also has to avoid local Hall effects from the influence of the ferromagnet. Spin coherence times as large as $3\,\mu\mathrm{s}$ have been reported in a $Si/Si_{0.75}Ge_{0.25}$ quantum well (QW) at 4.2 K [31], which corresponds to a spin relaxation length of over $100\,\mu\mathrm{m}$ for a 20 nm thick QW with a doping density $n \sim 3 \times 10^{11}\,\mathrm{cm}^{-2}$. This value is almost two orders of magnitude larger than that of GaAs.

### *1.4. Generation of spins*

Spin-polarized electrons can be generated in non-magnetic materials using the following methods: spin injection from a ferromagnet, a magnetic field, an electric field, circularly polarized photoexcitation, a thermal gradient and Zeeman splitting (see figure 4). One of the most common methods is spin injection from a ferromagnetic material, e.g., conventional ferromagnetic metals (Fe, Co, Ni and Gd), half-metallic ferromagnets (HMF) and DMS, attached to a non-magnetic metal or semiconductor through an ohmic contact or a tunnel barrier. A stray field at the edge of a ferromagnet can also

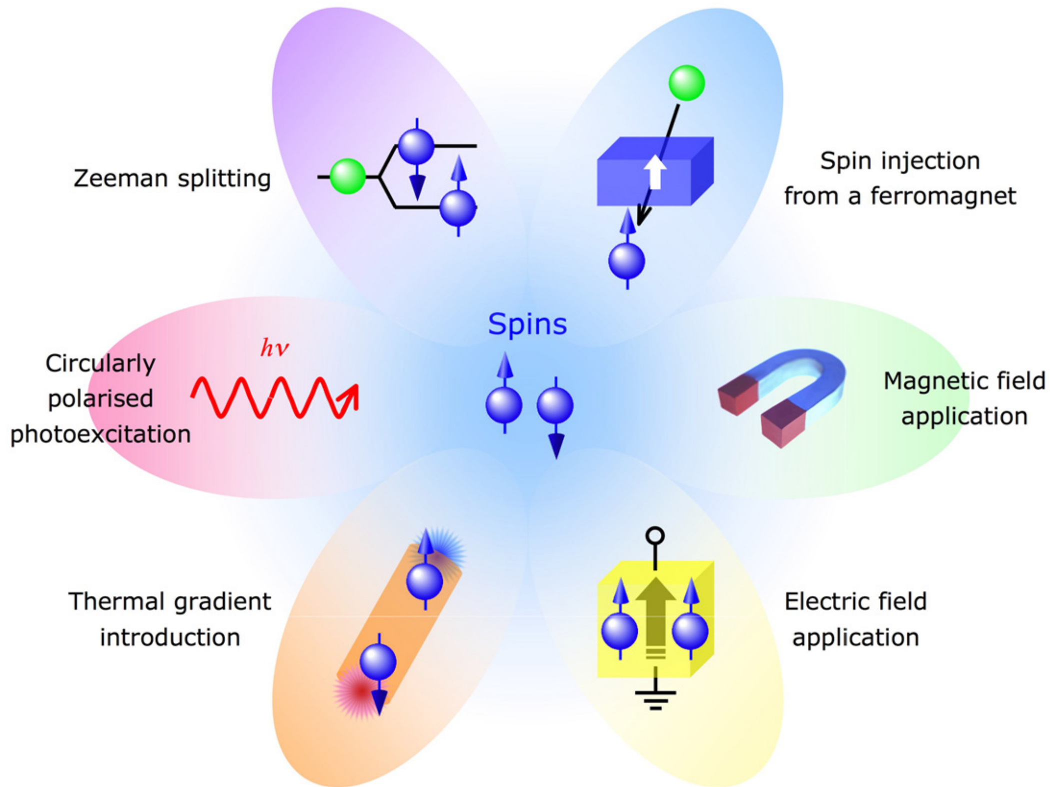


**Figure 4.** List of techniques to generate spin-polarized electrons in a non-magnetic medium.

be used to induce a population difference in spin-polarized electrons in a non-magnetic material. However this is difficult to control due to the precise definition of the edge shape. An electric field can provoke the motion of spin-polarized carriers in a non-magnetic material towards a favourable direction based on spin Hall effects. Circularly polarized light excites spin-polarized electrons in a semiconductor, dependent upon an optical selection rule. The reverse effect generates circularly polarized light emission by a spin-polarized electron current. This can be extended further to spin generation by electromagnetic waves, including spin pumping and high-frequency spin induction [32]. In addition, a thermal gradient has been found to produce a spin-polarized carrier flow due to a spin Seebeck effect. In a DMS, Zeeman splitting induces spin imbalance at the Fermi level.

Each of these techniques for spin-polarized carrier generation and corresponding spin-polarized transport properties are described in section 2. Representative device designs are explained in section 3. Section 4 discusses six key technologies to be developed for better spintronic device operation.

## 2. Spintronic device structures

Spintronic devices based on the manipulation of spin-polarized electrons offer the promise of significant advances in device performance in terms of speed, size scaling and power requirements [7, 8]. Spintronic devices may be grouped into four categories according to the material system and the corresponding electronic structures: (i) all-metal spin transistors including spin valves, (ii) magnetic tunnel junctions (MTJ), (iii) ferromagnet/semiconductor hybrid diode structures and (iv) organic devices, as listed in table 1. For spin-valve and tunnel junctions, spin-polarized electrons are electrically injected from a ferromagnet through an ohmic contact and a tunnel barrier, respectively. The output signals correspond to GMR and TMR effects, respectively. Finally, organic structures utilize organic materials as spin media with either ohmic or tunnel junctions at the spin injector (source) and detector (drain). For hybrid diodes, spin-polarized electrons are injected into a semiconductor either electrically through a ferromagnet/semiconductor ohmic contact (or Schottky barrier) or optically by introducing circularly polarized light into a semiconductor. These injected spins travel in the semiconductor and are detected using either optical light emission or an electrical signal at another ferromagnetic drain.

### 2.1. All-metal structures

*2.1.1. Diffusive transport.* The motion of electrons in a conducting material can be driven by applying an electric field generating an electric current via Ohm's law. For spin-polarized electrons, both conduction-electron transport in a conductor and spin-wave propagation in an insulator can be described by the Bloch–Torrey equation without spin-exchange diffusion [33]:

$$\frac{\partial \vec{M}}{\partial t} = \gamma(\vec{M} \times \vec{H}) - \frac{\vec{M}}{T_2} + \chi_0 \frac{\vec{H}}{T_1} + \frac{\vec{M} \cdot \vec{H}\vec{H}}{H^2} \times \left(\frac{1}{T_2} - \frac{1}{T_1}\right) + \nabla \cdot D\nabla(\vec{M} - \vec{M}_0), \quad (1)$$

**Table 1.** List of four major spin-polarized three-terminal devices after [8].

| | Spin-valve structures | Magnetic tunnel junctions | FM/SC hybrid structures | Organic structures |
|---|---|---|---|---|
| Effects | GMR | TMR | Diodes | TMR/GMR |
| Interfaces | Ohmic contacts<br>Diffusive | Tunnel barriers<br>Ballistic | Ohmic/Schottky barriers<br>Diffusive/ballistic (hot electrons) | Ohmic/tunnel barriers<br>Diffusive/ballistic |
| Spin media | Non-magnetic metals | Tunnel barriers | Semiconductor | Organic materials |
| Spin coherence | 30 nm–1 $\mu$m | $\sim$ a few nm | $\leqslant$100 $\mu$m | $\sim$ 200 $\mu$m |
| Device applications | Johnson transistors<br>Spin-valve transistors<br>Lateral spin valves | MOS junctions<br>Coulomb blockade structures<br>MRAM<br>Superconducting point contacts<br>Spin RTD<br>Magnetic tunnel transistors<br>SP-STM | FM/2DEG<br>Schottky diodes<br>Spin FET<br>Spin LED<br>Spin RTD | Lateral spin valves |

where $\vec{M}$, $\vec{H}$, $\gamma$, $\chi_0$, $T_1$, $T_2$, $D$ and $\vec{M}_0$ correspond to magnetization, a magnetic field, a gyromagnetic ratio, magnetic susceptibility, longitudinal relaxation time, transverse relaxation time, diffusion coefficient and equilibrium magnetization. The last term in equation (1) represents a diffusion process. For a simple spin diffusion process in a non-magnetic medium, spin-polarized electrons decay in proportion to $\exp(-D/d_{sd})$, where $D$ is distance from the spin source and $d_{sd}$ is the spin diffusion length in the non-magnetic conductor.

#### *2.1.2. Giant magnetoresistance (GMR).*

*(i) Fundamentals*

In 1988, Baibich *et al* found a large decrease of resistance in a [Fe (3 nm)/Cr (0.9 nm)]$_{60}$ structure under the application of a magnetic field. A 50% change was discovered using $(R_{max} - R_{min})/R_{max}$ at 4.2 K, as shown in figure 5 [13]. Since then, multilayered GMR structures have been widely investigated [16]. Thanks to the advancement in growth techniques, the GMR structure has been simplified down to a trilayer consisting of ferromagnet (FM)/non-magnet (NM)/FM.

The GMR effect depends on the spin-dependent scattering of electrons, as discussed below. The resistance shows a minimum ($R_{min}$) when the magnetization in neighbouring ferromagnetic layers are aligned parallel, while it shows a maximum ($R_{max}$) with antiparallel alignment. A GMR ratio is therefore defined as

$$\frac{\Delta R}{R} = \frac{R_{max} - R_{min}}{R_{min}}. \qquad (2)$$

For the case of a simple trilayer structure, typically a GMR ratio at RT is around 10%. In 1997, it was reported that a nano-oxide layer inserted between the pinned ferromagnetic layer and the antiferromagnet layer increases the GMR ratio due to specular reflection [34]. A hybrid free spin-valve with a thin free layer (e.g., NiFeTa), sandwiched between ferromagnetic and non-magnetic layers to reduce the current-shunting effect, and a synthetic spin-valve using a synthetic antiferromagnet

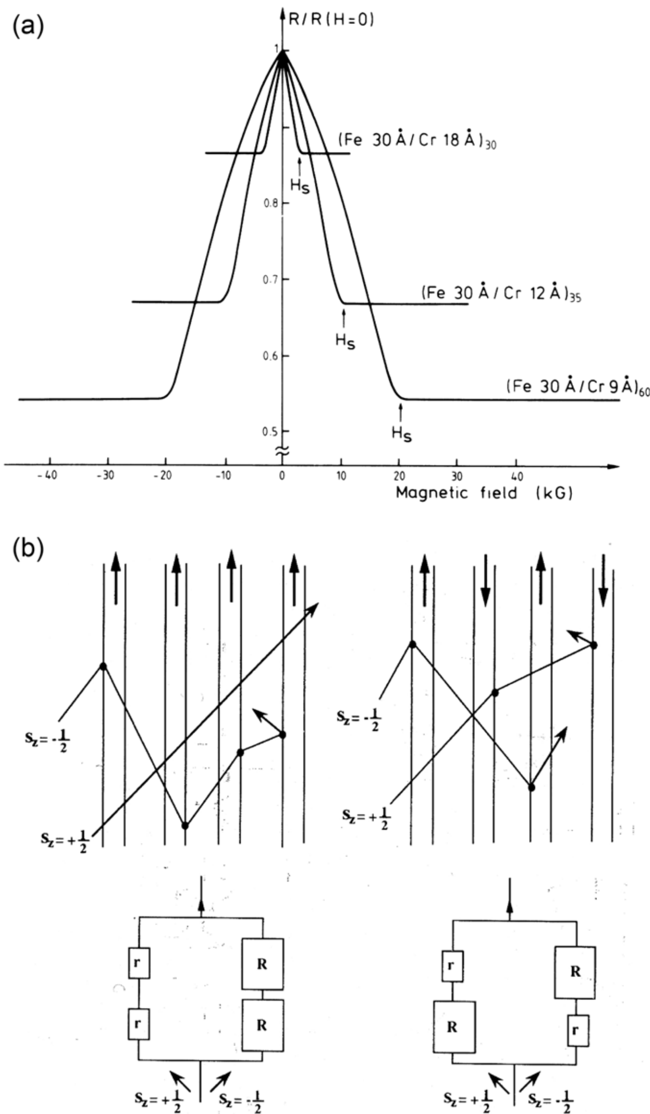


**Figure 5.** (*a*) GMR signals together with (*b*) schematic diagrams of the two-current model. Reproduced with permission from [13], Copyright 1988 American Physical Society.

of two antiferromagnetically coupled ferromagnetic layers, e.g., CoFe/Ru/CoFe, as either a pinning layer or a free layer, have been also demonstrated to show a large GMR effect [35]. In such advanced spin-valve systems, the GMR ratio can be up to 20% and has been used as a GMR read head.

*Geometrical effects*

A voltage application gives rise to the acceleration of the electrons in the direction of the electric field, either in the layer plane (CIP) or perpendicular to the plane (CPP) geometry [16]. It should be noted that the GMR effect depends on the NM interlayer thickness $t_{\mathrm{NM}}$. In the CIP geometry, the relevant length scale is given by the mean free path in the interlayer material (approximately 3–5 nm). If $t_{\mathrm{NM}}$ increases beyond this value, CIP-GMR decreases rapidly [16]. In CPP geometry, the relevant thickness is given by the spin diffusion length, which is around 100–1000 nm for non-magnetic interlayer materials [36].

*Models*

*Interlayer exchange coupling model.* Grünberg *et al* first identified interlayer exchange coupling between transition metal layers in Fe/Cr multilayers [37]. Parkin *et al* then found that the interlayer exchange coupling constant oscillates as a function of the NM interlayer thickness $t_{\mathrm{NM}}$ [38]. The oscillation period was observed to be approximately 1.0–1.5 nm, which was much larger than the theoretical prediction of ~0.25 nm from the Rudermann–Kittel–Kasuya–Yoshida (RKKY) interaction [39]:

$$U_{\mathrm{RKKY}} = \frac{1}{t_{\mathrm{NM}}^2}\sin(2k_{\mathrm{F}}t_{\mathrm{NM}}), \tag{3}$$

where $k_{\mathrm{F}}$ is the Fermi wave vector. Coehoorn [40] demonstrated RKKY oscillations with aliasing effects, which assumed that lattice planes located at discrete positions in the non-magnetic layer could only sample discrete points of the continuous RKKY oscillation, giving a long oscillation period $\lambda$:

$$\lambda = \frac{\pi}{|k_{\mathrm{F}} - (\pi n/t_{\mathrm{NM}})|}, \tag{4}$$

which was in a good agreement with experimental observation.

*QW model.* Edwards and Mathon proposed that quantum confinement dependent upon electronic band structures could explain the current transport in GMR structures [41]. For FM metals, the majority and minority 3*d* bands are shifted away from the Fermi level $E_{\mathrm{F}}$ due to the strong internal exchange interaction among 3*d* electrons. This gives rise to different energy levels for up and down spin electrons.

*Two current model.* As originally proposed by Mott [42], up and down spin electrons in 3*d* transition metals are assumed to carry electrical current independently at low temperature. In this model [43, 44], the resistivity is predominantly determined by interband scattering from 4*s* to 3*d* bands or vice versa, and the scattering probability is proportional to the density of states (DOS) in the 3*d* bands at the Fermi level $E_{\mathrm{F}}$. Accordingly, for 3*d* transition metals, the resistivity can be described as $\rho_\sigma \propto N^\sigma(E_{\mathrm{F}})$, where $\sigma = \uparrow, \downarrow$ and $N^\sigma(E_{\mathrm{F}})$ is the DOS at $E_{\mathrm{F}}$. For the transition metals and their alloys, *s*–*d* interband scattering can occur much more frequently than other scattering mechanisms such as *s*–*s* scattering due to the large DOS of 3*d* bands at $E_{\mathrm{F}}$. Since electrons scattered into the *d*-bands do not contribute significantly to the electrical conduction because of their large effective mass, this model predicts higher resistivities for the transition metals and their alloys as compared with those for simple metals. This is consistent with experimental data for bulk 3*d* transition metals.

For an FM1/NM/FM2 trilayer with magnetizations parallel in the two FM layers, down spin electrons are scattered into 3*d* bands in the FM1 layer, whose spins are aligned parallel to the electron spins. Up spin electrons cannot be scattered into 3*d* states because the up spin 3*d* bands are almost fully occupied. The same situation can be applied to the FM2 layer so that down spin electrons can flow through the trilayer without scattering. Up spin electrons suffer scattering at both the FM/NM interfaces and in each ferromagnetic layer. In an

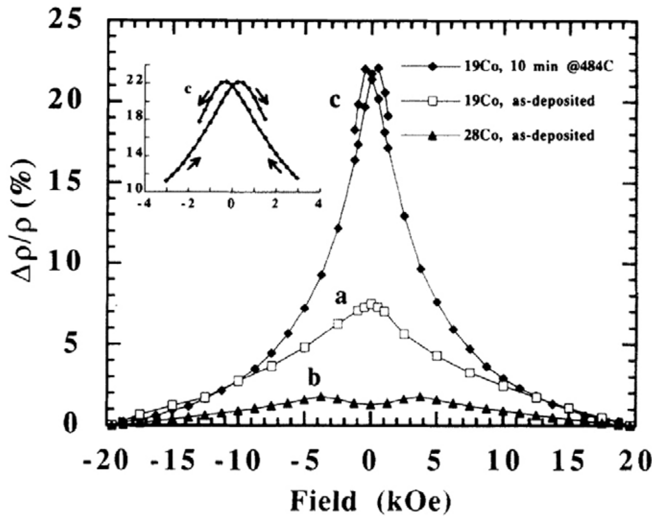


**Figure 6.** Field dependence of $\Delta\rho/\rho = (\rho_{H_c} - \rho_{H=20\,\text{kOe}})/\rho_{H=20\,\text{kOe}}$ for the three types of curves obtained. Inset: details of curve c. Curves *a* and *b* were measured at $T = 100$ K; curve *c* was measured at 10 K. Reproduced with permission from [47], Copyright 1992 American Physical Society.

antiparallel configuration, down spins are scattered in the FM1 layer and up spins are scattered in the FM2 layer, respectively. Consequently, the scattering probabilities of up and down spins averaged over the trilayer become equal, which means that the resistances for up and down spin currents are identical. Therefore the parallel configuration shows a lower resistivity than the antiparallel configuration.

From the application point of view, spin-valve structures are fabricated typically consisting of a ferromagnetic layer pinned by exchange coupling to a neighbouring antiferromagnetic layer, a non-magnetic spacer layer and a magnetically soft layer, which can be switched by a small external magnetic field [45, 46]. Such a spin-valve typically shows $\Delta R/R = 5$–6% at RT.

*(ii) Systems*

*Granular GMR*

In comparison to the conventional GMR in a multilayer with respect to the magnetization alignment as discussed above, Berkowitz *et al* and Xiao *et al* observed large GMR effects in a system with Co nanoparticles dispersed in a Cu matrix as shown in figure 6 [47, 48]. In such a granular system, the magnetic moments in the Co particles are randomly aligned without an external applied field and are aligned parallel in the saturated state. These nanoparticles contain a single magnetic domain whose alignment requires a relatively large magnetic field, typically in the order of a few kOe. A granular GMR effect has been reported in Co–Ag and Fe–Ag systems. Here, the change in resistivity $\Delta\rho/\rho$ can be well described by $1 - (M/M_S)^2$ [49].

*Ballistic GMR*

In a similar way to a superconducting point contact measurement [50], Upadhyay *et al* have reported that the spin filtering of ballistic electrons transmitted through ultrathin Co films can be identified from $I$–$V$ measurements using a Co nano-contact on a Pb film [51]. In such a system, spin-polarized electrons can flow through the Co/Pb interface only when the electron energy matches the superconducting energy gap. When these energies do not match, most of the electrons are reflected at the interface. Rippard and Buhrman have extended this study to Co/Cu/Co spin-valve structures in which only ballistic electron transport has been detected [52]. Such a nano-contact has been used to demonstrate STT and adapted to a magnetic random access memory (MRAM) bit as discussed in section 3.1.3.

*Spin-transfer torque (STT)*

In a system consisting of two ferromagnetic layers separated by a thin NM spacer, STT has been predicted to occur at the NM/FM interface by flowing an electrical current via another FM [53, 54]. Conduction electrons are spin-polarized by flowing through the first FM and exert a torque on localized electrons in the second FM across the NM spacer. This induces a rotation of the spins of the localized electrons in the second FM. In a nano-scale junction, such STT can reverse the magnetization of the target FM by flowing a current above the threshold, which is typically of the order below $10^7$ A cm$^{-2}$. STT was first demonstrated in a point contact [55] and later in CPP-GMR and TMR nano-pillars, as discussed in section 3.1.3 for the development of MRAM.

By utilizing the STT, magnetic moments in a domain can also be rotated by flowing an electrical current. This leads to the displacement of a magnetic DW in a micro- or nano-scale ferromagnetic wire [56]. For this case, a threshold current density is typically of the order of $10^{12}$ A cm$^{-2}$. This offers the basis for a new magnetic memory, i.e. racetrack memory (see sections 3.1.4 and 4.5).

### 2.2. Tunnel junctions

*2.2.1. Ballistic transport.* When a scattering event in a transport medium is negligible, one can assume the electron conduction is achieved in a ballistic regime for an ideal case. To obtain these conditions, one should either use a tunnel barrier, which mimics a vacuum, or reduce the dimension of the current path into one dimension (1D). This increases the mean free path of electrons and results in highly efficient transport.

#### 2.2.2. Tunnel magnetoresistance (TMR).

*(i) Fundamentals*

Jullière first reported a 14% MR ratio in Fe/GeO/Fe junctions at 4.2 K [17], as shown schematically in figure 7. Such junctions are the same as GMR structures with the non-magnetic metal layer replaced by an oxide barrier. TMR requires a CPP configuration to avoid ohmic conduction through the metallic layers.

*Origin*

Theoretically, a TMR ratio is understood in a diffusive limit to be similar to the GMR ratio:

$$\frac{R^{\text{AP}} - R^{\text{P}}}{R^{\text{P}}} = \frac{2P_{\text{FM1}}P_{\text{FM2}}}{1 - P_{\text{FM1}}P_{\text{FM2}}}, \qquad (5)$$

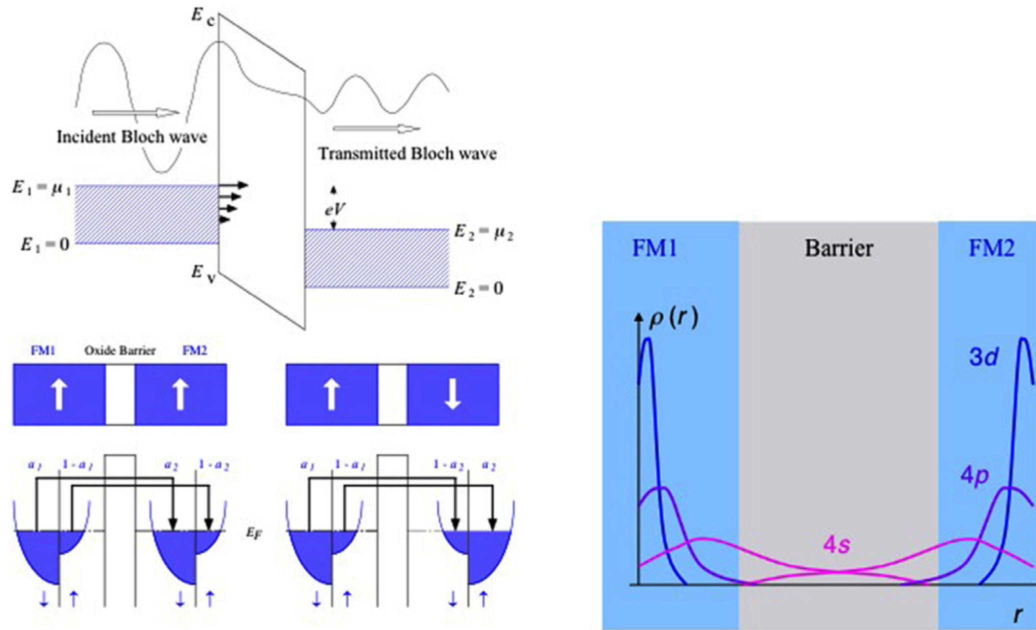


**Figure 7.** Schematic diagrams of (*a*) quantum electron tunnelling through an oxide barrier, (*b*) the mechanism of spin-polarized tunnelling and (*c*) the overlap of wavefunctions for the corresponding electrons.

where $P_{FM1}$ and $P_{FM2}$ are the spin polarization of the FM1 and FM2 layers, respectively, which are defined as

$$P \equiv \frac{N_{majority} - N_{minority}}{N_{majority} + N_{minority}}. \tag{6}$$

The conductance for parallel ($G^P$) and antiparallel ($G^{AP}$) configurations are obtained using the DOS at $E_F$ in the two ferromagnetic layers, $a_{FM1(FM2)} = N_{majority}/(N_{majority} + N_{minority})$, i.e. $P = 2a - 1$:

$$G^{AP} \propto a_{FM1}a_{FM2} + (1 - a_{FM1})(1 - a_{FM2}), \quad G^{P} \propto a_{FM1}(1 - a_{FM2}) + (1 - a_{FM1})a_{FM2}. \tag{7}$$

*(ii) Systems*

*Conventional TMR*

Although the TMR ratio can theoretically be almost 50% with conventional FM metals, a high TMR ratio was not reported until 1995. Miyazaki and Tezuka [19] used a coercivity difference in an $Fe/Al_2O_3/Fe$ junction, while Moodera *et al* [20] used an exchange-biased $CoFe/Al_2O_3/Co$ junction to obtain large effects. Similar to GMR studies, TMR also used spin-valve type structures such as NiFe/Co/AlO/Co/NiFe/FeMn/NiFe [57], which gave a TMR ratio of 40–50% [58]. TMR read heads for HDDs were first implemented by Seagate in 2004 and are now commonly used. The maximum TMR ratio has been reported with an amorphous Al–O tunnel barrier in an MTJ with structure $Si(0\,0\,1)/Si_3N_4/Ru/CoFeB/Al_2O_3/CoFeB/Ru/FeCo/CrMnPt$ [59]. In these MTJs, the interfaces between ferromegnets and insulators are not sharply defined and the insulators cannot be treated as an ideal barrier due to defects and grain boundaries. This results in spin-polarized electron tunnelling in a diffusive regime.

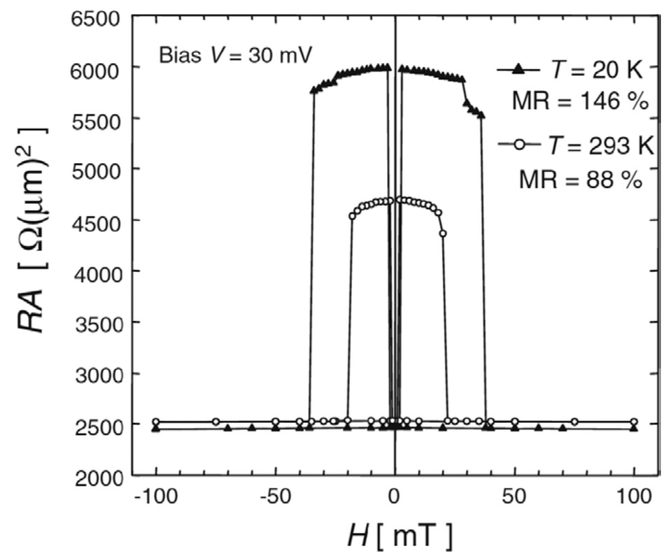


**Figure 8.** Magnetoresistance curves for an Fe(0 0 1)/MgO(0 0 1)(2 0 Å)/Fe(0 0 1) MTJ at $T = 293$ and 20 K. The MR ratios were 88% and 146%, respectively. Reproduced with permission from [62], Copyright 2004 Japan Society of Applied Physics.

*Coherent tunnelling*

Based on progress in growth techniques, purely ballistic transport was achieved in 2004. TMR ratios of over 1000% have been predicted theoretically at RT with oriented MgO barriers [60, 61]. Such a giant TMR effect is induced by the $\Delta_1$ band connection at the Fe(0 0 1)/MgO interface only for the majority spins. Coherent tunnelling achieved a TMR ratio experimentally of over 100% at RT [62–65] (see figure 8), which is expected to reduce the read head size in an HDD and to improve the read/write operation in an MRAM cell. To date,

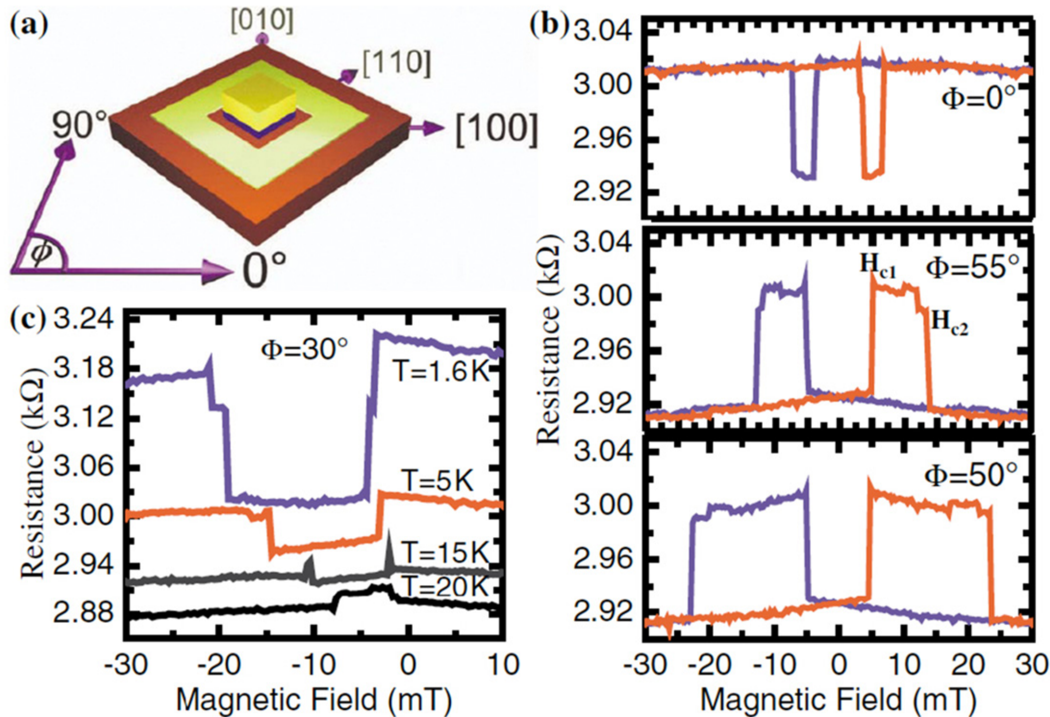


**Figure 9.** (*a*) Schematic device configuration showing the crystallographic directions. (*b*) Hysteretic magnetoresistance curves acquired at 4.2 K with 1 mV bias by sweeping the magnetic field along the 0, 50° and 55° directions. (*c*) TAMR along 30° for temperatures from 1.6 to 20 K, showing a change of sign of the signal. The curves are vertically offset for clarity. Reproduced with permission from [67], Copyright 2004 American Physical Society.

a record TMR ratio of 604% at RT has been reported in an MTJ consisting of $Co_{20}Fe_{60}B_{20}/MgO/Co_{20}Fe_{60}B_{20}$ [66].

*Tunnelling anisotropic magnetoresistance (TAMR)*
For a junction with a tunnel barrier sandwiched by a ferromagnetic electrode on one side and a non-magnetic layer on the other, its resistance can be controlled by magnetization rotation through the spin–orbit interaction at the interface. This is called tunnelling anisotropic magnetoresistance (TAMR). This effect was first demonstrated experimentally by Gould *et al* with a junction of 70 nm $Ga_{0.94}Mn_{0.06}As$/Al-O(1.4 nm)/Ti/Au, as shown in figure 9 [67]. A TAMR ratio of ∼0.4% has also been measured with GaAs as a tunnel barrier [68]. Similarly, 13% TAMR has been reported for a textured 1 nm Co(1 nm)/Pt(1 nm)/Co(1 nm)/Pt(0.5 nm)/Al-O(2 nm)/Pt(5 nm) junction with perpendicular magnetic anisotropy [69]. In this case the TAMR has also been reported to depend strongly on the crystalline structure of the tunnel barrier [70]. By comparing a highly textured MgO and an amorphous Al–O barrier in MTJs with $Co_{0.49}Fe_{0.21}B_{0.30}/Co_{0.70}Fe_{0.30}$/Oxide/$Co_{0.70}Fe_{0.30}/Co_{0.49}Fe_{0.21}B_{0.30}$, the former exhibits 377% TAMR at 10 K, while the latter shows only 89%. The effect was reported to become as large as 130% using a NiFe/IrMn/MgO/Pt multilayer [71].

*Electromotive force*
An electromotive force has been theoretically predicted from Faraday's law by Barnes and Maekawa [72], which becomes active in the presence of a time-dependent magnetization, e.g., magnetic domain motion. Their prediction has been proven experimentally in an MTJ, consisting of GaAs/zinc-blende MnAs nanoparticles/GaAs [73]. Here, the electromotive force is found to work on a timescale of $10^2$–$10^3$ s, which controls the spin-dependent tunnelling behaviour in the superparamagnetic MnAs nanoparticles. This induces a high MR of up to 100 000% at 3 K.

*Granular TMR*
TMR has also been measured in a nano-granular system with ferromagnetic nanoparticles dispersed in an insulating matrix. The first TMR effect was observed in granular Ni-$SiO_2$ films [74]; however, the TMR ratio was found to be about 1% at $T = 300$ K. In 1995, Fujimori *et al* reported an 8% TMR ratio at RT in a Co–Al–O system [75]. The effect is very similar to the conventional TMR effect but with a charging effect in the nanoparticles. A significant enhancement in the TMR ratio of more than 20% at 2 K has also been reported [76]. Such an enhancement by $2/(1 - P^2)$ as compared with sequential tunnelling ($P$ = spin polarization of the ferromagnet) is theoretically proposed to be induced by co-tunnelling across nanoparticles in the Coulomb blockade regime [77].

By inserting such a granular TMR system into an insulating layer in a conventional MTJ, Schelp *et al* successfully fabricated a double MTJ [78]. They sandwiched Co nanoparticles of 2–4 nm diameter dispersed in Al–O between Co layers. The TMR ratio was found to be approximately 15% at 4.2 K and 10% at RT. Significant enhancement of the TMR ratio has also been reported in a double MTJ with a CoFe/CoFe–Al–O/CoFe multilayer [79]. The Coulomb blockade was observed below 50 K for CoFe

nanoparticles with diameters between 2.0 and 4.5 nm. The bias voltage dependence of the TMR ratio increased from 10.5% at 20 mV at 7 K to 23.9% at 0.60 mV. This enhancement near zero bias agrees very well with the Takahashi–Maekawa theory [77].

### *2.3. Ferromagnet/semiconductor hybrid structures*

#### *2.3.1. Interfacial properties.*

*Schottky diode*

By depositing a ferromagnetic metal layer directly onto a semiconductor substrate, a Schottky barrier can be formed at the interface. The Schottky barrier acts as an intrinsic tunnelling barrier for electrons travelling across the interface. Since the barrier is formed at the surface region of the semiconductor, electron flow is prevented depending on the band-bending shape of the barrier, resulting in current rectification.

A spin-polarized electron current across the Fe/GaAs Schottky barrier has been measured by Filipe *et al* [80]. A spin-polarized electron beam from a GaAs photocathode was used to inject spins, which were filtered by the Fe layer dependent upon the Fe magnetization orientation. The efficiency of the filtering was estimated to be above 25%. A Schottky barrier has been utilized widely for both spin injection and detection into and from a semiconductor, as discussed in section 2.3.2.

*Magnetically dead layer*

At the ferromagnet/semiconductor interfaces, a magnetically dead layer can be formed by the elastic deformation of the ferromagnetic film due to a large lattice mismatch: the so-called the Poisson ratio. Early studies showed the presence of a magnetically dead layer at the interface of an Fe film grown by electrolytic deposition [81], which was calculated theoretically [82]. However, recent progress in ultrahigh vacuum (UHV) technology enables us to grow epitaxial pseudo single crystals onto a semiconductor and a non-magnetic metal.

*Conductance mismatch*

A spin-polarized current flow across a ferromagnet/two-dimensional electron gas (2DEG) interface is predicted theoretically to be of a detectable order [83, 84]. The electrons in the 2DEG are confined in a potential well and appear to possess a zero-field spin splitting due to the Rashba effect. Conductance calculations also reveal that the interfacial spin-flip scattering is enhanced.

In contradiction, it has been suggested by Schmidt *et al* [85] that there may be fundamental obstacles to achieving efficient spin transmission across ferromagnetic metal/semiconductor interfaces via a diffusive process, as shown in figure 10. Their calculations suggest that a few electrons with different spin polarization from the majority spins at the Fermi level may reduce the spin polarization in the semiconductor. Ideally, 100% spin polarization needs to be used for the source and drain to achieve highly efficient spin injection. It can be achieved in the following materials: DMS and HMFs, such as Heusler alloys, which are discussed in section 4.1.

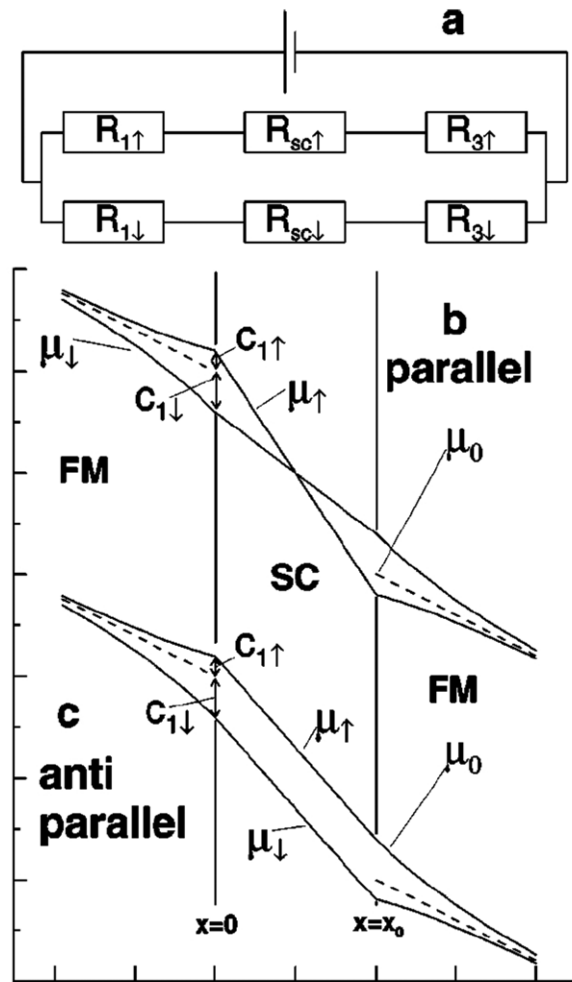


**Figure 10.** (*a*) Simplified resistor model for a device consisting of an SC with two FM contacts 1 and 3. The two independent spin channels are represented by the resistors $R_{1\uparrow,\downarrow}$, $R_{SC_{\uparrow,\downarrow}}$ and $R_{3\uparrow,\downarrow}$. Parts (*b*) and (*c*) show the electrochemical potentials in the three different regions for parallel (*b*) and antiparallel (*c*) magnetization of the ferromagnets. Reproduced with permission from [85], Copyright 2000 American Physical Society.

These obstacles can be overcome by using either ballistic electrons [86] or very thin tunnelling barriers between the ferromagnet and the semiconductor [87]. If the tunnel resistance is larger than the resistance in a semiconductor, which is much larger than that in a ferromagnet, spin injection with up to 100% polarization is expected.

#### *2.3.2. Spin injection/detection.*

*Electrical spin injection*

By flowing an electrical current from a ferromagnetic electrode into a semiconductor, spin-polarized electrons can be injected depending on the spin polarization of the initial ferromagnetic source. This method has been used conventionally as originally proposed by Aronov and Pikus [88] and later reintroduced by Datta and Das [89]. In order to detect the injected spin polarization in a semiconductor, another ferromagnetic electrode (drain) has been widely used to measure the spin-polarized current signal

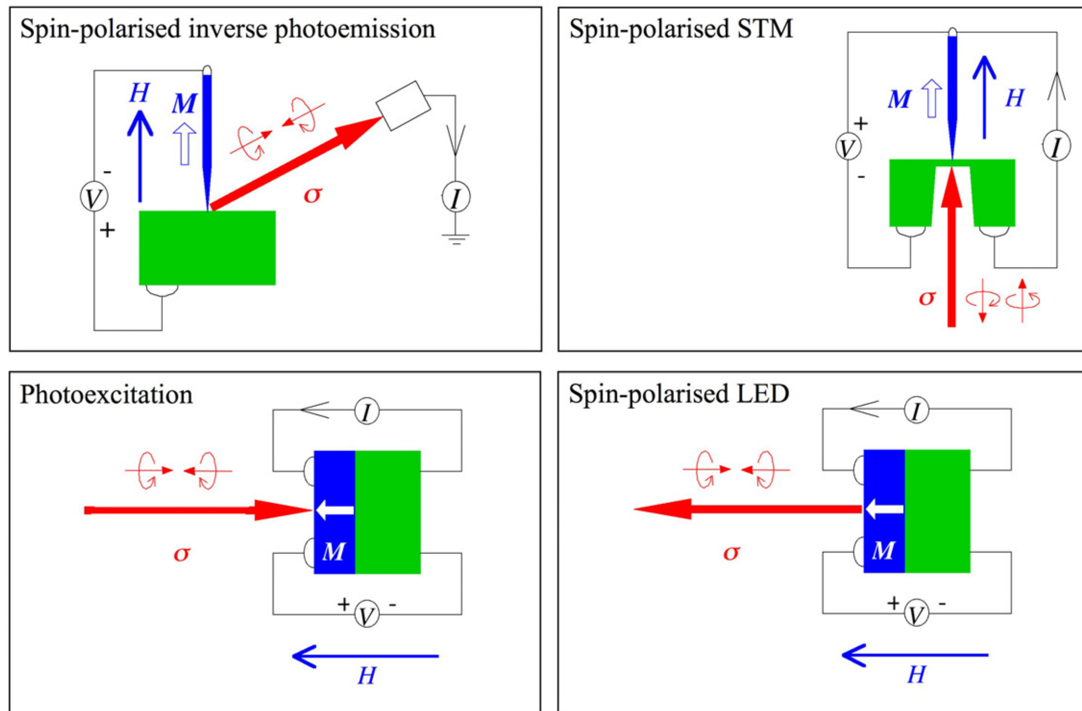


**Figure 11.** Major experimental techniques with circularly polarized photons: spin-polarized inverse photoemission, spin-polarized STM, photoexcitation and spin-polarized LED.

[80, 84, 86]. Recently, circularly polarized light emission from a semiconductor has been used as a measure of the spin polarization of the semiconductor electrons [26, 27]. Here spin-polarized electrons (or holes) have been injected into a semiconductor, whose efficiency has been estimated by using circularly polarized electroluminescence (EL) signals from a QW (see table 1).

*Optical spin injection*

The other method of injecting spin-polarized electrons is photoexcitation, which uses circularly polarized light to excite spin-polarized electrons and detects the spin polarization as an electrical signal (see figure 11). The possibility of passing a spin-dependent current through thin film tunnel junctions of both Co/$Al_2O_3$/GaAs and Co/$\tau$-MnAl/AlAs/GaAs with photoexcited spin-polarized electrons was first discussed by Prins *et al* [90]. For the former structure, a spin-dependent tunnelling current is observed, while only magnetic circular dichroism (MCD) signals are seen in the latter. In their experiment, a sample with a 2 nm $Al_2O_3$ tunnelling barrier showed the largest helical asymmetry of the photoexcited current of approximately 1.2% at 1.5 eV near the GaAs bandgap. Accordingly, many studies of spin-dependent tunnelling through metal/oxide/semiconductor (MOS) junctions have been carried out, e.g., [91], especially to achieve optically pumped SP-STM as described in section 3.3.1.

Accordingly, the evidence for the RT spin filtering of spin-polarized electrons has been investigated systematically at the ferromagnet/semiconductor interface in forward bias [92, 93]. The bias and GaAs doping density dependence of spin-filtered signals suggest that electron tunnelling is the transport mechanism. Further proof of this picture has been added by temperature-dependent measurements of bandgap engineered NiFe/AlGaAs barrier/GaAs structures [92, 93]. Spin-dependent effects were only observed in the bias and temperature range where electron tunnelling occurs. In addition, strong optical magnetocurrent effects at RT have been observed in spin-valve/semiconductor structures. The difference in the optical magnetocurrent obtained between parallel and antiparallel spin-valve configurations was extremely large (up to 2400%). This indicates that the spin-dependent electron transport across the spin-valve structures was determined by the relative spin alignment of the ferromagnetic layers and the initial spin polarization of the photoexcited electrons. The photon energy dependence of the optical magnetocurrent also proved that the photoexcited electrons tunnel into the ferromagnet ballistically. Recently, the effect of a QW in the semiconductor on spin-polarized electron transport across the ferromagnet/semiconductor interface has also been made [94]. Since 20 nm thick FeCo and Fe films are used for the measurement, MCD background signals dominate the polarized photocurrent, resulting in, at most, 0.5% of the photocurrent being attributable to a true spin-dependent signal at 10 K. The spin-filtering effect can be used for future spintronic devices, such as an optically assisted magnetic sensor [95].

A *p*–*n* junction was employed to demonstrate the spin voltaic effect by photoexcitation [96]. Across a *n*-GaAlAs/*p*-GaInAs/*p*-GaAs junction, a circularly polarized photocurrent was detected at 4 K, which was different from the MCD background. Similarly, the spin Hall effect was reported in a planar p–n junction [97, 98]. A planar 2DEG/two-dimensional hole gas (2DHG) photodiode was patterned into a Hall bar with

the $p$–$n$ interface at the centre. Due to the skew scattering in the bar, clear spin Hall signals were observed, dependent upon the circularly polarized light introduction. Such spin-dependent behaviour was explained by Žutić *et al* [99]. A monotonic change in the spin-polarized electron density was numerically calculated with respect to the applied bias voltage. Similar analysis was carried out on magnetic semiconductor junctions [100].

*Spin transport in GaAs*

In GaAs, which is widely used in spintronics, the valence band maximum and the conduction band minimum are aligned at the $\Gamma$-point. The centre of the Brillouin zone ($\boldsymbol{k} = 0$), with an energy gap $E_g = 1.43$ eV at RT, indicates that the only transition induced by photon energy $h\nu$ occurs at $\Gamma$ (direct-gap semiconductor) [101, 102]. The valence band ($p$-symmetry) splits into a four-fold degenerate $P_{3/2}$ state at $\Gamma_8$ and a two-fold degenerate $P_{1/2}$ state, which lie at $\Gamma_7$ ($\Delta = 0.34$ eV below $P_{3/2}$), whereas the conduction band ($s$-symmetry) is a two-fold degenerate $S_{1/2}$ state at $\Gamma_6$. The $P_{3/2}$ band consists of two-fold degenerate bands; heavy hole and light hole sub-bands.

When $h\nu = E_g$, circularly polarized light excites electrons from $P_{3/2}$ to $S_{1/2}$. According to the selection rule ($\Delta m_j = \pm 1$), two transitions for each photon helicity ($\sigma^+$ and $\sigma^-$) are possible. However the relative transition probabilities for the light and heavy holes need to be taken into account in order to estimate the net spin polarization. For example, if electrons are excited only from the valence band maximum ($\Gamma_8$) by circularly polarized light, three times more spins are excited from $m_j = \pm 3/2$ than from $m_j = \pm 1/2$ states. Although the maximum polarization is expected to be 50% in theory, the maximum observed experimentally is ~40% at the threshold. This is due to experimental limitations, such as spin depolarization in the GaAs layer and the interfaces [101, 103].

For $E_g + \Delta < h\nu$, the polarization decreases with increasing $h\nu$ due to the mixture of the light and heavy hole states with the split-off valence band states, which have the opposite sign. Such interband absorption occurs only through the spin-orbit interaction, since the electric field of the exciting light only influences electron orbital motion. For $E_g + \Delta \ll h\nu$, the spin-orbit interaction becomes negligible and spin depolarization during the cascade process can be significant. Therefore the electron optical orientation is absent.

Recently, spin injection has also been demonstrated into an indirect semiconductor Si, as described in section 3.2.1.

### 2.4. Organic structures

In general, organic materials contain carbon atoms, e.g., diamond, graphene, fullerenes or carbon nanotubes (CNT). Recently, organic materials have been used as an NM media to accumulate and carry spin-polarized electrons (holes). The main difference from the above metallic-based devices is that the magneto-transport properties are governed by the interfacial orbital bonding. Hence, orbital moments play a very important role in the FM/organic junctions, in addition to the spin moments [104]. It is critical to control the interfacial states in a reproducible manner.

*Graphene*

Graphene is a sheet of a carbon monolayer in a honeycomb alignment and has been widely prepared by exfoliation technique [105]. Large-area graphene has been able to be prepared using chemical vapour deposition (CVD) [106] and epitaxial growth on SiC [107]. MR measurements on multilayer epitaxial graphene have been performed [108]. Clear Hanle signals were observed and revealed the spin diffusion length up to approximately 200 $\mu$m.

Following these exciting discoveries, spin-polarized electron transport has been detected in a graphene sheet by measuring lateral spin-valve signals in a non-local geometry (see figure 12) [32, 109]. A Berry phase has also been observed by measuring the quantum Hall effect in bilayer graphene [110]. This phase was proposed by Berry in 1984 as a geometrical phase [111]. A pseudo-spin-valve has been proposed by sandwiching bilayer graphene with two pairs of ferromagnetic electrodes [112]. This also suggests the possibility of gate operation by an additional pair of ferromagnets. A graphene-based memory logic has been proposed and demonstrated by many groups, e.g., [113]. Such a system has an advantage of low-power operation and scalability. Further details can be found in, for example, [104].

*Carbon nanotubes (CNT)*

A new form of organic structure, a CNT, was demonstrated in 1991 by Sumio Iijima [114] by rolling a graphene sheet. The CNT can be categorized into three types; zig–zag, chiral and armchair. Only the first two possess both metallic and semiconducting characteristics due to the band overlap at the Fermi level between $\pi$ and $sp^2$, suggesting an ideal conductance of $2G_0$. The first spin-polarized electron transport across a CNT was measured in a metal-on-tube configuration, as shown in figure 13 [115]. This configuration is fabricated by a fine metal-patterning process onto a dispersed CNT on a substrate, and it has lower contact resistance without CNT distortion and interfacial oxide-barrier or contamination formation as compared with a tube-on-metal geometry. A buried-tube configuration by electrode melting can further reduce the contact resistance. For a single-wall (SW) CNT, these transport properties are especially pronounced. For the case when the contact resistance is larger than the quantum resistance, a Coulomb blockade has been observed [116]. An SW-CNT can be treated as an ideal 1D system, suggesting that acceleration of one electron induces acceleration of the whole system up to the Fermi velocity [117]. This is clear proof of the Tomonaga–Luttinger liquid proposed in 1950 [118, 119], which is different from the Fermi liquid, with different effective mass for independent electrons. The Kondo effect has also been observed below 1 K [120], showing a resistivity increase by spin flip during the transport, as proposed by Kondo in 1964 [121]. In addition, ambipolar hole/electron transport has been observed in an SW-CNT [122]. Optical emission from an SW-CNT has also been achieved [123]. These fundamental physical features clearly indicate that the CNT and related organic materials can be used in future spintronic devices.

*Fullerenes*

By folding a graphene sheet, fullerenes were discovered in 1985 by Kroto *et al* [124], and were named after an architect,

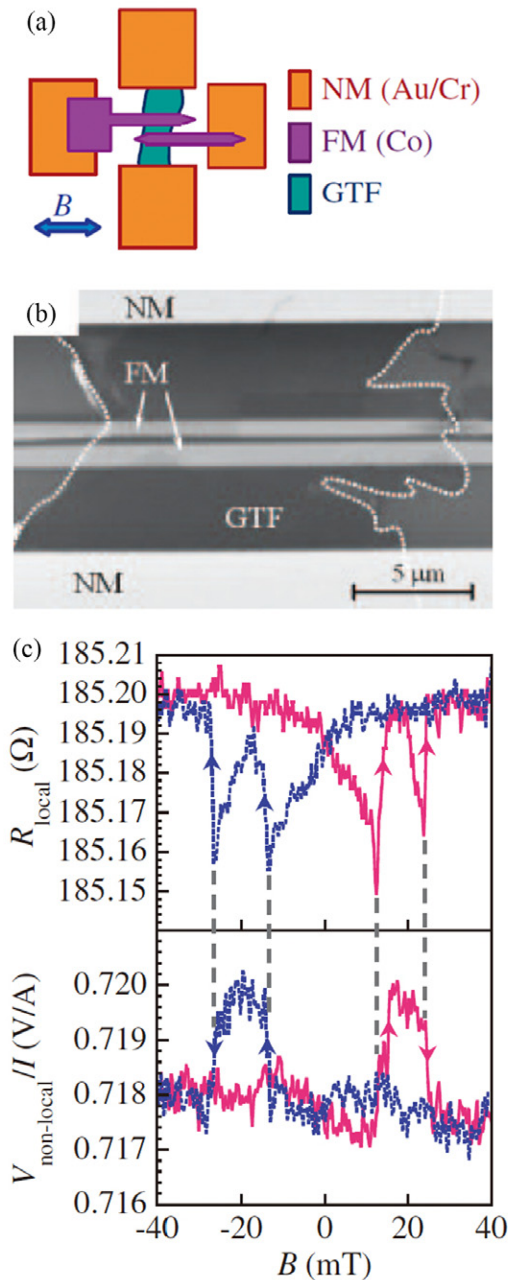


**Figure 12.** (*a*) A schematic of a graphene spin device. (*b*) A scanning electron microscope image of a graphene spin device. (*c*) Result of a local MR measurement (upper panel) and a non-local MR measurement at RT (lower panel). Reproduced with permission from [109], Copyright 2007 The Japan Society of Applied Physics.

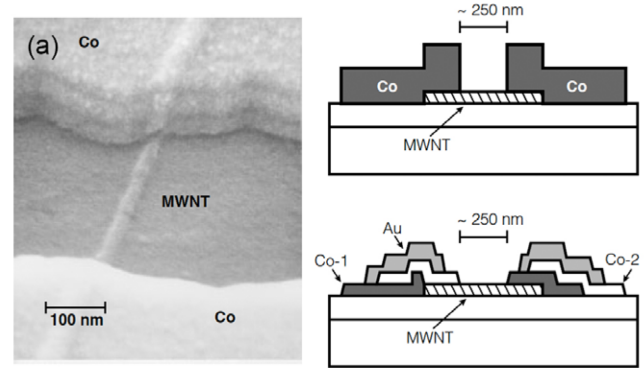


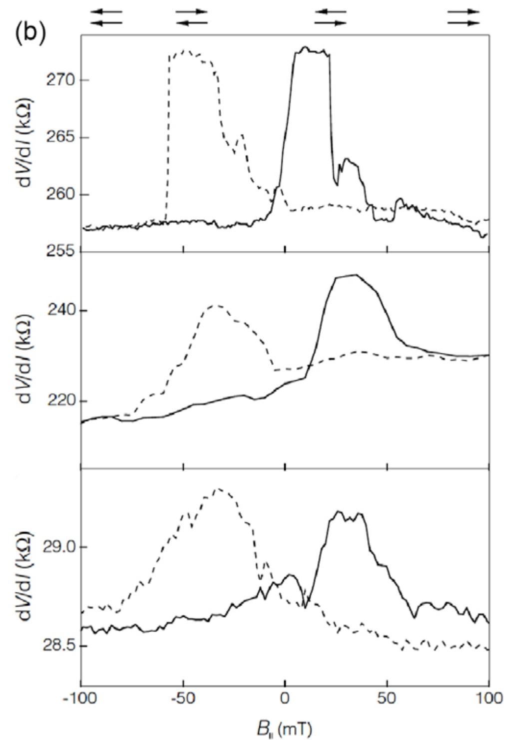


**Figure 13.** (*a*) Structure of our devices, consisting of a single multi-walled carbon nanotube (MWNT) electrically contacted by ferromagnetic Co. (*b*) Two-terminal differential resistance as a function of magnetic field for three different MWNT devices at 4.2 K. Reproduced with permission from [115], Copyright 1999 Nature.

Richard Fuller, who designed a net sphere. The fullerene is of great importance, as an extra atom can be inserted inside the structure providing additional metallic features, such as spin polarization by Gd inserted in $C_{60}$ [125]. By co-depositing fullerenes and ferromagnetic nanoparticles, granular TMR has been reported, showing a 26% TMR ratio at 2 K [126]. This has a great potential to be improved further.

*Other organic materials*

Another material that has been heavily investigated is the molecular organic semiconductor, 8-hydroxyquinolinato ($Alq_3$). A first attempt has been made to observe GMR in a $La_{0.67}Sr_{0.33}MnO_3$ (LSMO)/$Alq_3$/Co junction [127]. This provides a GMR ratio of 12% at 11 K. By sandwiching $Alq_3$ with permalloy (Py) and Co as well as an additional $Al_2O_3$ tunnel barrier, a TMR ratio of 6.0% at 300 K has been reported [128]. Without using the additional barrier, the spin polarization of an $Alq_3$/Al junction is estimated to be only 6%. The spin diffusion length in $Alq_3$ has been measured to be $10 \pm 1$ nm at 90 K [129].

In 1974, Aviram and Ratner proposed a molecular rectifier [130]. A molecular diode was demonstrated with a Langmuir–Blodgett (LB) film [131]. For instance, a spin-transistor demonstration has been reported using a CNT as a medium [132]. By using half-metallic LSMO as the spin source and drain, highly efficient spin-transistor operation can be achieved [133].

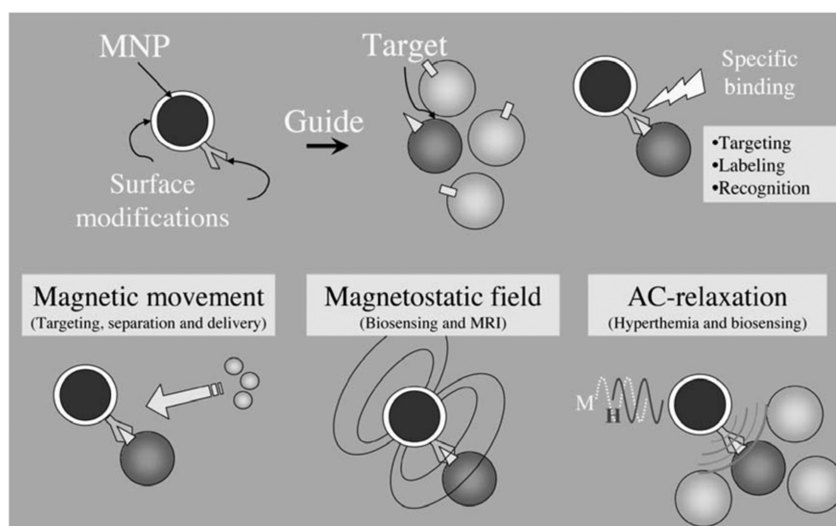


**Figure 14.** Major bio-applications of ferromagnetic nanoparticles. Reproduced with permission from [136], Copyright 2006 Springer.

## 3. Spintronic device designs

In this section, the operation and recent development of the current major spintronic devices are described. The devices are categorized by the number of terminal electrodes, operational modes (passive or active) and spectroscopic usage.

### *3.1. Two-terminal passive spintronic devices*

Here, the operation and recent development of the current major spintronic devices are described. The devices are categorized by the number of terminal electrodes, operational modes (passive or active) and spectroscopic usage.

*3.1.1. Magnetic field sensors.* From 1994, Non-Volatile Electronics Inc. (NVE) developed a series of magnetic field sensors and switches based on GMR [134]. These sensors can be used to detect position, a magnetic media, rotational speed and an electrical current at low cost. Using a polycrystalline Co/Cu/Co multilayer, a GMR ratio of more than 70% has been reported at RT [135].

Recently, magnetic biosensors have been developed using ferromagnetic nanoparticles as a magnetic marker, as listed schematically in figure 14 [136]. In principle, these magnetic markers can be used for both drug delivery and on-chip biosensors. For drug delivery, blood flow is employed to deliver a magnetically labelled drug or a micro-medical machine, and a local magnetic field specifies the point of delivery. For biosensors, a magnetic nanoparticle or magnetic bead is attached to a target molecule and is trapped by a stray field from a GMR-type sensor. In order to realize these bio-applications, three major issues need to be solved; biocompatibility, size uniformity and surface stability [137].

*3.1.2. Hard disk drives (HDD).* In 2005, a TMR head was introduced by Seagate [138], which was used in longitudinal recording based HDDs. This resulted in an areal density of $>$600 Gbit in$^{-2}$. These heads are attached to an arm, which is moved precisely over the platter using an actuator controlled by a linear motor. The write head for longitudinal recording was a ring-shaped magnet invented by Schuller (AEG).

In an HDD, the media consists of CoPtCr$X$ alloy ($X$ = B and Ta) thin films deposited on a metallic (Al) or glass platter [139]. These written bits are read out by a read head, where an MR head is used in order to detect a change of direction of a small stray field from the medium. Such a sharp change induces a change in the MR value, which is detected electrically.

*Perpendicular recording*

In 1967, perpendicular magnetic anisotropy [140] was first observed [141], which was then demonstrated in Co/Pd [142] and Au/Co/Au multilayers [143] in 1986. In 2000, Hitachi demonstrated an HDD with perpendicular recording with an areal density of 52.5 Gbit in$^{-2}$ using granular CoPtCr media [138]. In 2005–2006, perpendicular recording was finally introduced by Seagate, Hitachi and Toshiba. This is expected to achieve over 1 Tb in$^{-2}$. These perpendicular media contains CoPt$X$ alloys, which increase the HDD fabrication const. A search for alternative materials has been carried out intensively.

Such perpendicular recording media achieved over 300 Gbit in$^{-2}$ recently [144]. In order to increase the areal density further, coupled granular continuous (CGC) media were proposed [145]. The CGC media consist of a cylindrical granular layer sandwiched by a continuous soft under layer and cap layer. Due to the inter-granular coupling, the thermal stability and signal-to-noise ratio was improved by five times or more, achieving the areal density of 400 Gbit in$^{-2}$ [146].

Using a soft switching layer coupled to a hard under layer, an exchange coupled composite (ECG) medium was then proposed [147, 148]. Here, the soft layer assists the magnetization reversal in the hard layer by coherent rotation, as described by the Stoner–Wohlfarth model [149]. A combination of these two composite media has led to a new ECC/CGC medium [150]. The ECC/CGC media reduce the coercivity further with maintaining strong perpendicular anisotropy. This media is expected to achieve almost

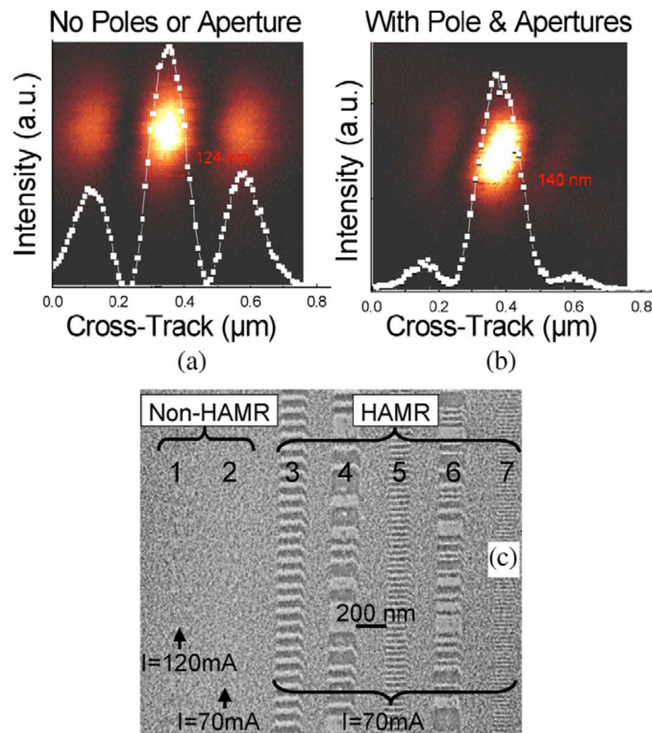


**Figure 15.** Scanning near-field optical microscope (SNOM) images of a HAMR head (*a*) with no poles and no aperture and (*b*) with the magnetic write poles and with an aperture. (*c*) Magnetic force microscopy image of high coercivity media being written without heat assist and with heat assist. Reproduced with permission from [155], Copyright 2008 IEEE.

1 Tbit in$^{-2}$. In order to overcome the areal density of Tbit in$^{-2}$, bit-patterned media was proposed [151]. By patterning nano-scale island-shaped bits typically consisting of 10–20 grains, the media can achieve 10 Tbit in$^{-2}$.

*Alternative recording methods*

For the further improvement in the HDD areal density, the trilemma has to be overcome among the areal density, thermal stability and writability [152]. A possible solution is to assist the magnetization switching for writing by energy, i.e. heat or microwave. Heat-assisted magnetic recording (HAMR) was proposed [153, 154]. A laser beam is employed to heat the media up locally and reduce the thermal stability of the data bit to be written. A scanning near-field optical microscope is implemented into a writing head and a successful demonstration has been reported (see figure 15) [155]. In 2012, TDK demonstrated a new HAMR head with the areal density of 1.5 Tbit in$^{-2}$ and bit-error rate of $10^{-2}$. Seagate also demonstrated a new HAMR drive in 2012.

Microwave-assisted magnetic recording (MAMR) was proposed by Zhu *et al* [156]. The MAMR utilizes microwaves to reduce the switching field by an order of magnitude [157].

*Spintronic read heads*

As replacements of the above TMR heads, coherent TMR, nano-oxide-layered (NOL) GMR and half-metallic GMR junctions have been investigated, as shown in figure 16. The requirements for the next-generation HDD is above 2 Tbit in$^{-2}$, achievable by satisfying both MR >50% and resistance–area

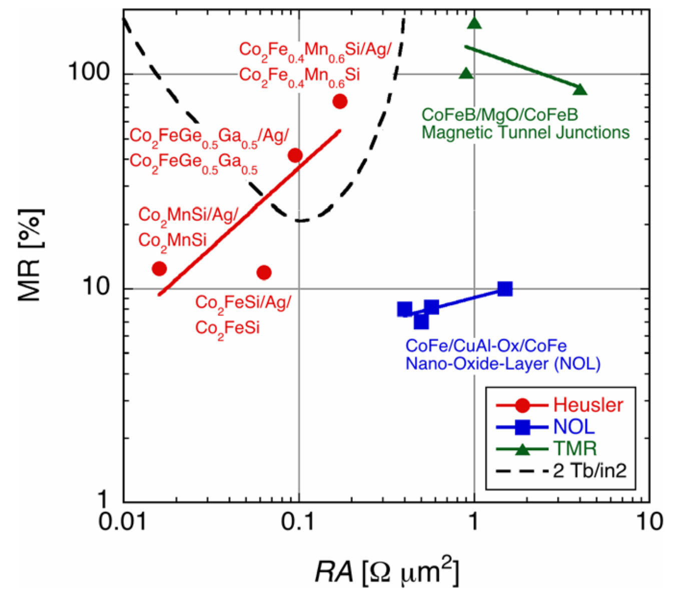


**Figure 16.** Current and target values of (*a*) MR ratios and *RA* for an HDD read head after. Reproduced with permission from [158], Copyright 2013 Springer.

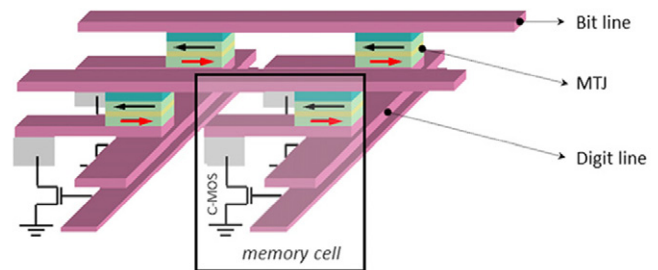


**Figure 17.** Schematic diagrams of MRAM. Reproduced with permission from [159], Copyright 2013 IOP.

product ($RA$) $< 0.1\,\Omega\,\mu\text{m}^2$ as indicated by the dotted region in figure 16 [158]. The coherent TMR junctions are required to lower their *RA* by one order of magnitude, and nano-oxide-layered GMR junctions are required to almost double their MR. Among these candidates, the half-metallic GMR junctions satisfy these requirements. Accordingly, Hitachi Global Storage Technologies (HGST, now a Western Digital company) has been investigating half-metallic Heusler alloy GMR junctions.

*3.1.3. MRAM/spin RAM.* After the commercial success of the GMR head [158], one of the major ongoing device studies is to realize a MRAM, as shown schematically in figure 17 [159]. MRAM can achieve the following features [158, 160, 161]:

(i) non-volatility similar to HDD without using a mechanical head
(ii) read and write times of the order of nano-seconds
(iii) high density
(iv) low-power consumption.

Hence MRAM is a good candidate for a universal memory. MRAM can also avoid the delay and unnecessary power

**Table 2.** List of major memories [173, 175].

| | Spin RAM | MRAM | FLASH | | DRAM | | FeRAM | SRAM |
|---|---|---|---|---|---|---|---|---|
| Rules | 32 nm | 90 nm | 32 nm | 90 nm | 45 nm | 90 nm | | 90 nm |
| Non-volatility | Y | Y | Y | Y | N | N | Y | N |
| Read time | $\sim$1 ns | 300 ns (GMR)<br>$<$60 ns (TMR) | 10–50 ns | 10–50 ns | 10 ns | 10 ns | 100–200 ns | 1.1 ns |
| Write time | $\sim$1 ns | $<$10 ns | 0.1–100 ms | 0.1–100 ms | 10 ns | 10 ns | $\sim$100 ns | 1.1 ns |
| Repetition | $>10^{15}$ | $>10^{15}$ | $>10^{6}$ | $>10^{6}$ | $>10^{15}$ | $>10^{15}$ | $10^{9}$–$10^{12}$ | $>10^{15}$ |
| Cell size | 0.01 $\mu m^2$<br>5 Gb $cm^{-2}$* | 0.25 $\mu m^2$<br>256 Mb $cm^{-2}$ | 0.02 $\mu m^2$<br>2.5 Gb $cm^{-2}$* | 0.1 $\mu m^2$<br>512 Mb $cm^{-2}$ | | 0.25 $\mu m^2$<br>256 Mb $cm^{-2}$ | | 1–1.3 $\mu m^2$<br>64 Mb $cm^{-2}$ |
| Cell density | 6 $F^2$ | 27 $F^2$ | | 4 $F^2$ | 6 $F^2$ | 8 $F^2$ | 8 $F^2$ | 92 $F^2$ |
| Chip capacity | | $>$1 Gb | | $>$1 Gb | | | $<$10 Mb | |
| Program energy per bit | | 120 pJ | 10 nJ | 30–120 nJ | | 5 pJ + refresh | | 5 pJ |
| Soft error hardness | | Y | | Y | | Y | Y | N |
| Process cost | | RT process | | Lower bit cost | | | HT process | |

*Note*: * represents target values.

consumption due to circuit leads, and can provide a high-density circuit by the converting passive current leads in conventional electronic devices into memory cells. The comparison between the MRAM and the other major memories are summarized in table 2.

Current volatile memory stores data in tiny capacitors. The data needs to be refreshed thousands of times per second for dynamic random access memory (DRAM) but not for static random access memory (SRAM). For non-volatile memory, flash memory (FLASH) is a form of electrically erasable programmable read-only memory (EEPROM) and uses an extra floating gate on a transistor to store data, a large section of which can be erased by applying a voltage pulse. However, because of the limited rewritability and long write time, FLASH was initially used as ROM. Many formats have been produced including: CompactFlash by SanDisk in 1994, SmartMedia (SSFDCC: Solid State Floppy Disk Card) by Toshiba in 1995, MultiMediaCard originally proposed by Siemens AG in 1998, Memory Stick by Sony in 1998, and SD (secure digital) memory cards developed by Toshiba, Matsushita and SanDisk in 2000.

MRAM was first proposed by Schwee in 1972 [162]. The functionality of MRAM was demonstrated with a Fe-Ni-Co alloy-based GMR cell [163]. In 1996, the first MTJ cell was implemented in an MRAM demonstration [164, 165]. IBM and Motorola independently developed 1 kbit and 512 kbit MRAM, respectively, in 1999 [166, 167]. Motorola developed a 1 Mbit, 2 Mbit and 4 Mbit MRAM [168, 169]. NEC-Toshiba also demonstrated 1 Mbit and 16 Mbit MRAM in 2003 and 2006, respectively [170]. Fast random access has been demonstrated at a speed of $\sim$5 ns for read and write [171]. In 2007, Freescale Semiconductor, which was spun off from Motorola in 2004, commercialized a 4 Mbit MRAM with a working temperature between $-40\,^{\circ}$C and $105\,^{\circ}$C, for automobile applications. In 2010, EverSpin Technologies, which was spun off from Freescale in 2008, started to ship a 16 Mbit MRAM. This is operated at a bias voltage of 3.3 V and a current of 60 mA for read-out and 110 mA for write-in at a speed of 35 ns. Currently, MRAM suffers from the implementation of an additional transistor for each cell, which prevents further miniaturization. To avoid this structural limitation, one-transistor (1T)/4MTJ was proposed [172], suggesting that there is further potential for MRAM as a high-density memory.

These research activities are recognized as one of the key future technologies and are heavily funded by several governments. For example, in 1997, the US Defence Advanced Research Projects Agency (DARPA) funded IBM, Motorola and Honeywell to demonstrate 16 kbit MRAM with an access time of less than 100 ns within 1 inch square chips [173]. This is based on a Honeywell radiation-hard CMOS underlayer process. The New Energy Development Organization (NEDO) in Japan also funded the Spintronics Nonvolatile Function Technology Project from 2006.

For MRAM operation, the reference voltage is normally set at the voltage given by $V_{\mathrm{half}} = (V_{\mathrm{H}} - V_{\mathrm{L}})/2$, where $V_{\mathrm{H}}$ and $V_{\mathrm{L}}$ represent the output voltages at the highest and the lowest resistance. In order to realize a Gbit MRAM, $V_{\mathrm{half}}$ needs to be of the order of 100 mV. This requirement can be achieved by either introducing a double tunnel junction with a ferromagnetic free middle layer [173] or fabricating a textured tunnel junction [174].

Thermal stability is also a crucial issue, as discussed in section 3.1.2. For an MRAM, due to the presence of half-selection in an MRAM bit, which occurs when a bit or write line current flows and induces a random read or write signal, a thermal stability $Kv/k_{\mathrm{B}}T > 100$ is then required. A synthetic ferromagnetic layer has been typically used to maintain high thermal stability [175].

In principle, cross-point architecture guarantees a very high areal density. However, in reality reliable read-out requires one additional transistor cell for each MRAM cell (1T/1MTJ) due to unwanted parallel current paths. For reliable cell selection, toggle switching has been proposed by Motorola to circumvent the half-selection in an MRAM bit [175].

The MRAM cells are initially proposed to be reversed by an Ampère field generated by a write current (see figure 17). However, with reducing cell size, the switching field increases, resulting in larger power consumption (see in figure 18 [176]). Therefore, current-induced magnetization switching (CIMS) by STT has been proposed [53, 54] and demonstrated experimentally [55]. A critical current density of switching of

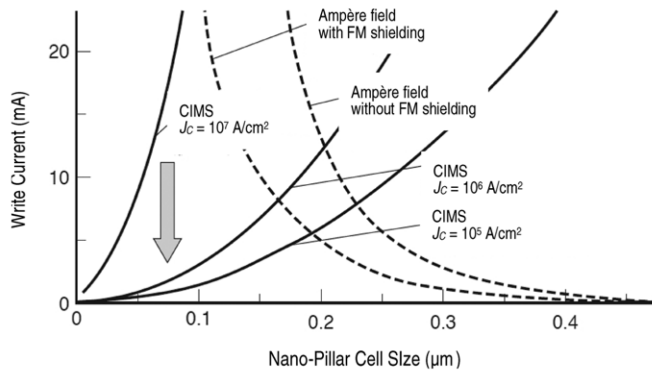


**Figure 18.** Required writing currents for several techniques dependent upon cell size. Reproduced with permission from [176], Copyright 2006 Toshiba Review.

$J_c \sim 10^7\,\mathrm{A\,cm^{-2}}$, which is at least one order of magnitude larger than the Gbit RAM requirement, has been reported. Using a CPP-GMR nano-pillar, an effective STT has been realized by combining two techniques: precise nanofabrication and precisely controlled film growth. A substantial decrease in a critical current density for CIMS has been achieved in a current-perpendicular-to-plane pseudo-spin-valve nano-pillar by inserting an ultrathin spin-scattering Ru layer [177] and an additional ferromagnetic layer [178]. This is an improved structure compared with a simple pseudo-spin-valve with a spin-scattering layer and has successfully achieved a critical current density of $2 \times 10^6\,\mathrm{A\,cm^{-2}}$. This was a crucial breakthrogh for Gbit-scale MRAM applications. Further reduction in the critical current density has been achieved by modifying the shape of the nano-pillar into a nano-ring where the magnetization in each ferromagnetic layer forms a vortex state at remanence [179, 180]. These magnetization directions are aligned to be either clockwise or anti-clockwise by carefully demagnetizing the nano-pillar so that a vertical current assists CIMS by inducing an Ampère field without magnetic-moment curling or domains, i.e. there is no stray field.

A TMR nano-pillar with an Al-O barrier has then been employed as a cell showing a TMR ratio of ∼30% and $J_c < 10^7\,\mathrm{A\,cm^{-2}}$ [181]. After the discovery of coherent tunnelling across an epitaxial MgO barrier, the improved operation of a TMR nano-pillar has been demonstrated with a TMR ratio of ∼100% and $J_c \sim 6 \times 10^6\,\mathrm{A\,cm^{-2}}$ with a pulsed current duration of 100 ms [182]. This has been followed by a further improvement with a TMR ratio of 160% and $J_c$ of $2.5 \times 10^6\,\mathrm{A\,cm^{-2}}$ [183].

Accordingly, Sony has proposed a Spin RAM, which utilizes STT-CIMS for writing rather than the Ampère field used for MRAM, demonstrating 4 kbit operation [184]. They have achieved a resistance–area product $RA$ of $20\,\Omega\,\mu\mathrm{m}^2$ and a TMR ratio of 160%, with a minimum writing current of 200 $\mu$A. In 2007, Hitachi–Tohoku University demonstrated a 2 Mbit Spin RAM with a cell size of $1.6 \times 1.6\,\mu\mathrm{m}^2$ ($16\,\mathrm{F}^2$), a TMR ratio of 100% and a writing current of 200 $\mu$A.

For the next-generation MRAM and Spin RAM, the following issues need to be solved: the reduction of the switching field or critical current density and a reduction of the fabrication rule. Based on the scalability of MRAM and Spin RAM bits, STT must be used as discussed above. For the reduction of power consumption, the thermal stability of the free layer has to be compromised. A synthetic ferromagnet, such as CoFeB/Ru/CoFeB, has been implemented as the free layer by AIST [185], resulting in a five times increase in thermal stability with only an 80% increase in the critical current density. This configuration can achieve a 10 Gbit Spin RAM device. The remaining issue to realize a high-density Spin RAM is the reduction of the fabrication rule, which may be achieved by replacing the additional transistor with a possible new device design as described above.

#### *3.1.4. 1D memory tracks.*

*DW resistance*

In order to minimize the total magnetic energy of a ferromagnetic structure, a DW with a width of the order of 100 nm can be formed between magnetic domains. The competition among the energy terms—magnetostatic, exchange and anisotropy—produces magnetic domains, mainly due to the magnetostatic energy in a mesoscopic ferromagnet. Within a DW, the spins gradually rotate from the direction of the domain to the direction in the neighbouring domain. If the ferromagnet is thick, the spin rotation within the wall is out-of-plane, forming a Bloch wall. For thin ferromagnet films, in-plane rotation, known as a Néel wall, occurs. For an intermediate ferromagnetic film thickness, a combination of these two walls, a cross-tie wall, forms [186].

Since such a wall is sandwiched by magnetic domains with their magnetization at certain angles, e.g., 90 or 180°, this system is expected to show large MR if a spin-polarized current is applied across the wall. Reported experimental observations of this effect are controversial. Positive DW resistivity has been reported [187, 188]. This has been supported theoretically using a spin-flip scattering model [189]. However, negative resistivity has also been reported [190, 191]. This has been explained using a weak localization theory [192]. This contradiction may be due to the relatively large measurement area, typically micrometre-scale. Accordingly, more confined and controlled samples have been prepared for detailed studies [193].

*DW displacement*

Following Slonczewski and Berger [53, 54], STT has also been applied to displace a DW by flowing an electrical current (see figure 19). A ferromagnetic micro-wire has been prepared with a DW, giving a current density between $10^{11}$ and $10^{12}\,\mathrm{A\,m^{-2}}$ for wall motion [194, 195]. The velocity of the wall motion has also been estimated to be 2–6 m s$^{-1}$ [56]. A similar experiment has also been performed in a DMS wire [196, 197].

The detailed behaviour can be analysed by solving the Landau–Lifshitz–Gilbert equation. A spin-transfer-torque term has been calculated in the ideal adiabatic limit to show a threshold current of the order of $10^{12}\,\mathrm{A\,m^{-2}}$ [198]. Additionally, spin relaxation of conduction electrons has been taken into consideration [193, 199–201]. Some studies suggest that spin relaxation is equivalent to damping [202]. However, to date, no conclusive model has been developed [203].

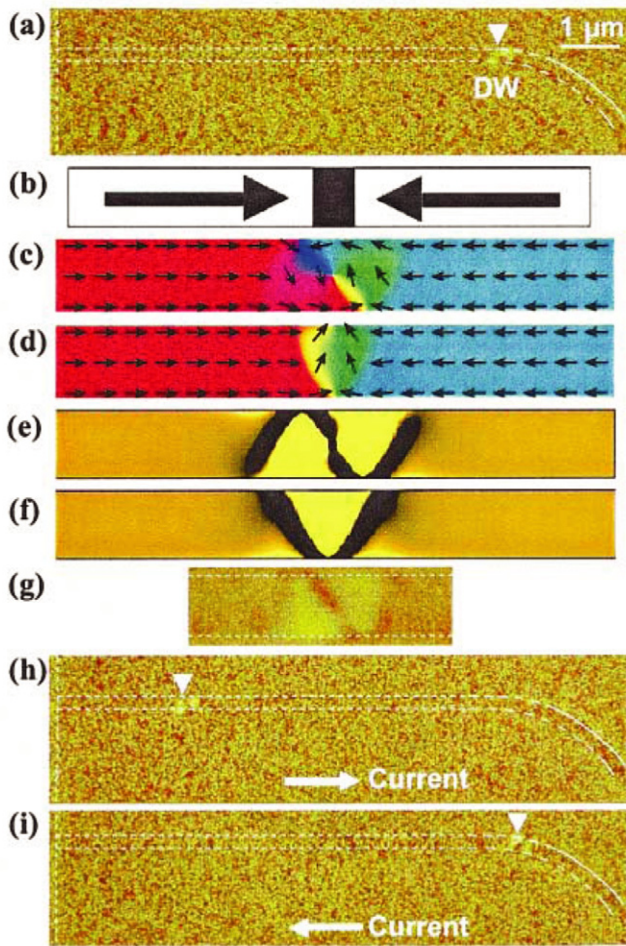


**Figure 19.** (*a*) MFM image after the introduction of a DW. DW is imaged as a bright contrast, which corresponds to the stray field from positive magnetic charge. (*b*) Schematic illustration of a magnetic domain structure inferred from the MFM image. DW has a head-to-head structure. (*c*) Result of micromagnetics simulation (vortex DW). (*d*) Result of micromagnetics simulation (transverse DW). (*e*) MFM image calculated from the magnetic structure shown in (*c*). (*f*) MFM image calculated from the magnetic structure shown in (*d*). (*g*) Magnified MFM image of a DW. (*h*) MFM image after an application of a pulsed current from left to right. The current density and pulse duration are $1.2 \times 10^{12}$ A m$^{-2}$ and 5 $\mu$s, respectively. DW is displaced from right to left by the pulsed current. (*i*) MFM image after an application of a pulsed current from right to left. The current density and pulse duration are $1.2 \times 10^{12}$ A m$^{-2}$ and 5 $\mu$s, respectively. DW is displaced from left to right by the pulsed current. Reproduced with permission from [56], Copyright 2004 American Physical Society.

By simply forming a nano-ring, both a flux-closure vortex state and a uniformly magnetized state, a so-called onion state, have been observed [204]. In the former state, the magnetic moment shows no stray field, while, for the latter case, two magnetic moments along the half-circle form a pair of head-to-head and tail-to-tail DWs. These two distinct states are proposed to be used for storing data. A nano-ring of this type has been used as a template to investigate magnetization switching dynamics [205], DW pinning [206], STT [207], GMR [208] and TMR [209].

An all-metallic DW logic device has been demonstrated at RT [210]. By forming a 'Y'-shaped junction consisting of two permalloy quarter-arc nano-wires, the magnetization reversal induced by the DW motion acts as a NOT circuit. Allwood *et al* have successfully demonstrated NOT-logic operation under the application of an oscillatory magnetic field with up to 11 junctions. The output signals were observed using the magneto-optical Kerr effect (MOKE). By tuning the shape of the 'Y'-junction, they have also realized an AND operation in a DW logic device [211].

*3.1.5. 1D nano-dot track.* An alignment of elongated single-domain quantum dots (QDs) can be treated as a majority gate for logic operation [212]. By employing either ferromagnetic or antiferromagnetic coupling between the neighbouring dots, a three-input gate device has been demonstrated which gives NAND or NOR operation. Based on fast magnetization reversal (~100 ps), the fast operation of ~100 MHz is expected to be achieved with very low-power consumption (~0.1 W for $10^{10}$ gates). This QD logic can be much smaller compared with the DW logic originally proposed by Cowburn and Welland [213].

### 3.2. Three-terminal active spintronic devices

*3.2.1. Spin transistors.* In order to replace a conventional electron with a spin as a data carrier, improved transistor operation with higher density is expected to be achieved. Accordingly, the following spin transistors have been proposed and demonstrated to date.

*All-metal bipolar spin switch*

In 1985, Johnson and Silsbee first demonstrated successful spin injection from a permalloy (Py) into Al and spin detection by the Py using a non-local geometry (see figure 20) [214]. The 65 nm thick Py micrometre-size electrodes ($15 \times 40$ $\mu$m$^2$) were prepared on a 100 $\mu$m wide and 50 $\mu$m thick Au wire using a shadow mask. A clear GMR-type signal was measured below 36.6 K for a Py separation of 300 $\mu$m with a current application of 47 mA, which generates diffusive spin-polarized electron transport in the Au bar. This study was then extended to a Johnson bipolar spin switch by sandwiching a thin Au layer between Py electrodes [215]. At 10 K, a clear spin signal was detected up to an Au thickness of $1.5\pm0.4$ $\mu$m. However, these devices may suffer from a stray field from the edges of the Py electrodes as well as current diffusion into the bulk region. Nanofabrication advancement then enables the patterning of 1D nano-wires, as discussed in sction 3.2.2.

*Spin-polarized field effect transistors (spin FET)*

In 1990, Datta and Das reintroduced a spin-polarized field effect transistor (spin FET), which requires efficient spin injection into a semiconductor [89]. The spin FET provides a key concept for three-terminal spintronic devices. Electron spins are injected from a source modulated by a gate bias and are detected at a drain. In an ideal one-dimensional spin FET, the spin orientation is proportional to the gate voltage, and the drain current can be modulated with the spin orientation from a minimum of 180° to a maximum at 360° [216].

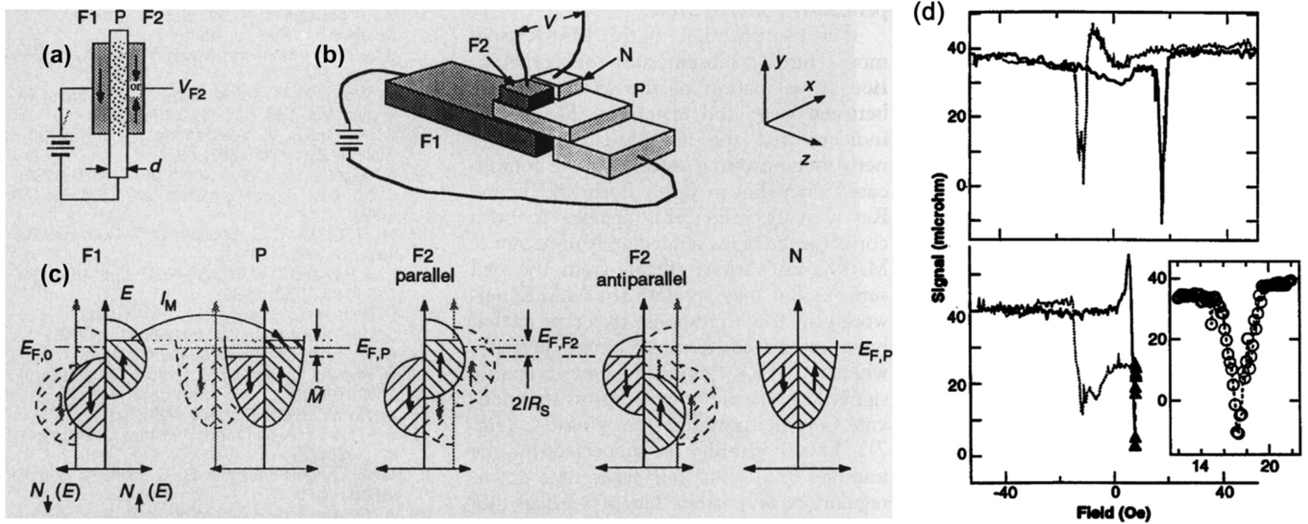


**Figure 20.** (*a*) Pedagogical model of a three-terminal device in cross-section. (*b*) Geometry of a spin-switch device. N is a non-magnetic metal counterelectrode. (*c*) Diagrams of the densities of state, N(E), as functions of energy, of the F1-P-F2 system depicted in (*a*). (*d*) Data from a prototype with $d = 98$ nm. Under constant bias current, the voltage is recorded as the magnetic field is changed. Reproduced with permission from [214], Copyright 1985 American Physical Society.

The spin–orbit interaction Hamiltonian can be derived from the Dirac equations [217]:

$$H_{SO} = \frac{q\hbar}{4m^2c^2}(\vec{\sigma} \cdot [\vec{E} \times \vec{p}]), \quad (8)$$

where $q$, $\hbar$, $m$, $c$, $\vec{\sigma}$, $\vec{E}$ and $\vec{p}$ are the electron charge, Planck constant, electron mass, speed of light, Pauli matrices, electric field and electron momentum, respectively. By comparison with the Rashba Hamiltonian $H_R = \eta(\vec{\sigma} \times \vec{k}) \cdot \vec{v}$ ($\vec{k}$: wave vector and $\vec{v}$: unit vector perpendicular to the plane),

$$H_R = \frac{q\hbar}{4m^2c^2}(\vec{\sigma} \cdot [\vec{E} \times \vec{p}]) = \frac{q\hbar}{4m^2c^2}\frac{V_G}{d}(\vec{\sigma} \times \vec{k}) \cdot \vec{v}. \quad (9)$$

Therefore, the spin–orbit interaction constant $\eta$ can be obtained using a gate voltage $V_G$ and distance between the electron path and the gate $d$:

$$\eta = \frac{q\hbar}{4m^2c^2}\frac{V_G}{d}. \quad (10)$$

As proposed by Datta and Das [89], a 2DEG in a semiconductor has been widely exploited as a possible medium for spin-polarized electron transport due to the high in-plane mobility. Spin injection (almost 1% change) has been reported for a ferromagnetic metal/InAs 2DEG device at 75 K by Hammar *et al* [218]. A potential difficulty is the exclusion of a Hall voltage associated with the strong magnetic field due to the ferromagnetic elements. Direct spin injection and detection of spin polarization in a NiFe/InAs QW/NiFe system has been reported at 4.2 K by Monzon and Roukes [219]. It is very difficult to distinguish a spin-dependent signal from the experimental background noise, although local Hall effects can be suppressed by minimizing magnetic fields in the low-density conduction channels. This can be achieved by engineering the nano-magnet switching properties and eliminating multiple magnetic domains in the injection region. In order to avoid local Hall effects, a multi-terminal geometry has been proposed [86] and used [220], however it was not successful. This can also be avoided by patterning into an asymmetric multi-terminal geometry.

Successful spin injection from epitaxial Fe into *n*-GaAs(0 0 1) has been demonstrated at 4 K by Crooker *et al* [221]. MOKE imaging has been used to detect spin polarization at both the spin injector and detector in the lateral device, as shown in figure 21. A detailed image of spin transport at the edge of an *n*-GaAs layer has also been investigated by focused cross-sectional MOKE imaging [222]. The image verifies the exponential decay of spin-polarized electrons injected from a $Co_{0.68}Fe_{0.32}$ electrode, which is attributed to the spin relaxation in GaAs. Even though the sample preparation and measurement are extremely difficult, this new technique offers a way to map the depth profile of spin-polarized electrons under an electric field in three-terminal spintronic devices.

Spin injection from Fe into ZnSe has also been investigated. Coherent band matching has been investigated theoretically for this system, as has been similarly reported for epitaxial MgO-based tunnel junctions [223]. The majority spins in the vicinity of the Fermi level are dominated by *s*-characteristics as compared with the minority spins, resulting in larger conductance for the majority bands. Further *ab initio* calculations have predicted that Fe/ZnSe(0 0 1) and Fe/GaAs(0 0 1) interfaces act as highly efficient spin filters with a spin polarization of 99% [224]. These results are very promising for future spin-injection devices.

*Spin-polarized lasers*

Circularly polarized light emission was initially studied in InGaAs QW [225]. A vertical cavity surface emitting laser (VCSEL) was fabricated with circular polarization in Voigt geometry, showing 35 mW power under a magnetic field

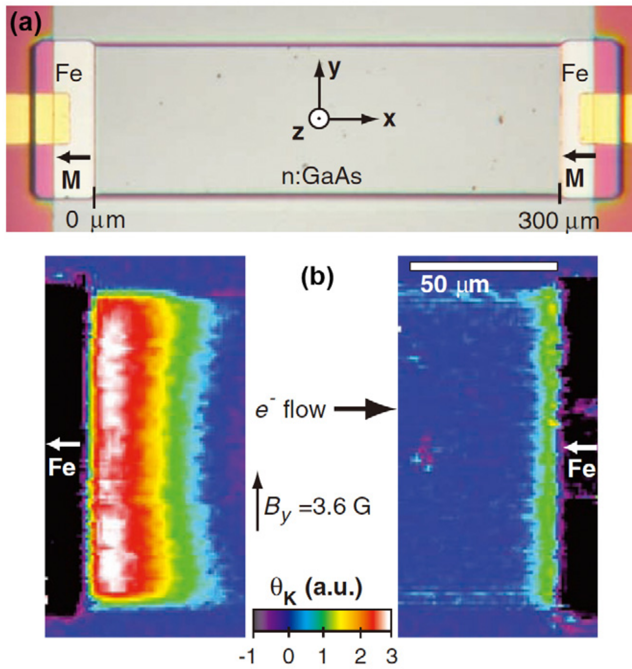


**Figure 21.** (*a*) Photomicrograph of the lateral ferromagnet/semiconductor device used for electron spin injection, transport, accumulation, and detection. (*b*) Images of the Kerr rotation angle $\theta_K$ ($\propto S_z$) near the source and drain contacts. $V_b = +0.4$ V. The region of spin accumulation near the drain contact also exhibits positive $\theta_K$, indicating that both the injected and accumulated spin polarizations are antiparallel to $M$. Reproduced with permission from [221], Copyright 2005 Science.

of 2 T. The VCSEL operation was then demonstrated both by optical and electrical injection [226]. By optimizing the structure to reduce spin–orbit coupling, just a 4% spin polarization of injected carriers led to a nearly complete (96%) polarization of emitted light reported with a QW-VCSEL [226], demonstrating that such lasers can be highly efficient spin filters and spin amplifiers, as predicted theoretically [227]. The behaviour of the spin lasers were analysed by the bucket model [228]. The model offers a way to design a desirable spin laser for both QW and QD configurations. Spin-injection modulation was also demonstrated to be able to eliminate parasitic frequency modulation (chirp) and to enhance the modulation bandwidth [229], improving the two key parameters in lasers. The operation frequency can be over 11 GHz, which is highly advantageous for future spintronic communications via circularly polarized light at RT [230].

*Spin-polarized light-emitting diodes (spin LED)*

Since DMS show a large Zeeman splitting and ferromagnetism [25], DMS can be used as a spin aligner to inject spin-polarized carriers, i.e. spin-polarized electrons or holes, into a semiconductor. The spin polarization of the injected carriers is detected optically through circularly polarized EL from the semiconductor (e.g., GaAs), which are called spin-polarized light-emitting diodes (spin LEDs). With ferromagnetic *p*-GaMnAs as a spin aligner, spin-polarized hole injection has been reported at low temperature [231]. At forward bias, spin-polarized holes from the *p*-GaMnAs, as well as unpolarized electrons from the *n*-GaAs layer, are injected into an InGaAs QW, so that the recombination of the spin-polarized holes can create a circularly polarized EL emission from the QW. However, as the spin relaxation time for the holes is much shorter than that for the electrons [232], the spin polarization signal through the recombination process in the GaAs is very small (about ± 1%). Using paramagnetic *n*-BeMnZnSe with a large Zeeman splitting as a spin aligner, highly efficient electron spin injection has been achieved with an applied field of ∼3 T (spin polarization in EL ∼90%) [233]. This is because the spin diffusion length of the electrons has been reported to be above 100 $\mu$m in the GaAs [29]. Similar results have been obtained using CdMnTe [234], ZnMnSe [235, 236], ZnSe [237] and MnGe [238], but only at low temperatures of typically $T < 80$ K. Since RT ferromagnetism has been predicted in several DMS compounds [239] but not yet observed, spin injection at RT with a DMS may be achievable in the near future (see section 4.1 for more details).

*Schottky diodes*

A ferromagnet/semiconductor Schottky diode consisting of an Fe (20 nm)/GaAs/InGaAs QW LED structure, has been used to measure circularly polarized EL by Zhu *et al* [240]. Spin injection from the Fe into the GaAs was achieved with an efficiency of about 2% at 25 K, which was independent of temperature. However, the right and left circularly polarized EL intensity did not show a clear difference. By examining the tails of the Gaussian-like EL intensity distributions, a heavy hole excitation contribution was estimated. Hanbicki *et al* [241] have performed a similar experiment with an Fe (12.5 nm)/AlGaAs/GaAs QW LED and have observed a spin injection efficiency of 30%. They clearly observed a significant difference between right and left circular EL intensity. The spin polarization was estimated to be 13% at 4.5 K (8% at 240 K). Taking the spin relaxation time in the QW into account, they reported a small temperature dependence of the spin injection efficiency, which is consistent with spin-polarized electron tunnelling.

Crooker *et al* measured a spin polarization of 32% at an Fe/GaAs Schottky junction [221]. In Fe/GaAs/Fe junctions, more up spin electrons were injected on one side and more down spins were ejected from the other end by flowing a current across the junction. This indicates that positive spin polarization is achieved in reversed bias, while negative polarization is achieved in forward bias. Both positive and negative spin polarizations have been measured in an Fe/GaAs Schottky junction introducing spin-polarized electrons by circularly polarized photoexcitation [242].

*Tunnel diodes*

Jonker's group in the Naval Research Laboratory also inserted a tunnel barrier at a ferromagnet/semiconductor interface to achieve ballistic spin injection. A spin polarization of 30% at 4.5 K was measured in an Fe/$Al_2O_3$/GaAs system [243]. Using coherent tunnelling with an epitaxial MgO(0 0 1) barrier, a spin polarization of 55% was achieved [244]. This leads to a spin injection efficiency of 32% at 290 K [245]. However, atomic mixing across the MgO barrier during annealing to crystalize the barrier needs to be prevented.

*Spin-polarized resonant tunnelling diodes (spin RTD)*
A DMS has been used for a spin RTD in AlAs/GaMnAs/AlAs [25] and BeTe/ZnMnSe/BeTe [246] structures. In the spin RTD, spin orientations can be controlled by a gate voltage, which relies on a giant Zeeman splitting of the $Mn^{2+}$ ions.

In 2000, Ohno *et al* have achieved a magnetic phase transition by applying a bias voltage in an InMnAs layer sandwiched within a FET [247]. A positive bias on the gate created an electric field which repels holes, causing the Mn magnetic moments to rotate randomly (paramagnetism). A negative voltage generates an electric field which attracts holes, causing the Mn magnetic moments to align along the field direction (ferromagnetism). Although these phenomena were only seen at 25 K with a bias voltage of ±125 V, this is a significant step towards the realization of three-terminal spintronic devices. A similar effect in a metallic film is discussed in section 4.2.

*Spin injection into Si*
Since Si has an indirect bandgap, poor spin injection is expected [248]. It has also long been believed that intrinsic spin polarization in Si is typically a few per cent at RT and hence spin injection into Si is very difficult. Present nano-electronic devices predominantly depend on Si-based technology, indicating the importance of spin injection into Si with high efficiency. A junction of $Co/Al_2O_3/Si$ has been used to demonstrate that the *RA* product can be tuned over eight orders of magnitude by inserting an ultrathin Gd layer which has a lower work function against Si [249]. Such tunability in the *RA* product is very useful to realize a spin MOSFET, which requires a narrow *RA* window against the Si doping density.

Spin injection into Si has been successfully demonstrated by Jonker *et al* in an $Fe/Al_2O_3/n$-Si with an LED structure underneath [250]. As seen in figure 22, circular light polarization of 5.6% at 20 K (2.8% at 125 K) was measured, indicating an injected spin polarization of approximately 30%. Recently Dash *et al* demonstrated spin injection into Si at RT [251], where the spin lifetime and diffusion length was estimated to be 142 ps and 230 nm, respectively. These experiments have opened the door to Si spintronics, which possesses a significant advantage for the implementation of spintronics into Si-based nano-electronics, e.g., spin-polarized metal-oxide-semiconductor (MOS) FET, as described in section 4.2.

Since then, many groups have been working on this topic. In particular, Si has been reported to possess a very long spin lifetime under optimum doping: up to 1.3 ns and 122 ps for *n*- and *p*-doped Si at RT [252]. This allows the reduction of the numbers of interconnections in the current multi-core architectures [253] and hence is very advantageous for device applications in addition to the perfect compatibility with the current CMOS technology. The next step is spin injection using a four-terminal configuration.

Similarly, spin injection into Ge has been investigated, e.g., [254]. In particular, *p*-Ge has an advantage for spin-polarized electrons to be injected through only a tunnel barrier (without Schottky barrier formation), resulting a clear Hanle signal at RT. Here it should be noted that the Hanle signal is a negative MR induced by a small perpendicular magnetic field application, while the inverted Hanle signal is a positive MR induced by an in-plane field. In three-terminal geometry, therefore, the Hanle signal is only sensitive to the accumulated spins under the injector, while the inverted Hanle signal is sensitive to the interfacial roughness between the injector and the NM layer due to the perpendicular component of the stray field. This is very useful for spin-transistor device applications.

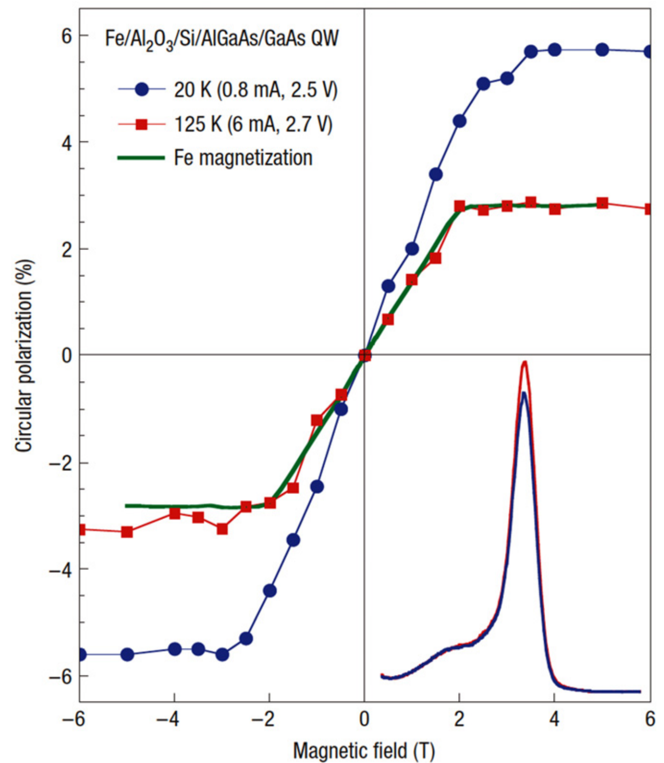


**Figure 22.** Magnetic-field dependence of $P_{circ}$ for the GaAs QW free exciton in the EL spectra from the $Fe/Al_2O_3/Si/AlGaAs/GaAs$ QW/AlGaAs n-i-p structure. $P_{circ}$ tracks the magnetization and majority electron spin orientation of the Fe film, shown as the solid line. The EL spectrum at 3 T and 20 K is shown in the inset, analysed for $\sigma+$ (red) and $\sigma-$ (blue) polarization. The main peak is the free exciton at 1.54 eV from the 10 nm GaAs QW. Reproduced with permission from [250], Copyright 2007 Nature.

*Spin-valve transistors*
Monsma *et al* successfully produced a spin-valve transistor (see figure 23) in 1995 [255], demonstrating large effects due to both electron injection into the spin-valve from a semiconductor across a Schottky barrier and ballistic electron detection at the spin-valve/semiconductor interface. A metal base consisting of $[Co(1.5\,nm)/Cu(2.0\,nm)]_4$ was fabricated by wafer-bonding in UHV and was sandwiched by a Si emitter and collector. Since the CPP configuration is very sensitive to a magnetic field, the transmitted current across the structure can be controlled by applying a field. Due to the complicated fabrication process, this device may not be relevant for mass production. Another disadvantage is that the gain (collector current/emitter current) is very small ($\sim 10^{-5}$). More recently, spin-polarized hot electrons have been injected from $Co_{0.84}Fe_{0.16}$ into a 10 $\mu$m thick Si layer and detected by a $Ni_{0.80}Fe_{0.20}$ layer which was also fabricated by wafer bonding [256].

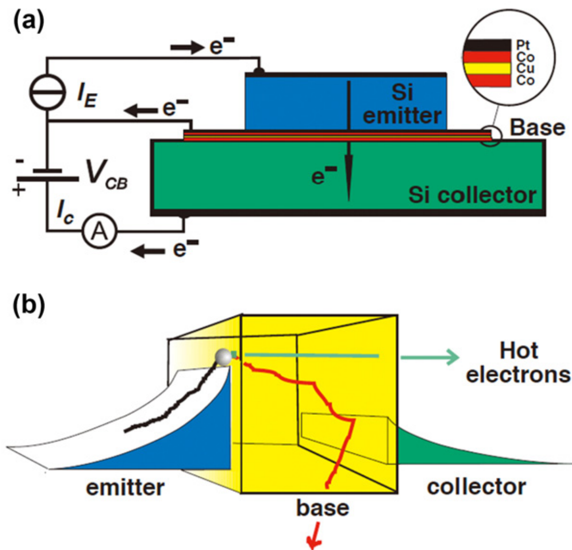


**Figure 23.** Schematic diagram of a spin-valve transistor. Reproduced with permission from [255], Copyright 1995 American Physical Society.

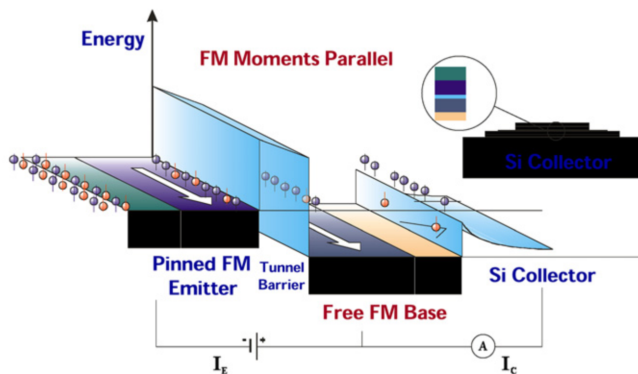


**Figure 24.** Schematic diagram of a magnetic tunnel transistor. Reproduced with permission from [257], Copyright 2003 AIP Publishing LLC.

*Magnetic tunnel diodes*

By replacing a spin-valve structure with a MTJ in the spin-valve transistor, a very large magnetocurrent change of over 3400% has been demonstrated in a magnetic tunnel diode, as shown in figure 24 [257]. Hot electrons were injected from the top Cu emitter into the bottom GaAs base through a tunnel barrier in the structure which was GaAs/$Co_{0.70}Fe_{0.30}$/Cu/$Ni_{0.81}Fe_{0.19}$/$Al_2O_3$/Cu. Here, the transmission spin polarization can be as high as 95%.

*Coulomb blockade diodes*

By confining the current path into a lateral nano-bridge (30 nm wide and 60 nm long), a clear Coulomb blockade has been observed in a Co–Al–O granular film [258]. At slightly above the threshold voltage of the Coulomb blockade regime, the TMR ratio was reported to exceed 30%. This device used NbZrSi as the injector and detector for the Coulomb blockade nano-bridge. The structure was further modified into a vertical Al/Co-Al-O/Co granular junction [259]. A bias-dependent oscillatory behaviour of the TMR ratio was clearly observed at 4.2 K, the sign change of which occurs at the step-points of the Coulomb staircase.

*Nano-ring diodes*

A nano-ring structure has the great advantage of forming a stray-field-free magnetic configuration. Gallo *et al* [260] proposed a spin FET with a split-nano-ring source and drain. The nano-ring is set to be in the vortex state, assuring that the source and the drain are antiferromagnetically coupled with a separation below 50 nm. Such a spin FET has been demonstrated experimentally [261]. A 2 $\mu$m-diameter Fe nano-ring with a 30 nm gap in the middle was fabricated by electron-beam lithography. Magnetic domains, both in vortex and onion form, were observed by magnetic force microscopy, confirming a similar magnetization reversal process to that in a conventional nano-ring. This is the first step towards the realization of a spin FET consisting of a nano-ring.

*3.2.2. 1D lateral nano-wires.* Significant effort has been devoted to fabricating an all-metal transistor based on the GMR effect. The first successful spin injection across NiFe/Au/NiFe junctions was reported by Johnson [214], which can be explained using GMR theory [262]. This finding led to the realization of a Johnson transistor, as discussed in the previous section. Even so, it was found to be very difficult to reduce the distance between the two ferromagnetic electrodes to below the spin diffusion length of the non-magnetic medium for consistent operation.

Recent development in nanometre-scale fabrication techniques has enabled the expansion of these vertical GMR structures into a lateral configuration consisting of ferromagnetic nano-wires and a non-magnetic nano-wire to bridge over the spin injector and detector. In such a lateral spin-valve configuration, spin-polarized electrons can be injected with an electron charge current (local geometry) and without a charge current (non-local geometry). Initially, an asymmetric multi-terminal geometry has been used to inject spin-polarized electrons into an InAs 2DEG wire. However, only an AMR effect at 4.5 K [220] or a very small signal (~0.2%) at below 10 K [263] have been measured. By inserting a 2 nm thick oxide layer between the Fe and GaAs layers, around a 5% change, dependent upon the magnetization orientations, has been measured below RT [80]. This result turned out to be due to the conductance mismatch, as discussed in section 2.3.1.

*Non-local spin-valves*

In 2000, Jedema *et al* re-energized spin-injection studies using a non-local geometry, as shown in figure 25. Using the non-local geometry, pioneering works have been carried out, successfully demonstrating diffusive spin injection from a ferromagnetic $Ni_{80}Fe_{20}$ nano-electrode, spin accumulation in a non-magnetic Cu nano-wire and spin detection by another NiFe nano-electrode. Spin polarization of the injected current was a few per cent and the spin diffusion length in the Cu was estimated to be 350 nm at RT. A non-local contact geometry was used to avoid the Hall effect inducing significant voltages [264]. They have extended their study to ballistic spin injection by inserting an Al–O tunnel barrier at the

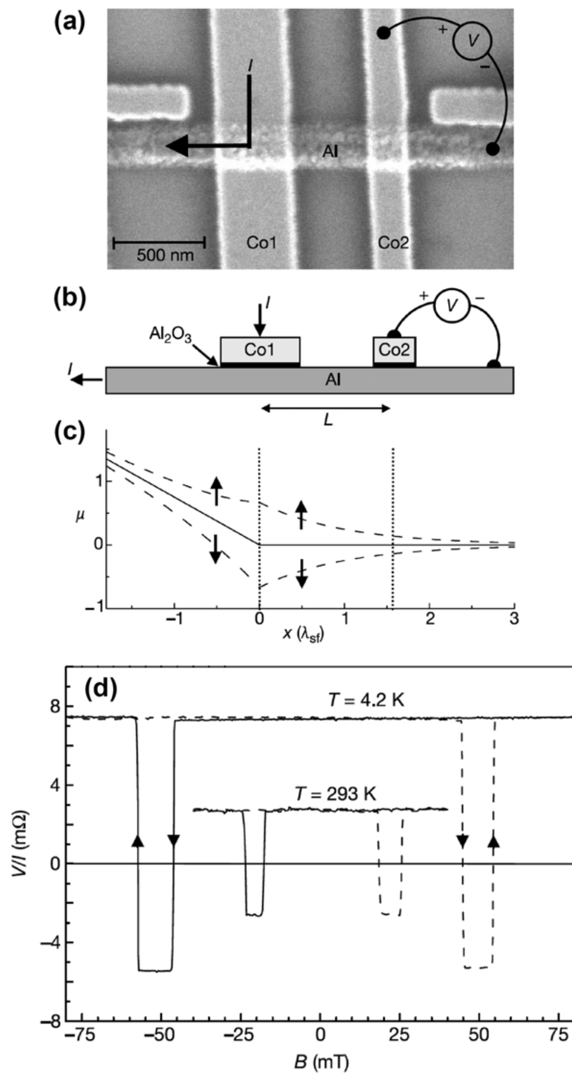


**Figure 25.** Geometry of our spin-valve device. (*a*) Scanning electron microscope image of the device. (*b*) Device cross-section. (*c*) The spatial dependence of the spin-up and spin-down electrochemical potentials ($\mu$, dashed lines) in the Al strip. (*d*), Output signal V/I as a function of the in-plane magnetic field $B$ for a sample with a Co electrode spacing $L = 650$ nm at $T = 4.2$ K and RT. Reproduced with permission from [265], Copyright 2002 Nature.

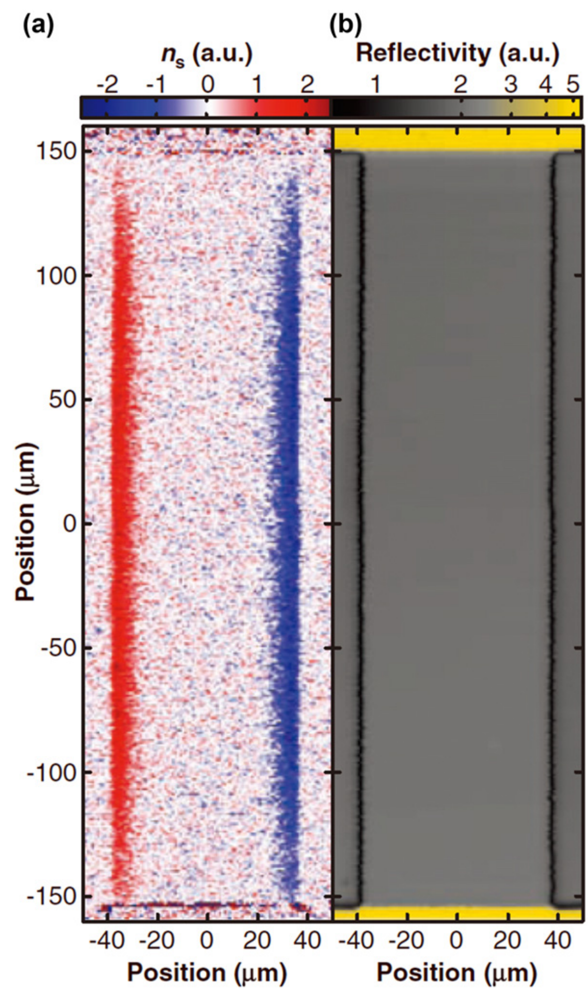


**Figure 26.** Two-dimensional images of spin density $n_s$ and reflectivity $R$, respectively, for the unstrained GaAs sample measured at $T = 30$ K and $E = 10$ mV $\mu$m$^{-1}$. Reproduced with permission from [273], Copyright 2004 Science.

ferromagnet/non-magnet interface [265]. Accordingly, non-local spin-valve systems have been extensively employed to investigate efficient spin injection by minimizing interfacial scattering in both diffusive contacts [266] and ballistic contacts [267], and also by optimizing the junction area [268]. A 185 nm wide Ag nano-wire has then been employed due to its longer spin diffusion length [269]. For a Py separation of 300 nm, a $\Delta R$ as large as 8.2 mΩ at 79 K has been reported.

In these devices, the junction resistance is a key parameter in controlling interfacial spin polarization. To date, a 24% spin polarization at a NiFe/Ag interface at 79 K [269] and 25% at a Co/Au interface at 4 K are the best values achieved. This is still only half of the expected value from ferromagnetic spin polarization.

*Spin Hall effect*

Non-local spin valves have also been used to detect both spin Hall and inverse spin Hall effects, clearly indicating the advantages of a lateral device configuration. A charge current in a paramagnetic metal has been predicted to induce a transverse spin imbalance without the application of a magnetic field, resulting in a spin Hall effect [270, 271]. A spin current can also induce a spin Hall voltage without a charge current or a magnetic field, i.e. an inverse spin Hall effect [272]. This is theoretically equivalent to an anomalous Hall effect in a ferromagnet and originates from the spin-orbit scattering of conduction electrons through skew and side-jump scattering. A spin Hall effect of this type was first observed at the edges of a GaAs semiconductor channel by magneto-optical Kerr imaging, as shown in figure 26 [273]. This is a new method to generate spin polarization as well as to manipulate electron spins without the application of a magnetic field.

The spin Hall effect has also been detected in a nano-wire lateral metallic spin-valve structure [274]. Here, a spin current was injected into a 60 nm wide Al wire from a 250 nm wide $Co_{0.80}Fe_{0.20}$ wire by the non-local method. The spin Hall voltage was then measured at the other end of the Al wire.

By employing a perpendicularly magnetized FePt layer and an Au Hall bar, both spin Hall and inverse spin Hall effects as large as 2.9 mΩ have been reported at RT for a separation between the injector and detector of 70 nm [275]. Such a large signal is very useful for the generation of spin polarization in a non-magnetic material.

The spin-injection Hall effect, which is a transverse voltage response to the local spin polarization of injected charge carriers, has also been reported in a 2DEG photovoltaic cell of GaAs/AlGaAs/GaAs [97]. The spin-dependent photovoltaic effect resulting from this effect has been found to convert the degree of circular polarization of light directly to a voltage signal.

*Spin Seebeck effect*

Similar to the conventional Seebeck effect, a thermal gradient in an FM/NM bilayer can induce the spin Seebeck effect [276]. By attaching Pt electrodes at both ends of a $Ni_{0.81}Fe_{0.19}$ strip with a temperature gradient across the strip, spin-polarized electrons with the opposite sign can be collected at both ends dependent upon the direction of magnetization of the strip and the temperature gradient. The structure is much larger than the nanometre scale with dimensions of up to a millimetre. However, the essence of the effect can be understood by a 1D modelling. A spin current is generated in the NM due to the thermal non-equilibrium between magnons in the FM and conduction electrons in the NM [277]. This effect converts thermal energy into a spin voltage, which is another method to generate spin-polarized electrons. Similarly, the spin Seebeck effect was observed in a magnetic insulator [278]. This indicates that the effect can be carried by spin waves even in an insulator. A spin Seebeck voltage of ∼15 $\mu$V was reported with a 25 K thermal gradient across 6 mm. These systems can be used for thermoelectric devices, which possess great potential to realize magnetic cooling and energy harvesting efficiently. Accordingly, a spin Seebeck device concept has recently been demonstrated by NEC and Tohoku University [279].

### 3.3. Spin-polarized spectroscopy

*3.3.1. Spin-polarized scanning tunnelling microscopy (SP-STM).* Spin-polarized scanning tunnelling microscopy (SP-STM) was proposed in 1990 by Johnson and Clarke [280] and Wiesendanger *et al* [281]. These reports were theoretically supported by Molotkov [282] and Laiho and Reittu [283] in 1993. This technique uses a direct-gap semiconductor tip. This is expected to be used to observe the surface magnetic configurations with an almost atomic resolution.

Spin-polarized electron tunnelling from a Ni STM tip into a GaAs substrate was first demonstrated by Alvarado and Renaud [284]. The Ni tip is magnetized by an electromagnet and is used as a spin injector. It scans over the sample surface in its measurement state. Spin-polarized electron tunnelling through the vacuum is detected as circularly polarized EL signals in which the change is ∼30% at RT. This value corresponded to a minority electron spin polarization of Ni(0 0 1) at the Fermi level. This suggests that minority spin electrons provide the dominant contribution to the tunnelling current.

After the first photoexcitation measurement by Prins *et al* [90], modulated circularly polarized light has been used to excite spin-polarized electrons in a semiconductor (e.g., GaAs). Although optically excited electrons are scattered mainly at the semiconductor surface with back illumination [285], Sueoka *et al* have demonstrated the possibility of detecting spin-polarized signals by scanning a Ni STM tip over a GaAs film with circularly polarized light shone through an AlGaAs membrane [286]. Suzuki *et al* have performed a similar observation by scanning a *p*-GaAs STM tip over a Co film with back illumination through a mica/Au/Co film, and have obtained magnetic domain images [287]. GaAs tips are fabricated using photolithography and anisotropic etching to prevent limitations due to facets {1 0 5}. A three monolayer (ML) Co film exhibits perpendicular magnetization and shows less than the MCD effect of 0.14%. This is much smaller than the observed polarization response of about 10%. Polarization modulation response images of the SP-STM show very good agreement with MFM images. In order to avoid the MCD effect and possible light scattering through the sample structures, Kodama *et al* introduced photon helicity into a GaAs tip in the vicinity of the sample, which is equivalent of front illumination [288]. They detected a change of approximately 7% in $I$–$V$ curves between right and left circular light irradiation of NiFe films.

*3.3.2. Andreev reflection.* Similarly, by implementing Andreev reflection and replacing the ferromagnetic STM tip with a superconductor, surface spin polarization at the Fermi level of various metals has been observed [50]. Due to Andreev reflection, the spin polarization can be estimated from the differential conductance of the point contact. The effect was used to observe the half-metallicity of $CrO_2$ with a spin polarization of 90 ± 3.6% at 1.6 K. Even though this technique is very sensitive to the surface spin polarization, it is commonly used to evaluate the spin polarization of new ferromagnetic materials such as Heusler alloys.

## 4. Future perspectives

Here, we identify seven major issues that need to be overcome to design a new spintronic device and to advance the current technologies, especially in their operation speed and efficiency.

### 4.1. Spin sources

The hybridization of a ferromagnetic metal with a semiconductor offers the possibility of engineering the electron spin DOS of the ferromagnet by tuning its lattice constant. A III–V semiconductor, in particular, has been utilized as a template for the epitaxial growth of Fe and Co due to the matching of the lattice constant. From the 1980s, by using molecular-beam epitaxy (MBE), ferromagnet/semiconductor direct interfacial properties, such as detailed growth modes, self organization, interfacial spin scattering and the formation of magnetic dead layers, have been widely investigated in, for example, single-crystal Fe/GaAs and Co/GaAs hybrid structures [289].

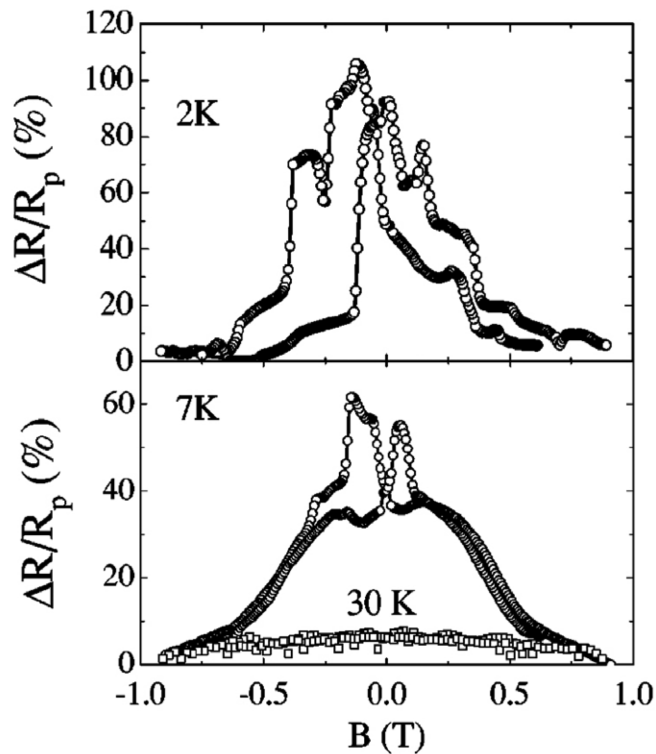


**Figure 27.** (*a*) MR as a function of the magnetic field at 2 K (well below the EuS $T_C$) and (*b*) at 7 K, and at 30 K (well above the EuS $T_C$). Reproduced with permission from [292], Copyright 2013 AIP Publishing LLC.

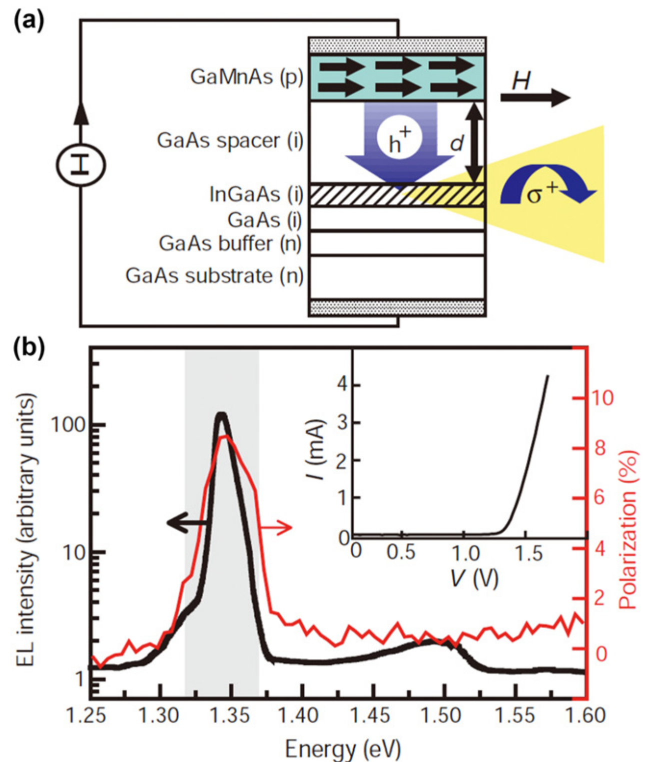


**Figure 28.** (*a*) Electrical spin injection in an epitaxially grown ferromagnetic semiconductor heterostructure, based on GaAs. (*b*) Total EL intensity of the device ($d = 20$ nm) under forward bias at temperature $T = 6$ K and magnetic field $H = 1000$ Oe is shown (black curve) with its corresponding polarization (red curve). Reproduced with permission from [231], Copyright 1999 Nature.

*Magnetic semiconductors*

The search for an applicable spin-filtering layer has successfully produced very large TMR using a large Zeeman splitting in the magnetic semiconductors EuO and EuS [290]. Spin filtering has also been reported using Europium and Chromium calcogenides rock-salt, e.g., EuO and EuSe, and the spinels, e.g., $CdCr_2S_4$ and $CdCr_2Se_4$ [291]. For example, EuS shows a TMR ratio of up to 110% at 2 K, as shown in figure 27, which disappears above $T_C \sim 16.8$ K [292].

Introduction of magnetic ions, typically Mn, into III–VI semiconductors has been carried out to form a DMS since the 1970s [293]. GaMnAs and InMnAs have been grwon by Munekata *et al* [23] and Ohno *et al* [294]. However, the Curie temperature is around 110 K with 5.5% Mn doping [295]. Recently it has been approaching RT (e.g., 250 K with $\delta$-doped Mn : GaAs [296]), which may be used in devices in the near future.

MBE-grown epitaxial DMS, such as (Ga,Mn)As and Zn(Be,Mn)Se, have demonstrated highly efficient spin injection into GaAs [26, 27], which has been applied to the realization of spin-polarized three-terminal devices: a spin FET, a spin-LED (see figure 28) and a spin RTD. However, DMS requires a large external magnetic field to induce Zeeman splitting at low temperature (below RT). A recent report demonstrated the possible operation of a bipolar magnetic junction at RT [297], which has been theoretically predicted [298] (table 3).

*Half-metallic ferromagnets (HMF)*

In order to exploit the 100% spin polarization induced by spontaneous magnetization, HMFs are under intensive investigation [299]. The HMF possesses a bandgap $\delta$ at the Fermi level $E_F$ only for its minority spins, achieving 100% spin polarization at $E_F$. Four types of HMFs have been predicted so far, as shown schematically in figure 29: oxide compounds (e.g., rutile $CrO_2$ [300] and spinel $Fe_3O_4$ [301]), perovskites (e.g., $(La,Sr)MnO_3$ [302]), zinc-blende compounds (e.g., CrAs [303] and MnAs [304]) and Heusler alloys (e.g., NiMnSb [305]). Even though both $CrO_2$ and $La_{0.7}Sr_{0.3}MnO_3$ have been reported to show almost 100% spin polarization at low temperature [300, 302], to date there has been no experimental report of their half-metallicity at RT, which is required for device applications.

*Heusler alloys*

Among these proposed HMFs, Heusler alloys hold the greatest potential to realize half-metallicity at RT due to their lattice constant matching with the III–V semiconductors and MgO. They have high Curie temperatures $T_C$ (above RT) and large $\delta$ at $E_F$. Heusler alloys are categorized into two distinct groups by their crystalline structures: half Heusler alloys of the form $XYZ$ in the $C1_b$ structure and full Heusler alloys of the form $X_2YZ$ in the $L2_1$ structure, where the $X$ and $Y$ atoms are transition metals, while $Z$ is either a semiconductor or a non-magnetic metal [305, 306]. The unit cell of the $L2_1$ structure consists of four face-centred cubic (fcc) sublattices, while that

**Table 3.** List of major spin-polarized three-terminal devices.

| | Spin FET | Spin LED | Spin RTD | Coulomb blockade |
|---|---|---|---|---|
| Diagram | | Input, Source, Control | Drain, Output | |
| Inputs | Spin-polarized electrons/holes | Spin-polarized electrons/holes | Spin-polarized electrons/holes | Spin-polarized electrons |
| Sources | FM | DMS | Double tunnel barriers | FM |
| Gates | Bias voltage | Bias voltage | Bias voltage | Bias voltage |
| Drains | FM | QW | QW | FM |
| Outputs | Electrical signals–spin-polarized electrons/holes | Circularly polarized EL | Circularly polarized EL | Electrical signals |
| Notes | | Low temperature High magnetic field | Low temperature | Low temperature |
| Refs. | [89, 399, 400] | [231, 233–236] | [246] | [258, 259] |

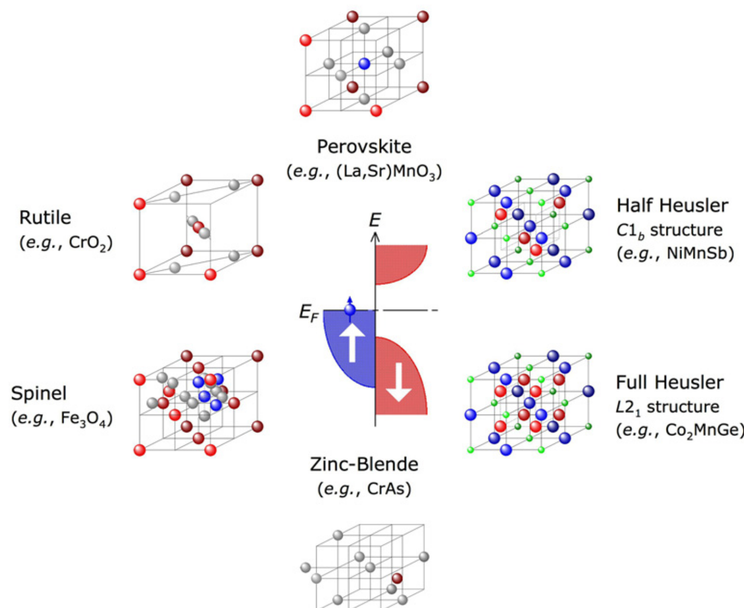


**Figure 29.** Schematic diagrams of half-metallic structures.

of the $C1_b$ structure is formed by removing one of the $X$ sites. In the Heusler alloys, half-metallicity is known to be fragile against atomic disorder. For the $L2_1$ structure, when the $Y$ and $Z$ atoms exchange their sites ($Y$–$Z$ disorder) and eventually occupy their sites at random, the alloy transforms into the $B2$ structure. In addition, $X$–$Y$ and $X$–$Z$ disorder finally leads to the formation of the $A2$ structure.

The recent excitement in this field has been triggered by Block *et al*, who measured large negative magnetoresistance at RT in a quarternary full Heusler $Co_2Cr_{0.6}Fe_{0.4}Al$ alloy [307], which proves the controllability of the spin DOS of the full Heusler alloys by substituting their constituent elements. They reported −30% MR at RT with pressed powder compacts, which act as a series of MTJs. As a result, many attempts have been made to utilize these alloy systems to achieve large MR. Also the first TMR using a $B2$ sputtered $Co_2Cr_{0.6}Fe_{0.4}Al$ film has been reported to be 26.5% at 5 K (16% at RT) by Inomata *et al* [308]. This alloy film with $L2_1$ ordering has then been grown fully epitaxially for the first time and has been implemented into a fully epitaxial MTJ [309]. The TMR ratio has later been increased to over 100% at RT using a MgO barrier [310]. In such MTJs, the oscillatory behaviour of tunnelling resistance has been found to be enhanced as compared with the coherent tunnelling with conventional ferromagnets [311], which is independent of temperature.

Recently, an MTJ with an epitaxial $L2_1$ $Co_2MnSi$ film has been reported to show very large TMR ratios of 70% at RT and 159% at 2 K [312]. These are the largest TMR ratios obtained in an MTJ with a Heusler alloy film and an Al-O barrier. The TMR is purely induced by the intrinsic spin polarization of the Heusler electrodes, which is different from an MTJ with an oriented MgO barrier, where a TMR ratio of 386% has been achieved at RT (832% at 9 K) for $Co_2FeAl_{0.5}Si_{0.5}$ [313]. The TMR ratio reported here is the highest ever in an MTJ with a Heusler alloy film but with the assistance of coherent tunnelling through an oriented MgO barrier. In addition, an MTJ using

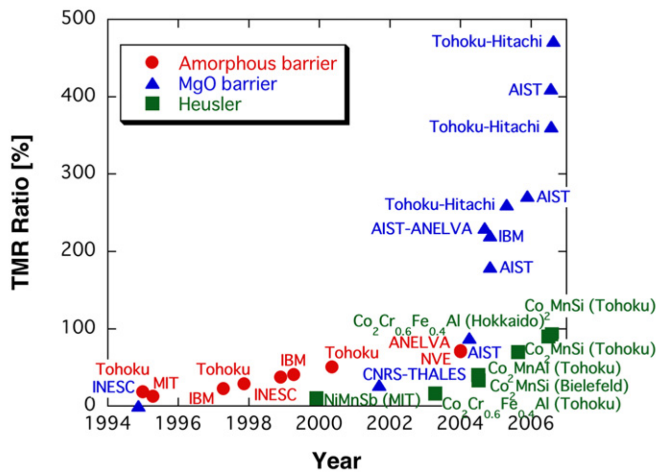


**Figure 30.** Recent development in a TMR ratio.

epitaxial $Co_2Fe(Al,Si)$ films with an epitaxial MgO barrier has been found to double the TMR ratios, with values as high as 150% at RT and 312% at 7 K [314]. This rapid decrease in the TMR ratio with increasing temperature does not follow the temperature dependence of the magnetization, which is known empirically to follow $T^{3/2}$. This suggests that a small fraction of atomically disordered phases cannot be ignored in spin-polarized electron transport at a finite temperature. The elimination of these disordered phases, especially near the barrier interface, should improve the TMR ratio further and realize half-metallicity at RT. Compositional analysis has shown that Si phase segregation occurs at the surface of $Co_2MnSi$ sputtered films after annealing and is independent of the grain size [315]. Such minor phase segregation is difficult to detect and characterize by macroscopic measurements, such as magnetization measurements and XRD, as bulk properties dominate the signals, especially for the case of epitaxial films. In addition, a half-metallic bandgap at RT has been demonstrated in the same Heusler alloy system [316, 317], showing the potential of Co-based Heusler alloys to realize absolute half-metallicity at RT. This could lead to an infinite TMR ratio at RT (see figure 30).

Accordingly, an attempt has been made to utilize a $Co_2FeSi$ layer to inject spin-polarized electrons into GaAs [318]. However, the measured spin polarization of the circularly polarized light emission was only 15–20% at 20 K. In addition, a fully epitaxial CPP-GMR device, consisting of $Co_2MnSi/Ag/Co_2MnSi$, exhibits a maximum GMR ratio of 36.4% at RT [319].

The Gilbert damping constant for Heusler alloys, which defines the switching speed of the magnetization precession as discussed in section 4.4, is expected to be small because of the weak spin–orbit interaction and low spin DOS at $E_F$. Experimentally, the Gilbert damping constants of $Co_2MnSi$ and $Co_2FeSi$ films are found to be 0.005 and 0.02, respectively [320]. These are similar to those of $Ni_{0.8}Fe_{0.2}$, and are independent of the atomic ordering. This fact implies that the magnetization of Heusler alloys relaxes on nanosecond timescales, which will be crucial for the fast operation of an MRAM device and a GHz oscillator.

*$Fe_3Si$*

$D0_3$-ordered $Fe_3Si$ is well known as a ferromagnetic Heusler alloy with a high Curie temperature (>800 K) and a spin polarization of ∼45% [321]. Despite the relatively low spin polarization, $Fe_3Si$ is an ideal candidate for injecting spin-polarized electrons into Si due to the perfect lattice match. An epitaxial $Fe_3Si$ film has been successfully grown on a GaAs(0 0 1) [322] and exhibits a magnetic moment of $(1.11 \pm 0.01)\mu_B$ per atom at RT, which agrees well with the bulk value. Using the Andreev reflection, the spin polarization of the film was estimated to be $(45 \pm 5)$%. An $Fe_3Si$ layer has also been grown epitaxially on a Si(1 1 1) substrate showing a magnetic moment of $\sim 3.16\mu_B$ per formula unit (f.u.) at RT [323]. The Schottky characteristic across the interface achieved the ideality factor of ∼1.08 due to the very sharp interface.

*Perovskites*

Perovskites, such as $(La,Sr)MnO_3$, exhibit both strong ferromagnetism and metallic conductivity with the partial substitution of $La^{3+}$ ions with $2^+$ ions such as Ca, Ba, Sr, Pb and Cd [324, 325]. Since only one spin band exists at the Fermi energy ($E_F$) in these films, 100% spin polarization can be achieved. Using these materials instead of a conventional ferromagnet, a very large MR of ∼150% at RT has been observed [326]. This is known as colossal magnetoresistance (CMR). Using Mn-perovskite thin films, a TMR ratio of up to 450% has been reported, but only below the Curie temperature [327]. CMR can be induced either by breaking the insulating symmetry of $Mn^{3+}$ and $Mn^{4+}$ alternating chain or by suppressing spin fluctuation near $T_C$.

*Rutiles*

Using Andreev reflection, $CrO_2$ has been proven to show a half-metallic nature at low temperature as suggested by *ab initio* calculations [328]. $CrO_2$ has a tetragonal unit cell with a magnetic moment of $2.03\mu_B$/f.u. at 0 K [329]. The ferromagnetism of $CrO_2$ appears below 391 K [330]. Above this temperature, another phase of $Cr_2O_3$ is known to show antiferromagnetism, which is the major cause of the reduction of the half-metallicity. Highly-ordered $CrO_2$ films are predominantly grown by CVD [331].

*Spinels*

The most commonly studied oxide of Fe is $Fe_3O_4$, which has a magnetic moment of $4.1\mu_B$/f.u. [332]. The Curie temperature is ∼850 K and the Verwey temperature is 123 K. Spin-resolved photoemission experiments show that $Fe_3O_4$ exhibits a spin polarization of up to −80% [333]. Very high spin polarization has also been suggested by the measurement of an MR ratio of over 500% through a nano-contact [334]. Epitaxial $Fe_3O_4$ films have been grown by various techniques, including MBE under an oxygen atmosphere, magnetron sputtering and laser ablation [331].

By replacing one of the Fe ions with a divalent metal ion, e.g., Mn, Co, Ni etc., a ferrite can be formed [331]. Pénicaud has predicted half-metallicity in Mn, Co and Ni ferrites [335]. In particular, $NiFe_2O_4$ shows a bandgap in the majority band, indicating that this compound can become an insulator or semi-metallic half-metal.

*Other oxides*

Another interesting oxide is metal-doped $TiO_2$ [336]. By replacing Ti with Co at a level up to 8%, a transparent ferromagnet has been successfully fabricated with a magnetic moment of $0.32\mu_B$/f.u. at RT. This film also shows 60% MR at 2 K. Most of these oxides have their $T_C$ below RT, which means that they cannot be used as spin sources for future devices operated at RT.

*Materials with perpendicular magnetic anisotropy*

In an MRAM cell, perpendicular magnetization requires lower energy for the reversal due to the lower potential barrier formation as compared with in-plane magnetization switching via an intermediate state between in-plane and plane normal. It is therefore critical to use perpendicularly magnetized FM for the spintronic devices, which also reduces the stray field from the FM layer and their cross-talk with the neighbouring cells.

FePt with $L1_0$ ordering shows the largest uniaxial anisotropy of $7 \times 10^7$ erg cm$^{-3}$ perpendicular to the plane [337]. The spin polarization of FePt is expected to be approximately 70% [338]. This is an ideal material for perpendicular recording media in an HDD. Great efforts have therefore been devoted to growing $L1_0$-ordered FePt films. Initially, substrate heating during the film deposition followed by annealing at 600 °C was widely used in order to transform the initial face-centred cubic (fcc) disordered structure, which has in-plane anisotropy, into the $L1_0$ phase [339]. However, this process induced island growth and led to a very rough surface [340]. Lower temperature growth was later optimized [341] and the epitaxial growth of both FePt(0 0 1) and FePt(1 1 0) onto MgO(0 0 1) and MgO(1 10 ) substrates was successfully achieved.

$L1_0$-ordered FePt films have been implemented in both TMR [342] and GMR [338] junctions. Mitani *et al* fabricated an MTJ with an $L1_0$-FePt/Al-O/FeCo structure, having a TMR ratio of 18% at RT (40% at 4.2 K) [342]. Using Jullière's model [17], they estimated the spin polarization of the FePt layer to be 33%. For FePt/Au/FePt GMR nano-pillars, STT has been demonstrated systematically by tuning the crystalline order of the FePt layer. The disordered fcc phase shows in-plane anisotropy and is used as a conventional reference. However, the $L1_0$-structure has been used to introduce a perpendicular magnetization in a nano-pillar. By combining these two different FePt structures, STT with a 90° magnetization configuration has been demonstrated by Seki *et al* [343], Mangin *et al* [344], and Meng and Wang [345], which is expected to achieve ultrafast magnetization switching [346]. As shown in figure 31, a GMR nano-pillar with the structure $L1_0$-FePt/Fe/Au/FePt/Fe/Au/FePt shows a perpendicular anisotropy of $6.7 \times 10^7$ erg cm$^{-3}$ and a critical current density of (5–6) $\times 10^7$ A cm$^{-2}$. This is almost one order of magnitude smaller than the conventional in-plane nano-pillar [343].

Recently, an epitaxial $Mn_{2.5}Ga$ film has also been found to exhibit strong perpendicular magnetic anisotropy ($K_{perp} = 1.2 \times 10^7$ erg cm$^{-3}$) with small saturation magnetization ($M_S = 250$ emu cm$^{-3}$) at RT [347]. This alloy system can also be used as a perpendicular magnetic medium.

It has also been reported that CoFeB/MgO shows perpendicular anisotropy [348]. This is induced by the perpendicular magnetization components of the CoFeB at the MgO interface. The STT-CIMS has also been demonstrated using a CoFeB/MgO/CoFeB stack with the TMR ratio over 120% and the switching current of 49 $\mu$A at a 40 nm-diameter junction. This may be the best building block for the MRAM cell.

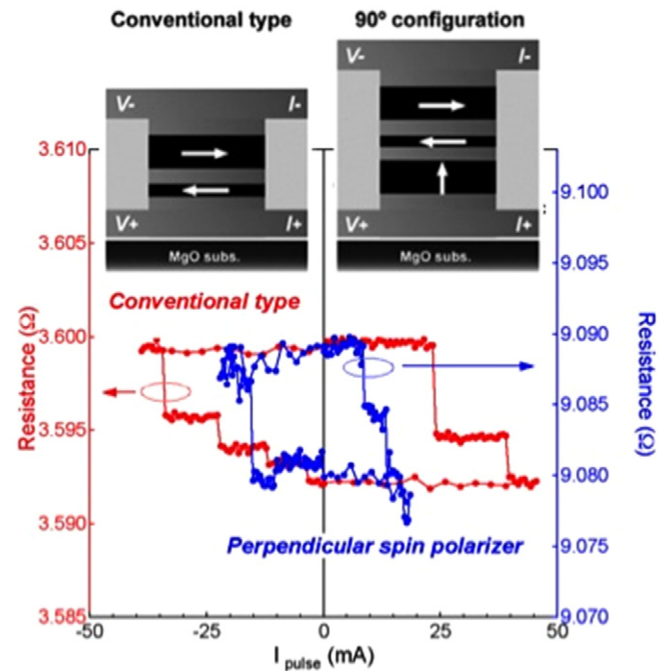


**Figure 31.** Resistance as a function of current pulse ($I_p$) measured at 77 K for a 90° configuration and the conventional type. Solid and open circles are the data for the 90° configuration and conventional type, respectively.

### 4.2. Gate operation

*Electric field operation*

Gate control of the spin–orbit interaction in InGaAs was demonstrated by Nitta *et al*, as shown in figure 32 [349]. This is clear evidence of the controllability of the spin–orbit interaction in a 2DEG by an electric field through a Rashba Hamiltonian. These workers have observed Schubnikov–de Haas oscillations in an $In_{0.53}Ga_{0.47}As/In_{0.52}Al_{0.48}As$ QW as a function of a gate voltage. Therefore, it is crucial to employ a semiconductor with a large spin–orbit interaction coefficient.

Recently, full gate-voltage operation has been demonstrated [350]. By applying a few V (up to ±3 V), a uniform oscillation was measured in a non-local geometry below 40 K. This result has unambiguously proven a gate operation by an electric field.

Using a 0.55 ns voltage pulse, Shiota *et al* demonstrated voltage-induced magnetization reversal in a $Ni_{0.8}Fe_{0.2}$/MgO/Fe nano-pillar junction [351]. Their method achieved a significant reduction in magnetization-reversal energy to as low as $5 \times 10^{-17}$ J. It should be noted that the applied voltage controls the surface magnetic anisotropy due to the screening effect by conduction electrons in the ferromagnet. The applied voltage is theoretically predicted to change the number of electrons at the Fermi level, resulting in the increase of an orbital moment along a preferred direction [352]. The effect was reported to be increased by the factor of two using ionic liquid [353]. In

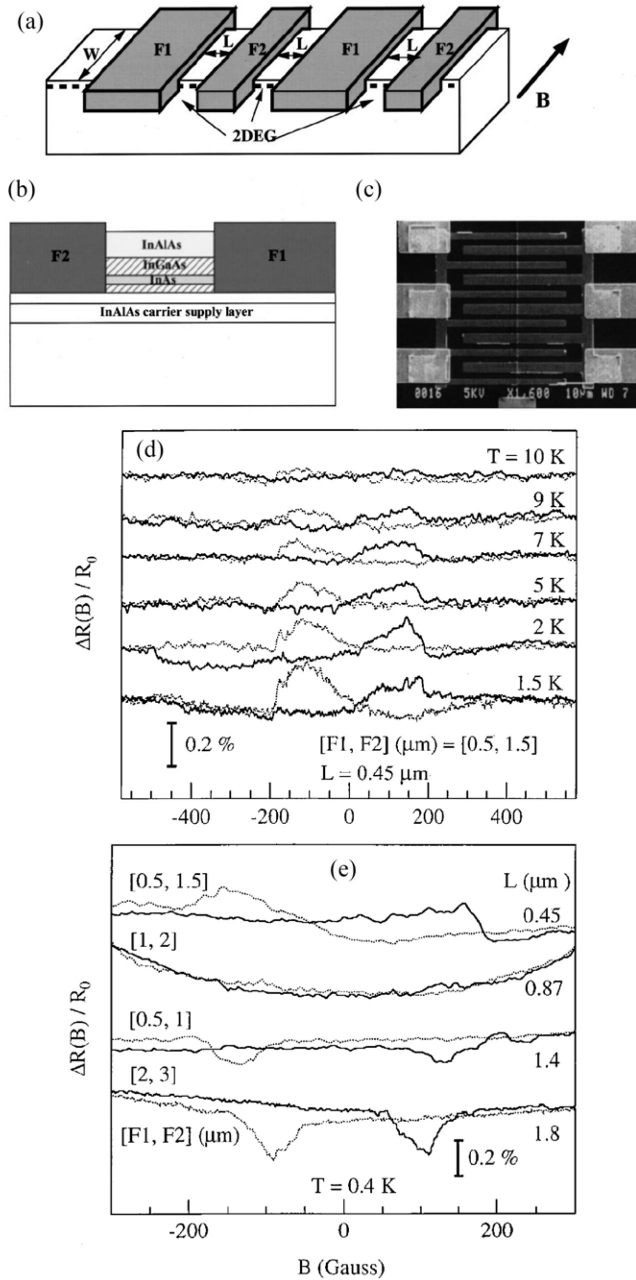


**Figure 32.** (*a*) Sketch of the device with interdigital ferromagnetic contacts connected to 2DEG channels. (*b*) Cross-sectional view of the junction and (c) top scanning electron microscopic (SEM) view of a device with $L = 1.8\,\mu$m, $W = 2\,\mu$m, $F1 = 2\,\mu$m and $F2 = 3\,\mu$m. $\Delta R(B)/R_0$ measured (*e*) for a device with 14 parallel units and $L = 0.45\,\mu$m at different temperatures (the $R_0$ of this device is about 100 Ω). Reproduced with permission from [349], Copyright 1997 American Physical Society.

addition, in an ultrathin Co film, a change in the Curie temperature was reported by applying an electric field [354], which may be used in a spin-torque transistor.

*Spin-polarized metal-oxide-semiconductor field effect transistor (spin MOSFET)*

In order to implement spintronic devices into current Si-based technology, a spin-polarized metal-oxide-semiconductor field effect transistor (spin MOSFET) has been proposed [355]. For the case of a conventional device, a transmittance from an

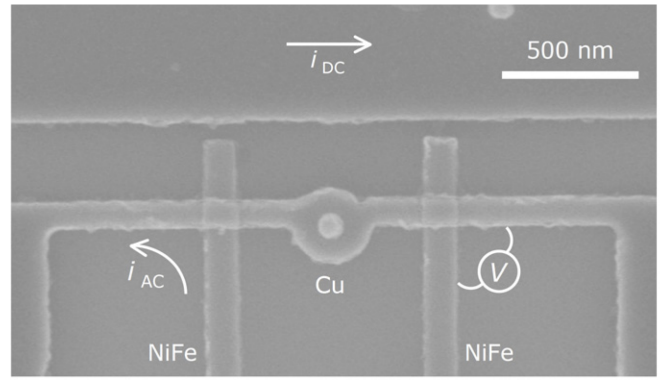


**Figure 33.** Scanning electron micrograph of the nano-ring spin operator.

emitter to a collector $\alpha (= J_C/J_E)$, where $J_C$ is the collector current density and $J_E$ is the emitter current density, is typically less than 0.1%, leading to a current amplification factor $\beta [= \alpha/(1-\alpha)]$ to be much smaller than 1. This clearly indicates that neither current nor voltage amplification for spin-polarized carriers can be achieved. This prevents the formation of a spin-polarized logic circuit. For the proposed spin MOSFET, a gate can amplify both a spin-polarized current and voltage with excellent compatibility with Si technology. The drain current density ($J_D$) has been calculated to be enhanced by almost two orders of magnitude for a parallel magnetization configuration between the emitter and the collector, as compared with the antiparallel case. In addition, a reconfigurable logic circuit can be designed with a spin MOSFET by connecting the gate to a word line, the source to an earth and the drain to a bit line. Such a circuit offers a very simple cell design based on one spin MOFET as a unit cell. This has a significant advantage over an MRAM device, due to its small fabrication scale and its simpler structure as compared with the current MRAM cell designs. Such a device, consisting of as little as ten spin MOSFETs, forms a two-input symmetric function for a logic device, which is similar to a neuron MOS [356].

*Magnetic field operation*

A lateral spin-valve structure has been fabricated using a non-magnetic Cu nano-ring in order to split a diffusive spin-current path for operation (see figure 33) [357]. By providing Larmor precession independently to each spin path with respect to the distance from a dc current path, this introduces a perpendicular Ampère field and acts as a gate in a three-terminal device. The difference in the non-local signals between the parallel and antiparallel configurations gives ~10% decrease with a dc current of $i_{dc} = 60$ mA. This is equivalent to a perpendicular field of 15 mT for a separation of 250 nm between the dc current path and a nano-ring with an outer diameter of 320 nm and an inner diameter of 70 nm. For a 180° phase shift, a perpendicular field of 175 mT is estimated to be required for this device. The calculation can also be applied to a semiconductor nano-ring for magnetic-field operation. It is therefore important to minimize the dimensions of the device to operate a spin-polarized electron current effectively.

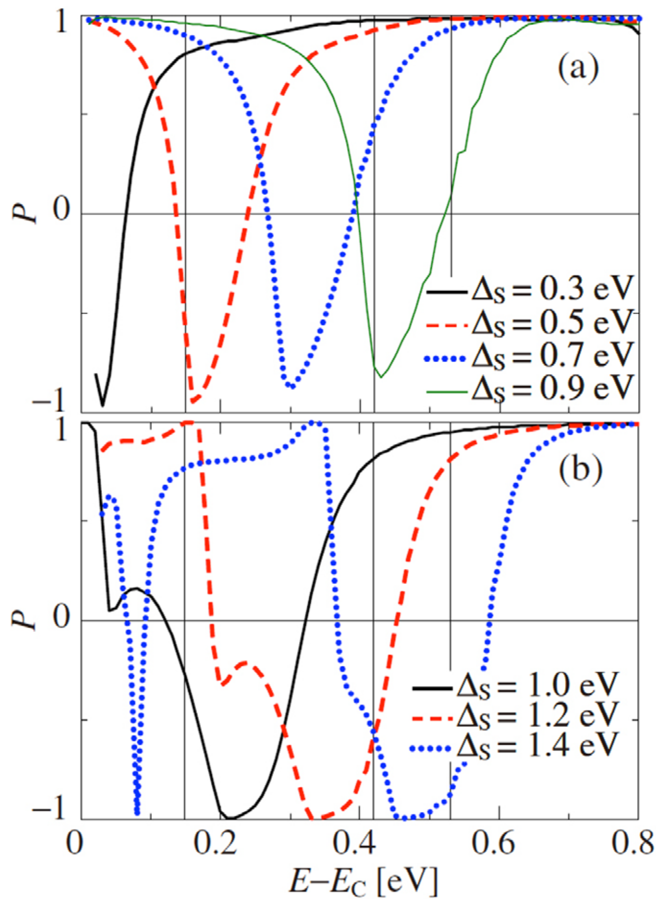


**Figure 34.** Calculated results of the spin polarization of the tunnel conductance as a function of energy for (*a*) Fe-As and (*b*) Fe-Ga contacts with the depletion layer thickness of 200 ML and various values of the Schottky barrier height $\Delta_S$. The vertical lines correspond to the energy $E - E_C$ ($E_C$: bottom of the conduction band). Reproduced with permission from [360], Copyright 2008 American Physical Society.

*Interface resonant states*

Dery and Sham [358] proposed a spin switch using spin filtering through localized electron states in a heavily doped semiconductor. In their model, *s* conduction electrons tunnel through a Schottky barrier and carry positive spin polarization into a ferromagnet. Localized *d* electrons transfer negative spin polarization, as the spin DOS for the down spins at $E_F$ is larger than that for the up spins. Chantis *et al* [359] also predicted negative spin polarization in a range of bias voltages across an Fe/GaAs (8 ML)/bcc Cu structure due to the formation of interface resonant states for down spin electrons formed at the interface with the Fe layer. Since the spin polarization is found to be dependent upon the photoexcitation energy, a new model has been proposed by Honda *et al* [360]. It is shown that band matching of resonant interface states within the Schottky barrier defines the sign of the spin polarization of the electrons transported through the barrier. The predictions agree very well with experimental results including those for the tunnelling of photoexcited electrons [242] and suggest that spin polarization (from −100% to 100%) is dependent on the Schottky barrier height (see figure 34). They also suggest that the sign of the spin polarization can be controlled with a bias voltage. A recent report [361] further confirms that the abrupt Fe/GaAs interface does not form an interfacial resonant state (IRS), while partially intermixed ones form IRSs. This finding provides a way to fabricate a spin FET with a consistent and reproducible spin polarization of an injected current.

Using equation (10), the electric-field operation requires further improvement in the spin–orbit interaction constant $\eta$ to achieve a realistic spin-transistor design. For magnetic field operation, as the spin modulation by the Hanle effect has already been demonstrated in non-local spin valves [221, 267], this technique may also be a promising method to modulate spin-polarized electrons in the non-magnetic medium. However, further miniaturization is crucial in order to implement a source of a magnetic field into the three-terminal devices. This should be able to be achieved by further improvement in nanofabrication techniques. For interfacial control, a clean and sharp interface is essential, which also requires further improvement in film growth techniques.

### 4.3. Spin current/voltage amplification

In a spin MOSFET made with an HMF, magnetocurrent amplification has been proposed theoretically, as shown in figure 35 [362]. A magnetocurrent ratio, the difference in drain currents between the parallel and antiparallel configurations which is divided by the drain current in the antiparallel configuration, is calculated to exceed $10^{10}$ with a small drain–source voltage of 0.1 V. According to this proposal, a spin MOSFET can also satisfy the scaling merit and give low voltage operation.

As shown in figure 36, a spin logic device, consisting of a semiconductor nano-wire with multiple ferromagnetic contacts, has been proposed to achieve fast and reconfigurable logic [363]. This is based on interconnected spin MOS junctions for data operation to maximize spin accumulation. Such a device is calculated to rotate the magnetization in 10 ns under a bias voltage of 0.5 V.

Even though the distance travelled by spin-polarized electrons in a non-magnetic medium should be within the spin diffusion length, it is crucial to develop a method to amplify the spin-polarized current or voltage. Especially for the case of a non-local spin-valve, the magnitude of the spin current introduced into the medium is estimated to be three orders of magnitude smaller than the originally injected spin-polarized (charge and spin) current. Therefore, spin amplification must be implemented to improve both the signal-to-noise ratio and the power consumption.

### 4.4. High-frequency oscillators

In order to integrate spintronic devices into current Si technology, which is operated at over 3 GHz, or to even improve on it, spin operation at a few GHz is required. As a first step towards high-frequency operation, both the fast settling of spin oscillation, which is defined by a damping constant, and the fundamental spin dynamics in devices need to be investigated.

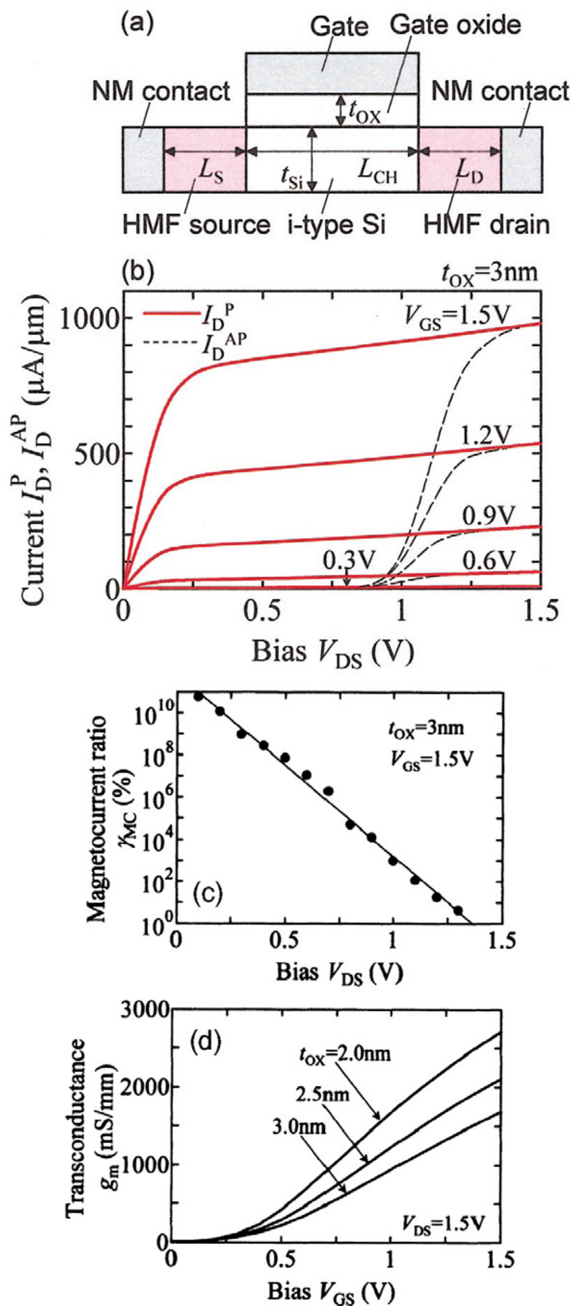


**Figure 35.** (*a*) Device structure used for the analysis. (*b*) Output characteristics of the spin MOSFET. The drain currents $I_D^P$ (solid curves) and $I_D^{AP}$ (dashed curves) in the parallel and antiparallel magnetic configurations, respectively, are plotted as a function of $V_{DS}$, where $V_{GS}$ is varied from 0.3 to 1.5 V. (*c*) Magnetocurrent ratio $\gamma_{MC}$ [$= (I_D^P - I_D^{AP})/I_D^{AP}$] as a function of $V_{DS}$ at $V_{GS} = 1.5$ V. (*d*) Trans-conductance $g_m$ ($= I_D^P/\partial V_{GS}$) as a function of $V_{GS}$ at $V_{DS} = 1.5$ V for $t_{ox} = 2.0$, 2.5 and 3.0 nm. Reproduced with permission from [362], Copyright 2004 AIP Publishing LLC.

*Damping constant*

Ferromagnetic resonance (FMR) has been measured for a permalloy film [364]. The Gilbert damping constant was measured to be of the order of $10^8$ s$^{-1}$ and was found to depend on the thickness of a Cu capping layer. This small value of the damping constant (∼0.02) is an important parameter for the reduction of the switching current. Magnetization reversal still has a significant advantage over current Si technology due to its reversal speed which is in the femtosecond region [365]. A focused circularly polarized beam (100 μm diameter and 40 fs pulse) has been used to reverse the magnetization of a $Gd_{22}Fe_{74.6}Co_{3.4}$ film.

A small Gilbert damping constant is essential for high-frequency operation. To date, permalloy films have been used. However, Heusler alloy films also have a similar damping constant to permalloy and may have more advantages due to their very large spin polarization of 100% in theory.

*Nano-pillars*

In an STT nano-pillar, microwave oscillation has been realized due to the angular dependence of the STT without the application of an external magnetic field [366, 367]. The nano-pillar consisted of a stack of $Ni_{0.81}Fe_{0.19}$ (4 nm)/Cu (10 nm)/$Ni_{0.81}Fe_{0.19}$ (15 nm) and showed a frequency-dependent STT, as shown in figure 37. Similarly, for a spin-valve nano-pillar of a structure of $Ni_{0.81}Fe_{0.19}$ (5 nm)/Cu (40 nm)/$Ni_{0.81}Fe_{0.19}$ (60 nm), microwave oscillation has been reported in the frequency range between 300 kHz and ∼1.1 GHz. High-frequency operation has then been extended to a MTJ formed from a nano-pillar of $Co_{0.60}Fe_{0.20}B_{0.20}$/MgO/$Co_{0.60}Fe_{0.20}B_{0.20}$ to demonstrate microwave generation in the vicinity of 7 GHz [368] and 3–8 GHz [369]. The frequency of these devices can be controlled by a bias current or a bias voltage. However, even though extensive efforts have been devoted to this area, the linewidth of the microwave oscillation in an MTJ is still of the order of ∼100 MHz, which is much wider than that required for device applications. Typically a Q-factor of 10 000 is required for reliable device operation, leading to a linewidth of <1 MHz. These devices also have an output power of ∼0.1 μW, which is three orders of magnitude larger than conventional GMR-based oscillators.

By reversing these microwave oscillations induced by a dc current, i.e. applying a microwave ac current, a dc voltage was observed to be generated in nano-pillar junctions [370, 371]. This is called the spin-torque diode effect and takes the maximum at the resonant frequency. This effect can be used in a microwave detector with very high sensitivity.

Magneto-optical Kerr imaging has been employed to observe spin dynamics in GaAs [372]. Time-resolved spin dynamics in GaAs, which is introduced by the extrinsic spin Hall effect, was measured magneto-optically. A single homogeneous spin decoherence time has been determined in GaAs, which is responsible for the limitation of high-frequency spin dynamics at the sample edges.

*Vortex oscillators*

Vortex core oscillation has been reported in the frequency range between 300 kHz and 1.1 GHz in a structure of Py (60 nm)/Cu (40 nm)/Py (5 nm) nano-pillars [373]. The electrical switching of a vortex core has also been demonstrated with an ac current in a 50 nm thick Py disc with a diameter of 1 μm [374].

In theory, these ferromagnetic discs and FM/NM/FM stacks can be operated at almost the FMR frequency of ∼ a few GHz, which can be better than the current Si-based devices. In preliminary demonstrations, a point contact can

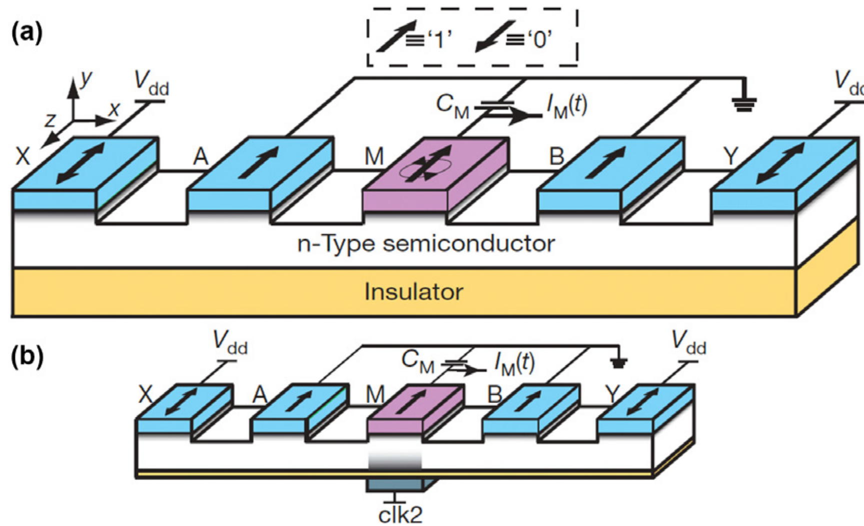


**Figure 36.** Design of the reprogrammable magnetologic gate. (*a*) Steady-state currents, driven by $V_{dd}$, flow between A(B) and X(Y). The output is given by a transient current response, $I_M(t)$, caused by an in-plane single rotation of M. The amplitude of $I_M(t)$ is proportional to the spin accumulation in the semiconductor. (*b*) A similar structure but with a pinned middle contact. The transient current, $I_M(t)$, is triggered by a voltage signal, clk2, applied to a (non-magnetic) back-contact beneath the mid-section. Semiconductor regions beneath the contacts are heavily doped. Reproduced with permission from [363], Copyright 2007 Nature.

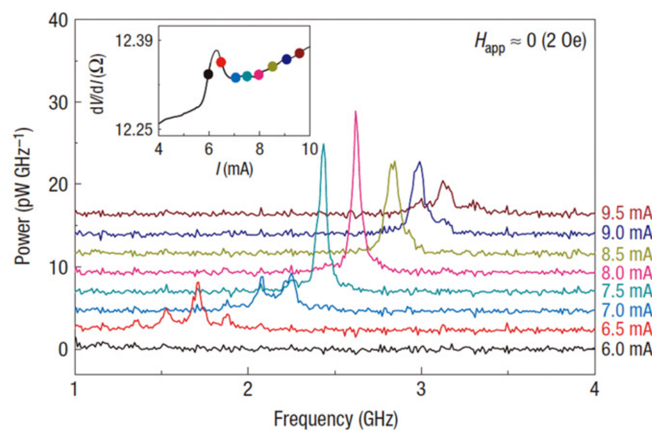


**Figure 37.** Microwave power spectra for the Co (8 nm)/Cu (10 nm)/Py (8 nm) nano-pillar for an applied field close to zero ($H_{app} = 2$ Oe) at different currents corresponding to the coloured symbols in the inset. Inset: $dV/dI$ versus $I$ for $H_{app} = 2$ Oe. Reproduced with permission from [366], Copyright 2003 Nature.

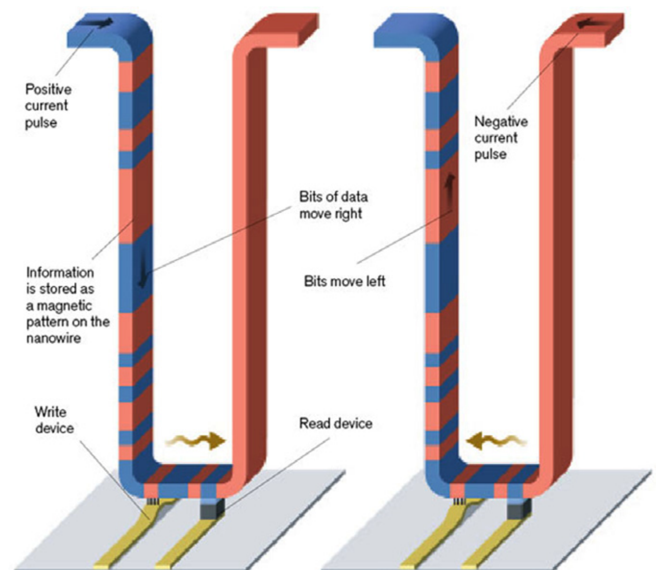


**Figure 38.** Schematic diagram of a proposed racetrack memory. Reproduced with permission from [379], Copyright 2010 The American Association for the Advancement of Science.

realize a very large Q-factor for the frequency-dependence of the power spectral density [375]. However, by patterning the ferromagnetic layer or the entire GMR/TMR stack into a nano-pillar or disc, the Q-factor decreases significantly due to the presence of the edges. In order to overcome this issue, a new design needs to be developed.

### *4.5. 3 D racetrack memories*

The DW displacement discussed in section 3.1.4 can also be used to produce a racetrack memory, as shown in figure 38 [58, 376]. This memory, originally proposed by Parkin, potentially extends a device structure into a 3 D configuration. Experimentally, the DW needs to be pinned at a precise position after wall motion is induced by a current. Since a vortex-like component in the wall can induce the random movement of the wall after the current injection, a step-like motion is required for memory applications. At this stage, wall motion at a speed of 100 m s$^{-1}$ under a current density of $2 \times 10^{12}$ A m$^{-2}$ has been achieved [377, 378]. This type of DW motion has been implemented into an MRAM device to switch the magnetization in the free layer of a bit, which has been demonstrated by NEC with a wall separation of 45 to 60 nm [379].

In order to achieve fast read/write operation, the DW motion, dependent upon the current-pulse width, has been

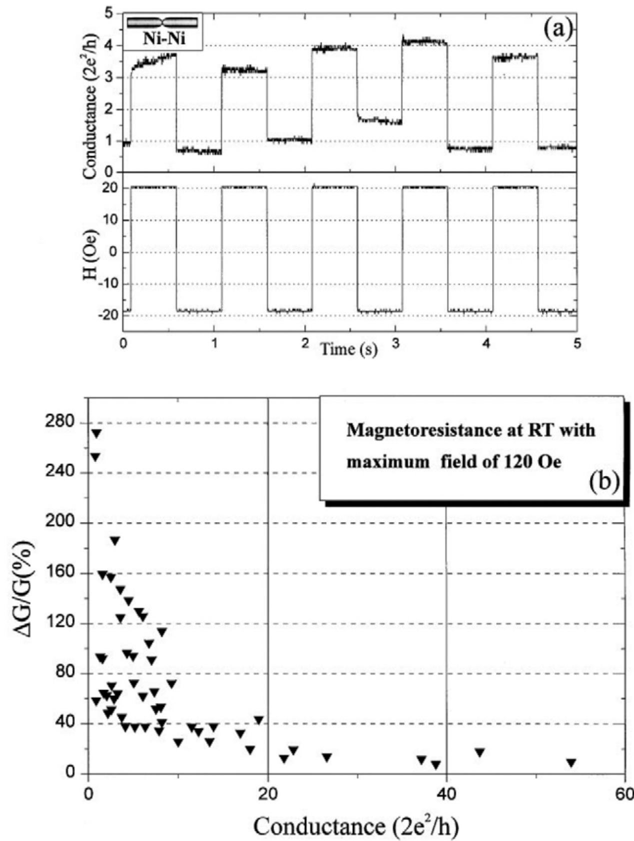


**Figure 39.** Measurements on Ni–Ni nano-constrictions. (*a*) Two nickel wires of millimetre radius are used to form nano-constriction. (*b*) Dependence of magnetoresistance on the conductance level: the applied magnetic fields range from 20 to 120 Oe. Reproduced with permission from [390], Copyright 1999 American Physical Society.

studied [380, 381]. Thomas *et al* have observed the amplification of the DW oscillation, even after pulsed current injection. By carefully matching the time constants of these phenomena, they have reported the possibility of reducing the critical current density for DW motion using numerical calculations. During the DW motion, there are known to be complex oscillatory motions depending on the shape of the vortex components of the DW [382]. By tuning the current pulse, a coherent and reproducible smooth motion of the DW has been achieved.

In order to realize the operation of a racetrack memory, micro- or nanometre wide ferromagnetic wire needs to be fabricated either with very smooth edges, which ensures uniform DW displacement, or with periodical DW traps at the edge. It is also crucial to fabricate these wires in the shape of a 'U' figure, as shown in figure 38. These requirements are very severe for current nanofabrication techniques.

A similar concept was utilized in a magnetic ratchet [383], where magnetic domains are shifted as data bits in a multilayered vertical wire. There have also been great efforts to employ a skyrmion [384] and magnon [385] instead of a DW, which are expected to warrant reproducible motion by a lower current density as compared with the studies described as above.

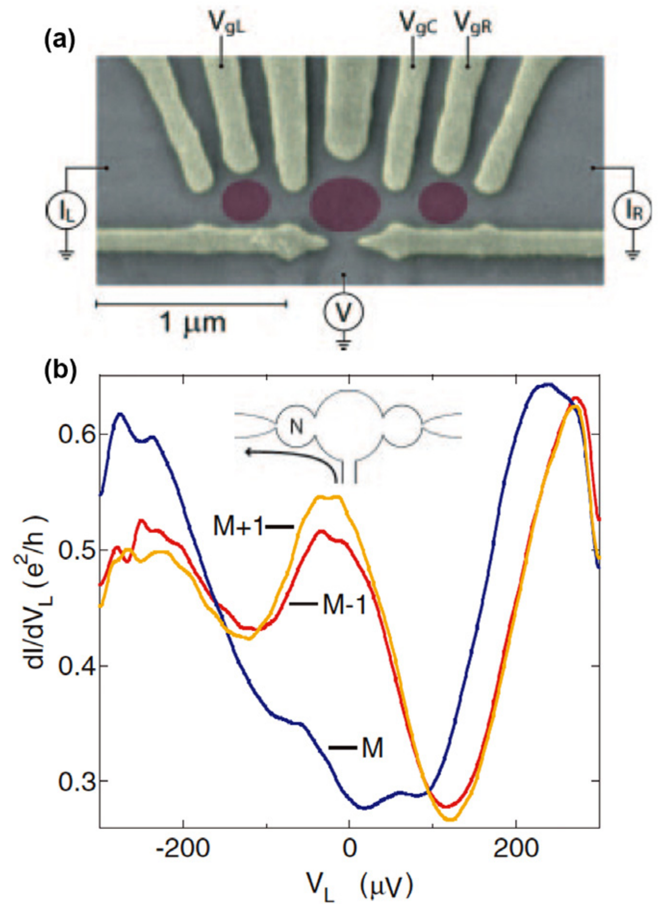


**Figure 40.** (*a*) Scanning electron micrograph of a device identical in design to the one measured, with schematic ovals indicating locations of dots upon gate depletion. (*b*) Differential conductance $dI/dV_L$ of the left dot for an odd number of electrons, $N$. When the right dot contains an even number of electrons ($M \pm 1$), a zero-bias peak in $dI/dV_L$ is seen, indicating a Kondo state. Reproduced with permission from [397], Copyright 2004 The American Association for the Advancement of Science

### 4.6. Topological insulators

Topological insulators are a new class of materials allowing an electron flow at the surface, while prohibiting that in the bulk region [386]. This is due to the formation of the Dirac point (2 D) or cone (3 D) between the valence and conduction bands. At the Dirac point in a 2 D system, up- and down-spins flow in the opposite directions, where an impurity cannot induce the backscattering of these spin-polarized electrons. This minimizes the energy loss of a spin-polarized current, realizing a device with low-power consumption. This phenomena can be observed as a spin Hall effect and was first predicted in graphene [386]. The first experimental measurement of the spin Hall effect was reported on $Hg_{1-x}Cd_xTe/HgTe/Hg_{1-x}Cd_xTe$ QW [387]. Fu *et al* then formalized the criteria to become a topological insulator [388]. By introducing ferromagnetic atoms at the surface of the topological insulator, electrical-gate-controlled magnetism was demonstrated in $Mn_xBi_{2-x}Te_{3-y}Se_y$ [389]. Such a system can offer a fundamental building block for an impurity- or defect-resistant spintronic memory.

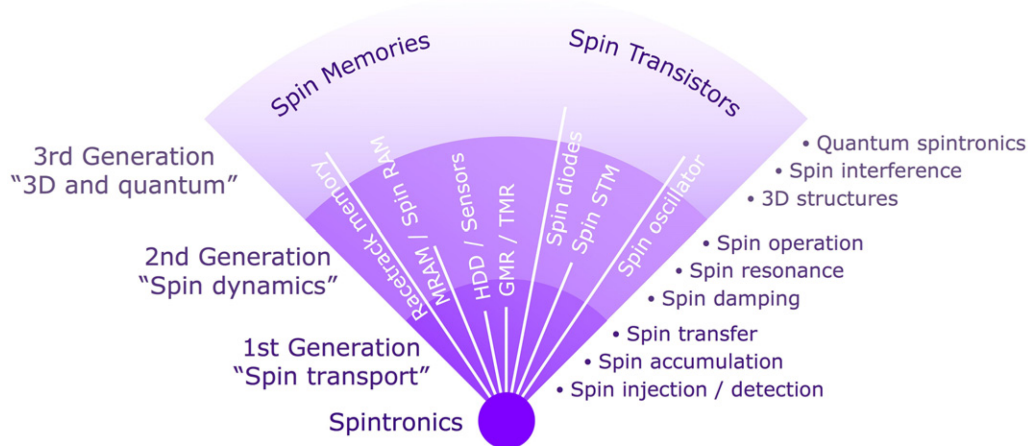


**Figure 41.** Recent developments in spintronic studies and devices.

### *4.7. Quantum spintronic devices*

*Ballistic magnetoresistance (BMR)*

A ballistic magnetoresistance (BMR) of 280% was first discovered in Ni nano-constricted point contacts, as shown in figure 39. These consist of a chain of atoms, under an applied field of 120 Oe at RT, reported by Garcia *et al* [390]. In such a system, the conductance is found experimentally to be quantized as integer multiples of $e^2/h(= G_0/2)$, where the factor of two corresponds to the spin degeneracy as compared with those made of non-magnetic materials [391]. BMR has been explained theoretically to be induced by spin-dependent electron transport across a confined magnetic DW trapped at the point contact [392–394]. The length scale of such an abrupt change of magnetization direction at the DW is much shorter than that for conventional Bloch and Néel walls. However, these point contacts are normally fabricated by pulling off both ends of two bulk electrodes across the contact, which leaves the possibility of MR induced by magnetostriction [395]. Recently, distinct non-linear current-voltage behaviour has been reported only in a ferromagnetic point contact without applying an external magnetic field. This proves the intrinsic presence of BMR [396]. However, a reproducible sample fabrication process needs to be established for future device applications.

*Spin-polarized QDs*

In the Kondo regime, the control of spin states has been demonstrated by applying a non-local voltage into a QD (see figure 40) [397]. Magnetic impurities in QDs can be treated as a Kondo system [121]. Two QDs were designed to be coupled, which was suppressed and split by changing the number of electrons trapped in the dot non-locally. This technique may be applied to future quantum data processing systems.

These quantum spintronic devices are still under development. At the moment most of the devices can only be operated at very low temperatures; however, the operating temperature is expected to be increased by further miniaturization and improvements in design.

## 5. Concluding remarks

After the implementation of GMR into an HDD read head, device applications have been driving spintronic research for over two decades, as summarized in figure 41. Recent progress further enables us to demonstrate spin memories and spin transistors, both of which are expected to be applied to devices. The spin memories utilize spin-polarized electron (hole) transport, while the spin transistors employ spin–orbit interactions as described to be Mott- and Dirac-type devices, respectively, in [398]. In this article, both the physical principles and device designs have been reviewed. Future 3 D and quantum spintonic devices need to be developed.

## Acknowledgments

The authors would like to thank Professor Kevin O'Grady for proofreading the manuscript. This work was partially supported by the JST PRESTO program.

## References

[1] Ziese M and Thornton M J (ed) 2001 *Spin Electronics* (Berlin: Springer)
[2] Maekawa S and Shinjo T (ed) 2002 *Spin Dependent Transport in Magnetic Nanostructures* (London: Taylor and Francis)
[3] Johnson M (ed) 2004 *Magnetoelectronics* (Amsterdam: Elsevier)
[4] Maekawa S (ed) 2006 *Concepts in Spin Electronics* (Oxford: Oxford University Press)
[5] Kronmüller H and Parkin S S P (ed) 2007 *Handbook of Magnetism and Advanced Magnetic Materials* (Chichester: Wiley)
[6] Dietl T, Awschalom D D, Kaminska M and Ohno H (ed) 2008 *Spintronics* (Amsterdam: Elsevier)
[7] Prinz G A 1998 *Science* **282** 1660
[8] Johnson M 2000 *IEEE Spectrum* **37** 33
[9] Wolf S A, Awschalom D D, Burhman R A, Daughton J M, von Molnár S, Roukes M L, Chtchelkanove A Y and Treger D M 2001 *Science* **294** 5546
[10] Chambers S A 2002 *Mater. Today* **2** 34
[11] Žutić I, Fabian J and Das Sarma S 2004 *Rev. Mod. Phys.* **76** 323
[12] Chappert C, Fert A and van Dau F N 2007 *Nature Mater.* **6** 813

[13] Baibich M N, Broto J M, Fert A, Van Dau F N, Petroff F, Etienne P, Creuzet G, Friederich A and Chazelas J 1988 *Phys. Rev. Lett.* **61** 2472
[14] Binasch G, Grünberg P, Saurenbach F and Zinn W 1989 *Phys. Rev.* B **39** 4828
[15] Grünberg P 1990 *US patent* 4,949,039
[16] Hartmann U (ed) 2000 *Magnetic Multilayers and Giant Magnetoresistance* (Berlin: Springer)
[17] Jullière M 1975 *Phys. Lett.* A **54** 225
[18] Maekawa S and Gäfvert U 1982 *IEEE Trans. Magn.* **18** 707
[19] Miyazaki T and Tezuka N 1995 *J. Magn. Magn. Mater.* **139** L231
[20] Moodera J S, Kinder L R, Wong T M and Meservey R 1995 *Phys. Rev. Lett.* **74** 3273
[21] Moodera J S and Mathon J 1999 *J. Magn. Magn. Mater.* **200** 248
[22] Moodera J S and Meservey R H 2004 Spin-polarized tunnelling *Magnetoelectronics* ed M Johnson (Amsterdam: Elsevier) p 163
[23] Munekata H, Ohno H, von Molnar S, Segmüller A, Chang L L and Esaki L 1989 *Phys. Rev. Lett.* **63** 1849
[24] Crooker S A, Baumberg J J, Flack F, Samarth N and Awschalom D D 1996 *Phys. Rev. Lett.* **77** 2814
[25] Ohno H 1998 *Science* **281** 951
[26] Ohno H 2002 Ferromagnetic III–V semiconductors and their heterostructures *Semiconductor Spintronics and Quantum Computation* ed D D Awschalom *et al* (Berlin: Springer) p 1
[27] Schmidt G and Molenkamp L W 2002 Electrical spin injection: spin-polarized transport from magnetic into non-magnetic semiconductors *Semiconductor Spintronics and Quantum Computation* ed D D Awschalom *et al* (Berlin: Springer) p 93
[28] Hubert A and Schäfer R 1998 *Magnetic Domains* (Berlin: Springer)
[29] Kikkawa J M and Awschalom D D 1999 *Nature* **397** 139
[30] Fujiwara A and Takahashi Y 2001 *Nature* **410** 560
[31] Tyryshkin A M, Lyon S A, Jantsch W and Schäffler F 2005 *Phys. Rev. Lett.* **94** 126802
[32] Tombros N, Jozsa C, Popinciuc M, Jonkman H T and van Wees B J 2007 *Nature* **448** 571
[33] Torrey H C 1956 *Phys. Rev.* B **104** 563
[34] Egelhoff W F Jr, Chen P J, Powell C J, Stiles M D, McMichael R R, Judy J H, Takano K and Berkowitz A E 1997 *J. Appl. Phys.* **82** 6142
[35] Araki S, Sano M, Li S, Tsuchiya Y, Redon O, Sasaki T, Ito N, Terunuma K, Morita H and Matsuzaki M 2000 *J. Appl. Phys.* **87** 5377
[36] Levy P M 1994 *Solid State Phys.* **47** 367
[37] Grünberg P, Schreiber R, Pang Y, Brodsky M D and Sowers H 1986 *Phys. Rev. Lett.* **57** 2442
[38] Parkin S S P, More N and Roche K P 1990 *Phys. Rev. Lett.* **64** 2304
[39] Yoshida K 1957 *Phys. Rev.* **106** 893
[40] Coehoorn R 1991 *Phys. Rev.* B **44** 9331
[41] Edwards D and Mathon J 1991 *J. Magn. Magn. Mater.* **93** 85
[42] Mott N F 1935 *Proc. Phys. Soc.* **47** 571
[43] Mott N 1964 *Adv. Phys.* **13** 325
[44] Fert A and Cambell I A 1968 *Phys. Rev. Lett.* **21** 1190
[45] Dieny B, Speriosu V, Parkin S S P, Gurney B, Wilhoit D R and Mauri D 1991 *Phys. Rev.* B **43** 1297
[46] Pratt W P Jr, Loloee R, Schroeder P A and Bass J 1991 *Phys. Rev. Lett.* **66** 3060
[47] Berkowitz A E, Mitchell J R, Carey M J, Young A P, Zhang S, Spada F E, Parker F T, Hutten A and Thomas G 1992 *Phys. Rev. Lett.* **68** 3745
[48] Xiao J Q, Jiang J S and Chien C L 1992 *Phys. Rev. Lett.* **68** 3749
[49] Zhang S and Levy P M 1991 *J. Appl. Phys.* **69** 4786
[50] Soulen R J Jr *et al* 1998 *Science* **282** 85
[51] Upadhyay S K, Louie R N and Buhrman R A 1991 *Appl. Phys. Lett.* **74** 3881
[52] Rippard W H and Buhrman R A 2000 *Phys. Rev. Lett.* **84** 971
[53] Slonczewski J 1996 *J. Magn. Magn. Mater.* **159** L1
[54] Berger L 1996 *Phys. Rev.* B **54** 9353
[55] Albert F J, Katine J, Buhrmn R A and Ralph D C 2000 *Appl. Phys. Lett.* **77** 3809
[56] Yamaguchi A, Ono T, Nasu S, Miyake K, Mibu K and Shinjo T 2004 *Phys. Rev. Lett.* **92** 077205
[57] Sato M and Kobayashi K 1997 *Japan. J. Appl. Phys.* **36** L200
[58] Parkin S S P *et al* 1999 *J. Appl. Phys.* **85** 5828
[59] Wang D, Nordman C, Daughton J M, Qian Z and Fink J 2004 *IEEE Trans. Magn.* **40** 2269
[60] Butler W H, Zhang X-G, Schulthess T C and MacLaren J M 2001 *Phys. Rev.* B **63** 054416
[61] Mathon J and Umerski A 2001 *Phys. Rev.* B **63** 220403(R)
[62] Yuasa S, Fukushima A, Nagahama T, Ando K and Suzuki Y 2004 *Japan. J. Appl. Phys.* **43** L588
[63] Parkin S S P, Kaiser C, Panchula A, Rice P M, Hughes B, Samant M and Yang S-H 2004 *Nature Mater.* **3** 862
[64] Yuasa S, Nagahama T, Fukushima A, Suzuki Y and Ando K 2004 *Nature Mater.* **3** 868
[65] Tsunekawa K, Djayaprawira D D, Nagai M, Maehara H, Yamagata S, Watanabe N, Yuasa S, Suzuki Y and Ando K 2005 *Appl. Phys. Lett.* **87** 072503
[66] Ikeda S, Hayakawa J, Ashizawa Y, Lee Y M, Miura K, Hasegawa H, Tsunoda M, Matsukura F and Ohno H 2008 *Appl. Phys. Lett.* **93** 082508
[67] Gould C, Rüster C, Jungwirth T, Girgis E, Schott G M, Giraud R, Brunner K, Schmidt G and Molenkamp L W 2004 *Phys. Rev. Lett.* **93** 117203
[68] Moser J, Matos-Abiague A, Schuh D, Wegscheider W, Fabian J and Weiss D 2007 *Phys. Rev. Lett.* **99** 056601
[69] Park B G, Wunderlich J, Williams D A, Joo S J, Jung K Y, Shin K H, Olejník K, Shick A B and Jungwirth T 2008 *Phys. Rev. Lett.* **100** 087204
[70] Gao L, Jiang X, Yang S-H, Burton J D, Tsymbal E Y and Parkin S S P 2007 *Phys. Rev. Lett.* **99** 226602
[71] Park B G *et al* 2011 *Nature Mater.* **10** 347
[72] Barnes S E and Maekawa S 2007 *Phys. Rev. Lett.* **98** 246601
[73] Hai P N, Ohya S, Tanaka M, Barnes S E and Maekawa S 2009 *Nature* **458** 489
[74] Gittleman J I, Goldstein Y and Bozowski S 1972 *Phys. Rev.* B **5** 3609
[75] Fujimori H, Mitani S and Ohnuma S 1995 *Mater. Sci. Eng.* B **31** 219
[76] Mitani S, Takahashi S, Takanashi K, Yakushiji K, Maekawa S and Fujimori H 1998 *Phys. Rev. Lett.* **81** 2799
[77] Takahashi S and Maekawa S 1998 *Phys. Rev. Lett.* **80** 1758
[78] Schelp L F, Fert A, Fettar F, Holody P, Lee S F, Maurice J L, Petroff F and Vaurès A 1997 *Phys. Rev.* B **56** 5747(R)
[79] Sukegawa H, Nakamura S, Hirohata A, Tezuka N and Inomata K 2005 *Phys. Rev. Lett.* **94** 068304
[80] Filipe A, Drouhin H-J, Lampel G, Lassailly Y, Nagle J, Peretti J, Safarov V I and Schuhl A 1998 *Phys. Rev. Lett.* **80** 2425
[81] Liebermann L, Fredkin D R and Shore H B 1969 *Phys. Rev. Lett.* **22** 539
[82] Wu R and Freeman A J 1992 *Phys. Rev.* B **45** 7532
[83] Heinrich B and Bland J A C (ed) 1994 *Ultrathin Magnetic Structures II* (Berlin: Springer)
[84] Johnson M 1999 *Phys. Rev.* B **58** 9635
[85] Schmidt G, Ferrand D, Molenkamp L W, Filip A T and van Wees B J 2000 *Phys. Rev.* B **62** R4790
[86] Tang H X, Monzon F G, Lifshitz R, Cross M C and Roukes M L 2000 *Phys. Rev.* B **61** 4437
[87] Rashba E I 2000 *Phys. Rev.* B **62** 16267

[88] Aronov A G and Pikus G E 1976 *Sov.—Phys. Semicond.* **10** 698
[89] Datta S and Das B 1990 *Appl. Phys. Lett.* **56** 665
[90] Prins M W J, van Kempen H, van Leuken H, de Groot R A, van Roy W and de Boeck J 1995 *J. Phys.: Condens. Matter* **7** 9447
[91] Nakajima K, Okuno S N and Inomata K 1998 *Japan. J. Appl. Phys.* **37** L919
[92] Bland J A C, Steinmüller S J, Hirohata A and Taniyama T 2005 Optical studies of electron spin transmission *Ultrathin Magnetic Structures* vol 4, ed B Heinrich and J A C Bland (Berlin: Springer) p 59
[93] Hirohata A, Steinmüller S J and Bland J A C 2005 Electron spin filtering across a ferromagnetic metal/semiconductor interface measured by photoexcitation *Spintronic Materials and Technology* ed Y B Xu and S M Thompson (Berlin: Springer) p 305
[94] Isakovic A F, Carr D M, Strand J, Schultz B D, Palmstrøm C J and Crowell P A 2001 *Phys. Rev.* B **64** R161304
[95] Bland J A C and Hirohata A, An optically addressed spin-polarised diode sensor *Basic British Patent* (AU8608701) and PCT/GB01/04088 (WO 02/23638 A2)
[96] Kondo T, Hayafuji J and Munekata H 2006 *Japan. J. Appl. Phys.* **45** L663
[97] Wunderlich J, Irvine A C, Sinova J, Park B G, Zârbe L P, Xu X L, Kaestner B, Novák V and Jungwirth T 2009 *Nature Phys.* **5** 675
[98] Endres B, Clorga M, Schmid M, Ultz M, Bougeard D, Weiss D, Bayreuther G, Back C H 2013 *Nature Commun.* **4** 2068
[99] Žutić I, Fabian J and Das Sarma S 2001 *Phys. Rev.* B **64** 121201
[100] Žutić I, Fabian J and Das Sarma S 2002 *Phys. Rev. Lett.* **88** 066603
[101] Pierce D T and Meier F 1976 *Phys. Rev.* B **13** 5484
[102] Adachi S 1994 *GaAs and Related Materials* (Singapore: World Scientific)
[103] Meier F and Zakharchenya B P 1984 *Optical Orientation* (Amsterdam: North-Holland)
[104] Seneor P, Dlubak B, Martin M-B, Anane A, Jaffres H and Fert A 2012 *MRS Bull.* **37** 1245
[105] Novoselov K, Geim A K, Morozov S V, Jiang D, Zhang Y, Dubonos S V, Grigorieva I V, Firsov A A 2004 *Science* **306** 666
[106] Avsar A *et al* 2011 *Nano Lett.* **11** 2363
[107] Sprinkle M *et al* 2009 *Phys. Rev. Lett.* **103** 226803
[108] Dlubak B, Martin M B, Deranlot C, Servet B, Xavier S, Mattana R, Seneor P and Fert A 2012 *Nature Phys.* **8** 557
[109] Ohishi M, Shiraishi M, Nouchi R, Nozaki T, Shinjo T and Suzuki Y 2007 *Japan. J. Appl. Phys.* **46** L605
[110] Novoselov K S, McCann E, Morozov S V, Fal'ko V I, Katsnelson M I, Zeitler U, Jiang D, Schedin F and Geim A K 2006 *Nature Phys.* **2** 177
[111] Berry M V 1984 *Proc. R. Soc. Lond.* A **392** 45
[112] San-Jose P, Prada E, McCann E and Schomerus H 2009 *Phys. Rev. Lett.* **102** 247204
[113] Dery H, Wu H, Ciftcioglu B, Huang M, Song Y, Kawakami R, Shi J, Krivorotov I, Žutić I and Sham J 2012 *IEEE Trans. Magn.* **59** 259
[114] Iijima S 1991 *Nature* **354** 56
[115] Tsukagoshi K, Alphenaar B W and Ago H 1999 *Nature* **401** 572
[116] Cobden D H and Nygård J 2002 *Phys. Rev. Lett.* **89** 046803
[117] Ishii H *et al* 2003 *Nature* **426** 540
[118] Tomonaga S 1950 *Prog. Theor. Phys.* **5** 544
[119] Luttinger J M 1963 *J. Math. Phys.* **4** 1154
[120] Nygård J, Cobden D H and Lindelof P E 2000 *Nature* **408** 342
[121] Kondo J 1964 *Prog. Theor. Phys.* **32** 37
[122] Martel R, Derycke V, Lavoie C, Appenzeller J, Chan K K, Tersoff J and Avouris P 2001 *Phys. Rev. Lett.* **87** 256805
[123] Misewich J A, Martel R, Avouris P, Tsang J C, Heinze S and Tersoff J 2003 *Science* **300** 783
[124] Kroto H W, Heath J R, O'Brien S C, Curl R F and Smalley R E 1985 *Nature* **318** 162
[125] Bolskar R D, Benedetto A F, Husebo L O, Price R E, Jackson E F, Wallace S, Wilson L J and Alford J M 2003 *J. Am. Chem. Soc.* **125** 5471
[126] Sakai S, Yakushiji K, Mitani S, Takanashi K, Naramoto H, Avramov P V, Narumi K, Lavrentiev V and Maeda Y 2006 *Appl. Phys. Lett.* **89** 113118
[127] Xiong Z H, Wu D, Vardeny Z V and Shi J 2004 *Nature* **427** 821
[128] Santos T S, Lee J S, Migdal P, Lekshmi I C, Satpati B and Moodera J S 2007 *Phys. Rev. Lett.* **98** 016601
[129] Drew A J *et al* 2009 *Nature Mater.* **8** 109
[130] Aviram A and Ratner M A 1974 *Chem. Phys. Lett.* **29** 277
[131] Service R F 2001 *Science* **294** 2442
[132] Cottet A, Kontos T, Sahoo S, Man H T, Belzig W, Bruder C and Schönenberger C 2006 *Semicond. Sci. Technol.* **21** 578
[133] Hueso L E, Pruneda J M, Ferrari V, Brunell G, Valdes-Herrera, Simmons B D, Littlewood P B, Artacho E, Fert A and Mathur N D 2007 *Nature* **445** 410
[134] Daughton J, Brown J, Beech R, Pohm A and Kude W 1994 *IEEE Trans. Magn.* **30** 4608
[135] Parkin S S P, Li Z G and Smith D J 1991 *Appl. Phys. Lett.* **58** 2710
[136] Krishnan K M, Pakhomov A B, Bao Y, Blomqvist P, Chun Y, Gonzales M, Griffin K, Ji X and Roberts B K 2006 *J. Mater. Sci.* **41** 793
[137] Pankhurst Q A, Thanh N K T, Jones S K and Dobson J 2009 *J. Phys. D: Appl. Phys.* **42** 224001
Roca A G, Costo R, Rebolledo A F, Veintemillas-Verdaguer S, Tartaj P, González-Carreño T, Morales M P and Serna C J 2009 *J. Phys. D: Appl. Phys.* **42** 224002
Berry C C 2009 *J. Phys. D: Appl. Phys.* **42** 224002
[138] Mao S *et al* 2006 *IEEE Trans. Magn.* **42** 97
[139] Moser A, Takano K, Margulies D T, Albrecht M, Sonobe Y, Ikeda Y, Sun S and Fullerton E E 2002 *J. Phys. D: Appl. Phys.* **35** R157
[140] Nakamura Y 1999 *J. Magn. Magn. Mater.* **200** 634
[141] Gradmann U and Müller J 1968 *Phys. Status Solidi* b **27** 313
[142] Carcia P F, Meinhaldt A D and Suna A 1986 *Appl. Phys. Lett.* **47** 178
[143] Chappert C, Renard D, Beauvillain P and Renard J 1986 *J. Magn. Magn. Mater.* **54** 795
[144] Marchon B, Pitchford T, Hsia Y T and Gangopadhyay S 2013 *Adv. Tribol.* **2013** 521086
[145] Sonobe Y, Weller D, Ikeda Y, Schabes M, Takano K, Zeltzer G, Yen B, Best M E, Greaves S, Muraoka H and Nakamura Y 2001 *IEEE Trans. Magn.* **37** 1667
[146] Sonobe Y, Muraoka H, Miura K, Nakamura Y, Takano K, Moser A, Do H, Yen B, Ikeda Y, Supper N and Weresin W 2002 *IEEE Trans. Magn.* **38** 2006
[147] Suess D, Schrefl T, Fahler S, Kirschner M, Hrkac G, Dorfbauer F and Fidler J 2005 *Appl. Phys. Lett.* **87** 012504
[148] Victora R and Shen X 2005 *IEEE Trans. Magn.* **41** 537
[149] Stoner E C and Wohlfarth E P 1948 *Phil. Trans.* **240** 599
[150] Nolan T, Vaclu B and Richter H J 2011 *IEEE Trans. Magn.* **47** 63
[151] Terris B D and Thomson T 2005 *J. Phys. D: Appl. Phys.* **38** R199
[152] Richter H J 2007 *J. Phys. D: Appl. Phys.* **40** R149
[153] Katayama H, Sawamura S, Ogimoto Y, Nakajima J, Kojima K and Ohta K 1999 *J. Magn. Soc. Japan* **23** **S1** 233
[154] Rottmayer R *et al* 2006 *IEEE Trans. Magn.* **42** 2417
[155] Seigler M A *et al* 2008 *IEEE Trans. Magn.* **44** 119
[156] Zhu J-G, Zhu H and Tang Y 2008 *IEEE Trans. Magn.* **44** 125
[157] Seki T, Utsumiya K, Nozaki Y, Imamura H and Takanashi K 2013 *Nature Commun.* **4** 1726

[158] Hirohata A, Sagar J, Lari L, Fleet L R and Lazarov V K 2013 *Appl. Phys.* A **111** 423
[159] Prejbeanu *et al* 2013 *J. Phys. D: Appl. Phys.* **46** 074002
[160] de Boeck J and Borghs G 1999 *Phys. World* **12** 27
[161] Oogane M and Miyazaki T 2009 Magnetic random access memory *Epitaxial Ferromagnetic Films and Spintronic Applications* ed A Hirohata and Y Otani (Kerala: Research Signpost) p 335
[162] Schwee L J 1972 *IEEE Trans. Magn.* **8** 405
[163] Granley G B, Daughton J M, Pohm A V and Comstock C S 1991 *IEEE Trans. Magn.* **27** 5517
[164] Wang Z G and Nakamura Y 1996 *IEEE Trans. Magn.* **32** 4022
[165] Daughton J M 1997 *J. Appl. Phys.* **81** 3758
[166] Scheunerlein R E, Gallagher W, Parkin S S P, Lee A, Ray S, Robertazzi R and Reohr W 2000 *IEEE Int. Solid-State Circuits Conf. (San Francisco, CA)* Digest of Technical Papers p 128
[167] Durlan M, Naji P, DeHerrera M, Tehrani S, Kerszykowski G and Kyler K 2000 *IEEE Int. Solid-State Circuits Conf. (San Francisco, CA)* Digest of Technical Papers p 130
[168] Durlam M *et al* 2003 *Int. Electron Devices Meeting (IEDM)* Technical Digest p 995
[169] Engel B N *et al* 2005 *IEEE Trans. Magn.* **41** 132
[170] Iwata Y *et al* 2006 *IEEE Int. Solid-State Circuits Conf. (San Francisco, CA)* Digest of. Technical Papers p 477
[171] DeBrosse J *et al* 2004 *IEEE J. Solid-State Circuit* **39** 678
[172] Tanizaki H, Tsuji T, Otani J, Yamaguchi Y, Murai Y, Furuta H, Ueno S, Oishi T, Hayashikoshi M and Hidaka H 2006 *Asian Solid-State Circuits Conf. (Hangzhou)* Digest of Technical Papers p 303
[173] Inomata K, Ogiwara H, Saito Y, Yusa K and Ichihara K 1997 *Japan. J. Appl. Phys.* **36** L1380
[174] Yu J H, Lee H M, Ando Y, Miyazaki T 2003 *Appl. Phys. Lett.* **82** 4735
[175] Inomata K, Koike N, Nozaki T, Abe S and Tezuka N 2003 *Appl. Phys. Lett.* **82** 2667
[176] Nakamura S, Saito Y and Morise H 2006 *Toshiba Rev.* **61** 40
[177] Jiang Y, Abe S, Ochiai T, Nozaki T, Hirohata A, Tezuka N and Inomata K 2004 *Phys. Rev. Lett.* **92** 167204
[178] Jiang Y, Nozaki T, Abe S, Ochiai T, Hirohata A, Tezuka N and Inomata K 2004 *Nature Mater.* **3** 361
[179] Yang T, Hirohata A, Kimura T and Otani Y 2006 *Phys. Rev.* B **74** 153301
[180] Yang T, Hirohata A, Kimura T and Otani Y 2006 *Appl. Phys. Lett.* **89** 252505
[181] Fuchs G D, Emley N C, Krivorotov I N, Braganca P M, Ryan E M, Kiselev S I, Sankey J C, Ralph D C, Buhrman R A and Katine J A 2004 *Appl. Phys. Lett.* **85** 1205
[182] Kubota H, Fukushima A, Ootani Y, Yuasa S, Ando K, Maehara H, Tsunekawa K, Djayaprawira D D, Watanabe N and Suzuki Y 2005 *Japan. J. Appl. Phys.* **44** L1237
[183] Hayakawa J, Ikeda S, Lee Y M, Sasaki R, Meguro T, Matsukura F, Takahashi H and Ohno H 2005 *Japan. J. Appl. Phys.* **44** L1267
[184] Hosomi M *et al* 2005 *Int. Electron Devices Meeting (Washington, DC)* Technical Digest p 459
[185] Yakata S, Kubota H, Seki T, Yakushiji K, Fukushima A, Yuasa S and Ando K 2010 *IEEE Trans. Magn.* **46** 2232
[186] Chikazumi S 1997 *Physics of Ferromagnetism* (Oxford: Oxford University Press)
[187] Gregg J F, Allen W, Ounadjela K, Viret M, Hehn M, Thompson S M and Coey J M D 1996 *Phys. Rev. Lett.* **77** 1580
[188] Ebels U, Radulescu A, Henry Y, Piraux L and Ounadjela K 2000 *Phys. Rev. Lett.* **84** 983
[189] Levy P M and Zhang S 1997 *Phys. Rev. Lett.* **79** 5110
[190] Hong K and Giordano N 1995 *Phys. Rev.* B **51** 9855
[191] Ruediger U, Yu J, Zhang S, Kent A D and Parkin S S P 1998 *Phys. Rev. Lett.* **80** 5639
[192] Tatara G and Fukuyama H 1997 *Phys. Rev. Lett.* **78** 3773
[193] Hirohata A (ed) 2011 *J. Phys. D: Appl. Phys.* **44** 380301
[194] Grollier J, Boulenc P, Cros V, Hamzić A, Vaurès A, Fert A and Faini G 2003 *Appl. Phys. Lett.* **83** 509
[195] Tsoi M, Fontana R E and Parkin S S P 2003 *Appl. Phys. Lett.* **83** 2617
[196] Yamanouchi M, Chiba D, Matsukura F and Ohno H 2004 *Nature* **428** 539
[197] Chiba D, Chiba D, Matsukura F and Ohno H 2006 *Phys. Rev. Lett.* **96** 096602
[198] Tatara G and Kouhno H 2004 *Phys. Rev. Lett.* **92** 086601
[199] Zhang S and Li Z 2004 *Phys. Rev. Lett.* **93** 127204
[200] Thiaville A, Nakatani Y, Miltat J and Suzuki Y 2005 *Europhys. Lett.* **69** 990
[201] Tserkovnyak Y, Skadsem J, Brataas A and Bauer G E W 2006 *Phys. Rev.* B 144405
[202] Barnes S E and Maekawa S 2005 *Phys. Rev. Lett.* **95** 107204
[203] Barnes S E 2006 *Phys. Rev. Lett.* **96** 189701;
Tatara G and Kohno H 2006 *Phys. Rev. Lett.* **96** 189702
Hirohata A (ed) 2011 *J. Phys. D: Appl. Phys.* **44** (special issue)
[204] Rothman J, Kläui M, Lopez-Diaz L, Vaz C A F, Bleloch A, Bland J A C, Cui Z and Speaks R 2001 *Phys. Rev. Lett.* **86** 1098
[205] Hayward T J, Moore T A, Tse D H Y, Bland J A C, Castaño F J and Ross C A 2005 *Phys. Rev.* B **72** 184430
[206] Kläui M *et al* 2005 *Appl. Phys. Lett.* **87** 102509
[207] Kläui M, Vaz C A F, Bland J A C, Wernsdorfer W, Faini G, Cambril E, Heyderman L J, Nolting F and Rüdiger U 2005 *Phys Rev. Lett.* **94** 106601
[208] Castaño F J, Morecroft D, Jung W and Ross C A 2005 *Phys. Rev. Lett.* **95** 137201
[209] Chen C C, Chang C C, Kuo C Y, Horng L, Wu J C, Wu T, Chern G, Huang C Y, Tsunoda M and Takahashi M 2006 *IEEE Trans. Magn.* **42** 2766
[210] Allwood D A, Xiong G, Cooke M D, Faulkner C C, Atkinson D, Vernier N and Cowburn R P 2002 *Science* **296** 2003
[211] Allwood D A, Xiong G, Faulkner C C, Atkinson D, Petit D and Cowburn R P 2005 *Science* **309** 1688
[212] Imre A, Csaba G, Ji L, Orlov A, Bernstein G H and Porod W 2006 *Science* **311** 205
[213] Cowburn R P and Welland M E 2000 *Science* **287** 1466
[214] Johnson M and Silsbee R H 1985 *Phys. Rev. Lett.* **55** 1790
[215] Johnson M 1993 *Science* **260** 324
[216] Bournel A, Dollfus P, Bruno P and Hesto P 1999 *Mater. Sci. Forum* **297** 205
[217] Dirac P A M 1958 *The Principles of Quantum Mechanics* (Oxford: Clarendon)
[218] Hammar P R, Bennet B R, Yang M J and Johnson M 1999 *Phys. Rev. Lett.* **83** 203
[219] Monzon F G and Roukes M L 1999 *J. Magn. Magn. Mater.* **632** 198–199
[220] Filip A T, Hoving B H, Jedema F J, van Wees B J, Dutta B and Borghs S 2000 *Phys. Rev.* B **62** 9996
[221] Crooker S A, Furis M, Lou X, Adelmann C, Smith D L, Palmstrøm C J and Crowell P A 2005 *Science* **309** 2191
[222] Kotissek P, Bailleul M, Sperl M, Spitzer A, Schuh D, Wegscheider W, Back C H and Bayreuther G 2007 *Nature Phys.* **3** 872
[223] MacLaren J M, Zhang X-G, Butler W H and Wang X 1999 *Phys. Rev.* B **59** 5470
[224] Wunnicke O, Mavropoulos P, Zeller R and Dederichs P H 2002 *Phys. Rev.* B **65** 241306(R)
[225] Hallstein S, Berger J D, Hilpert M, Schneider H C, Rühle W W, Jahnke F, Koch S W, Gibbs H M, Khitrova G and Oestreich M 1997 *Phys. Rev.* B **56** R7076

[226] Rudolph J, Döhrmann S, Hägele D and Oestreich M 2005 *Appl. Phys. Lett.* **87** 241117
[227] Gothgen C, Oszwaldowski R, Petrou A and Žutić I 2008 *Appl. Phys. Lett.* **93** 042513
[228] Lee J, Oszwaldowski R, Gøthgen C and Žutić I 2012 *Phys. Rev.* B **85** 045314
[229] Boéris G, Lee J, Vyborny K and Žutić I 2012 *Appl. Phys. Lett.* **100** 121111
[230] Gerhardt N C, Li M Y, Jähme H, Höpfner H, Ackermann T and Hofmann M R 2011 *Appl. Phys. Lett.* **99** 151107
[231] Ohno Y, Young D K, Beschoten B, Matsukura F, Ohno H and Awschalom D D 1999 *Nature* **402** 790
[232] Flatté M E and Byers J M 2000 *Phys. Rev. Lett.* **84** 4220
[233] Fiederling R, Keim M, Reuscher G, Ossau W, Schmidt G, Waag A and Molenkamp L W 1999 *Nature* **402** 787
[234] Oestreich M, Hübner J, Hägele D, Klar P J, Heimbrodt W, Rühle W W, Ashenford D E and Lunn B 1999 *Appl. Phys. Lett.* **74** 1251
[235] Jonker B T, Park Y D, Bennett B R, Cheong H D, Kioseoglou G and Petrou A 2000 *Phys. Rev.* B **62** 8180
[236] Jonker B T, Hanbicki A T, Park Y D, Itskos G, Furis M, Kioseoglou G, Petrou A and Wei X 2001 *Appl. Phys. Lett.* **79** 3098
[237] Malajovich I, Kikkawa J M, Awschalom D D, Berry J J and Samarth N 2000 *Phys. Rev. Lett.* **84** 1015
[238] Park Y D, Hanbicki A T, Erwin S C, Hellberg C S, Sullivan J M, Mattson J E, Ambrose T F, Wilson A, Spanos G and Jonker B T 2002 *Science* **295** 651
[239] Dietl T, Ohno H, Matsukura F, Cibert J and Ferrand D 2000 *Science* **287** 1019
[240] Zhu H J, Ramsteiner M, Kostial H, Wassermeier M, Schönher H-P and Ploog K H 2001 *Phys. Rev. Lett.* **87** 016601
[241] Hanbicki A T, Jonker B T, Itskos G, Kioseoglou G and Petrou A 2002 *Appl. Phys. Lett.* **80** 1240
[242] Kurebayashi H, Steinmuller S J, Laloë J B, Trypiniotis T, Easton S, Ionescu A, Yates J R and Bland J A C 2007 *Appl. Phys. Lett.* **91** 102114
[243] van't Erve O H J, Kioseoglou G, Hanbicki A T, Li C H, Jonker B T, Mallory R, Yasar M and Petrou A 2004 *Appl. Phys. Lett.* **84** 4334
[244] Wang R, Jiang X, Shelby R M, Macfarlane R M, Parkin S S P, Bank S R and Harris J S 2005 *Appl. Phys. Lett.* **86** 052901
[245] Jiang X, Wang R, Shelby R M, Macfarlane R M, Bank S R, Harris J S and Parkin S S P 2005 *Phys. Rev. Lett.* **94** 056601
[246] Gruber T, Keim M, Fiederling R, Ossau G, Schmidt G and Molenkamp L W 2001 *Appl. Phys. Lett.* **78** 1101
[247] Ohno H, Chiba D, Matsukura F, Omiya T, Abe E, Dietl T, Ohno Y and Ohtani K 2000 *Nature* **408** 944
[248] Žutić I, Fabian J and Erwin S C 2006 *Phys. Rev. Lett.* **97** 026602
[249] Min B-C, Motohashi K, Lodder J C and Jansen R 2006 *Nature Mater.* **5** 817
[250] Jonker B T, Kioseoglou G, Hanbicki A T, Li C H and Thompson P E 2007 *Nature Phys.* **3** 542
[251] Dash S P, Sharma S, Patel R S, de Jong M P and Jansen R 2009 *Nature* **462** 491
[252] Shikoh E, Ando K, Kubo K, Saitoh E, Shinjo T and Shiraishi M 2013 *Phys. Rev. Lett.* **110** 127201
[253] Dery H, Song Y, Li P and Žutić I 2011 *Appl. Phys. Lett.* **99** 082502
[254] Saito H, Yuasa S and Ando K 2005 *Phys. Rev. Lett.* **95** 086604
[255] Monsma D J, Lodder J C, Popma Th J A and Dieny B 1995 *Phys. Rev. Lett.* **74** 5260
[256] Appelbaum I, Huang B and Monsma D J 2007 *Nature* **447** 295
[257] van Dijken S, Jiang X and Parkin S S P 2003 *Appl. Phys. Lett.* **83** 951
[258] Yakushiji K, Mitani S, Takanashi K, Takahashi S, Maekawa S, Imamura H and Fujimori H 2001 *Appl. Phys. Lett.* **78** 515
[259] Yakushiji K, Ernult F, Imamura H, Yamane K, Mitani S, Takanashi K, Takahashi S, Maekawa S and Fujimori H 2005 *Nature Mater.* **4** 57
[260] Gallo P, Arnoult A, Camps T, Havard E, Fontaine C, Lombez L, Amand T, Marie X and Bournel B 2007 *J. Appl. Phys.* **101** 024322
[261] Lee J H *et al* 2009 *Appl. Phys. Lett.* **95** 172505
[262] Fert A and Lee S F 1997 *J. Magn. Magn. Mater.* **165** 115
[263] Hu C-M, Nitta J, Jensen A, Hansen J B and Takayanagi H 2001 *Phys. Rev.* B **63** 125333
[264] Jedema F J, Filip A T and van Wees B J 2000 *Nature* **410** 345
[265] Jedema F J, Heersche H B, Filip A T, Baselmans J J A and van Wees B J 2002 *Nature* **416** 713
[266] Kimura T, Hamrle J, Otani Y, Tsukagoshi K and Aoyagi Y 2004 *Appl. Phys. Lett.* **85** 3501
[267] Garzon S, Zutic I and Webb R A 2005 *Phys. Rev. Lett.* **94** 176601
[268] Kimura T, Otani Y and Hamrle J 2006 *Phys. Rev.* B **73** 132405
[269] Godfrey R and Johnson M 2006 *Phys. Rev. Lett.* **96** 136601
[270] Dyakonov M I and Perel V I 1971 *Phys. Lett.* A **35** 459
[271] Hirsch J E 1999 *Phys. Rev. Lett.* **83** 1834
[272] Saitoh E, Ueda M, Miyajima H and Tatara G 2006 *Appl. Phys. Lett.* **88** 182509
[273] Kato Y K, Myers R C, Gossard A C and Awschalom D D 2004 *Science* **306** 1910
[274] Valenzuela S O and Tinkham M 2006 *Nature* **442** 176
[275] Seki T, Hasegawa Y, Mitani S, Takahashi S, Imamura H, Maekawa S, Nitta J and Takanashi K 2008 *Nature Mater.* **7** 125
[276] Uchida K, Takahashi S, Harii K, Ieda J, Koshibae W, Ando K, Maekawa S and Saitoh E 2008 *Nature* **455** 778
[277] Xiao J, Bauer G E W, Uchida K, Saitoh E and Maekawa S 2010 *Phys. Rev.* B **81** 214418
[278] Uchida K *et al* 2010 *Nature Mater.* **9** 894
[279] Kirihara A, Uchida K, Kajiwara Y, Ishida M, Nakamura Y, Manako T, Saitoh E and Yorozu S 2012 *Nature Mater.* **11** 686
[280] Johnson M and Clarke J 1990 *J. Appl. Phys.* **67** 6141
[281] Wiesendanger R, Güntherodt H-J, Güntherodt G, Gambino R J and Ruf R 1990 *Phys. Rev. Lett.* **65** 247
[282] Molotkov S N 1993 *Surf. Sci.* **1098** 287–288
[283] Laiho R and Reittu H J 1993 *Surf. Sci.* **289** 363
[284] Alvarado S F and Renaud P 1992 *Phys. Rev. Lett.* **68** 1387
[285] Sze S M 1981 *Physics of Semiconductor Devices* 2nd ed (New York: Wiley)
[286] Sueoka K, Mukasa K and Hayakawa K 1993 *Japan. J. Appl. Phys.* **32** 2989
[287] Suzuki Y, Nabhan W, Shinohara R, Yamaguchi K and Mukasa K 1999 *J. Magn. Magn. Mater.* **198–199** 540
[288] Kodama H, Uzumaki T, Oshiki M, Sueoka K and Mukasa K 1999 *J. Appl. Phys.* **83** 6831
[289] Printz G A 1994 Magnetic metal films on semiconductor substrates *Ultrathin Magnetic Structures II* ed B Heinrich and J A C Bland (Berlin: Springer) p 1
[290] Moodera J S and Meservey R H 2004 Spin-polarized tunnelling *Magnetoelectronics* ed M Johnson (Amsterdam: Elsevier) p 163
[291] Kasuya T and Yanase A 1968 *Rev. Mod. Phys.* **40** 684
Radovanovic P V and Gamelin D R 2003 *Phys. Rev. Lett.* **91** 157202
[292] LeClair P, Ha J K, Swagten H J M, Kohlhepp J T, van de Vin C H and de Jonge W J M 2002 *Appl. Phys. Lett.* **80** 625

[293] Kossut J and Dobrowlski W 1993 *Handbook of Magnetic Materials* vol 7 ed K H J Buschow (Amsterdam: North-Holland) p 231
[294] Ohno H, Akiba N, Matsukura F, Shen A, Ohtani K and Ohno Y 1998 *Appl. Phys. Lett.* **73** 363
[295] Matsukura F, Ohno H, Shen A and Sugawara Y 1998 *Phys. Rev.* B **57** R2037
[296] Nazmul A M, Amemiya T, Shuto Y, Sugahara S and Tanaka M 2005 *Phys. Rev. Lett.* **95** 017201
[297] Rangaraju N, Peters J A and Wessels B W 2010 *Phys. Rev. Lett.* **105** 117202
[298] Fabian J and Žutić I 2004 *Phys. Rev.* B **69** 115314
[299] Galanakis I and Dederichs P H (ed) 2005 *Half-metallic Alloys* (Berlin: Springer)
[300] Schwarz K 1986 *J. Phys. F: Met. Phys.* **16** L211
[301] Yamase A and Shiratori K 1984 *J. Phys. Soc. Japan* **53** 312
[302] Okimoto Y, Katsufuji T, Ishikawa T, Urushibara A, Arima T and Tokura Y 1995 *Phys. Rev. Lett.* **75** 109
[303] Akinaga H, Manago T and Shirai M 2000 *Japan. J. Appl. Phys.* **39** L1118
[304] Engel-Herbert R, Mohanty J, Ney A, Hesjedal T, Dãweritz L and Ploog K H 2004 *Appl. Phys. Lett.* **84** 1132
[305] de Groot R A, Mueller F M, van Engen P G and Buschow K H J 1983 *Phys. Rev. Lett.* **50** 2024
[306] Hirohata A, Kikuchi M, Tezuka N, Inomata K, Claydon J S, Xu Y B ang van der Laan G 2006 *Curr. Opin. Solid State Mater. Sci.* **10** 93
[307] Block T, Felser C, Jakob G, Ensling J, Mühling B, Gütlich P and Cava R J 2003 *J. Solid State Chem.* **176** 646
[308] Inomata K, Okamura S, Goto R and Tezuka N 2003 *Japan. J. Appl. Phys.* **42** L419
[309] Hirohata A, Kurebayashi H, Okamura S, Masaki T, Nozaki T, Tezuka N and Inomata K 2005 *J. Appl. Phys.* **97** 103714
[310] Marukame T and Yamamoto M 2007 *J. Appl. Phys.* **101** 083906
[311] Marukame T, Ishikawa T, Taira T, Matsuda K, Uemura T and Yamamoto M 2010 *Phys. Rev.* B **81** 134432
[312] Sakuraba Y, Nakata J, Oogane M, Kubota H, Ando Y, Sakuma A and Miyazaki T 2005 *Japan. J. Appl. Phys.* **44** L1100
[313] Tezuka N, Ikeda N, Mitsuhashi F and Sugimoto S 2009 *Appl. Phys. Lett.* **94** 162504
[314] Wang W, Sukegawa H, Shan R and Inomata K 2008 *Appl. Phys. Lett.* **93** 122506
[315] Hirohata A, Ladak S, Aley N P and Hix G 2009 *Appl. Phys. Lett.* **95** 252506
[316] Sukegawa H, Wang W, Shan R, Nakatani T, Inomata K and Hono K 2009 *Phys. Rev.* B **79** 184418
[317] Shan R, Sukegawa H, Wang W H, Kodzuka M, Furubayashi T, Ohkubo T, Mitani S, Inomata K and Hono K 2009 *Phys. Rev. Lett.* **102** 246601
[318] Ramsteiner M, Brandt O, Flissikowski T, Grahn H T, Hashimoto M, Herfort J and Kostial H 2008 *Phys. Rev.* B **78** 121303(R)
[319] Sakuraba Y, Izumi K, Iwase T, Bosu S, Saito K, Takanashi K, Miura Y, Futatsukawa K, Abe K and Shirai M 2010 *Phys. Rev.* B **82** 094444
[320] Kubota T, Tsunegi S, Oogane M, Mizukami S, Miyazaki T, Naganuma H and Ando Y 2009 *Appl. Phys. Lett.* **94** 122504
[321] Fujii S, Ishida S and Asano S 1995 *J. Phys. Soc. Japan.* **64** 185
[322] Ionescu A *et al* 2005 *Phys. Rev.* B **71** 094401
[323] Hamaya K, Ueda K, Kishi Y, Ando Y, Sadoh T and Miyao M 2008 *Appl. Phys. Lett.* **93** 132117
[324] Coey J M D, Viret M and von Molnr S 1999 *Adv. Phys.* **48** 167
[325] Tokura Y and Tomioka Y 1999 *J. Magn. Magn. Mater.* **200** 1
[326] von Hemlolt R, Wecker J, Holzapfel B, Schults L and Samwer K 1993 *Phys. Rev. Lett.* **71** 2331
[327] Viert M, Drouet M, Nassar J, Contour J P, Fermon C and Fert A 1997 *Europhys. Lett.* **39** 545
[328] Swartzendruber L J 1991 *J. Magn. Magn. Mater.* **100** 573
[329] Siratori K and Iida S 1960 *J. Phys. Soc. Japan.* **15** 210
[330] Flippen R B 1963 *J. Appl. Phys.* **34** 2026
[331] Vaz C A F 2009 Magnetization reversal in epitaxial FePt thin layers by spin-polarized current *Epitaxial Ferromagnetic Films and Spintronic Applications* ed A Hirohata and Y Otani (Kerala: Research Signpost) p 145
[332] Gorter E W 1955 *Proc. IRE* **43** 1945
[333] Huang D J, Chang C F, Chen J, Tjeng L H, Rata A D, Wu W P, Chung S C, Lin H J, Hibma T and Chen C T 2002 *J. Magn. Magn. Mater.* **239** 261
[334] Versluijs J J, Bari M A and Coey J M D 2001 *Phys. Rev. Lett.* **87** 026601
[335] Pénicaud M, Siberchicot B, Sommers C B and Kübler J 1992 *J. Magn. Magn. Mater.* **103** 212
[336] Matsumoto Y, Murakami M, Shono T, Hasegawa T, Fukumura T, Kawasaki M, Ahmet P, Chikyow T, Koshihara S and Koinuma H 2001 *Science* **291** 854
[337] Ovanov O A, Solina L V, Demshina V A and Magat L M 1973 *Phys. Met. Metallogr.* **35** 81
[338] Mitani S 2011 *J. Phys. D: Appl. Phys.* **44** 384003
[339] Cebollada A, Weller D, Sticht J, Harp G R, Farrow R F C, Marks R F, Savoy R and Scott J C 1994 *Phys. Rev.* B **50** 3419
[340] Shima T, Takanashi K, Takahashi Y K and Hono K 2002 *Appl. Phys. Lett.* **81** 1050
[341] Seki T, Shima T, Takanashi K, Takahashi Y, Matsubara E and Hono K 2003 *Appl. Phys. Lett.* **82** 2461
[342] Mitani S, Tsukamoto K, Seki T, Shima T and Takanashi K 2005 *IEEE Trans. Magn.* **41** 2606
[343] Seki T, Mitani S, Yakushiji K and Takanashi K 2006 *Appl. Phys. Lett.* **89** 172504
[344] Mangin S, Ravelosona D, Katine J A, Carey M J, Terris B D and Fullerton E E 2006 *Nature Mater.* **5** 210
[345] Meng H and Wang J P 2006 *Appl. Phys. Lett.* **88** 172506
[346] Kent A D, Özyilmaz B and del Barco E 2004 *Appl. Phys. Lett.* **84** 3897
[347] Wu F, Mizukami S, Watanabe D, Naganuma H, Oogane M, Ando Y and Miyazaki T 2009 *Appl. Phys. Lett.* **94** 122503
[348] Ikeda S, Miura K, Yamamoto H, Mizunuma K, Gan H D, Endo M, Kanai S, Hayakawa J, Matsukura F and Ohno H 2010 *Nature Mater.* **9** 721
[349] Nitta J, Akazaki T, Takayanagi H and Enoki T 1997 *Phys. Rev. Lett.* **78** 1335
[350] Koo H C, Kwon J H, Eom J, Chang J, Han S H and Johnson M 2009 *Science* **325** 1515
[351] Shiota Y, Nozaki T, Bonell F, Murakami S, Shinko T and Suzuki Y 2012 *Nature Mater.* **11** 39
[352] Duan C-G, Velev J P, Sabirianov R F, Zhu Z, Chu J, Jaswal S S, Tsymbal E Y 2008 *Phys. Rev. Lett.* **101** 137201
[353] Shimamura K, Chiba D, Ono S, Fukami S, Ishiwata N, Kawaguchi M, Kobayashi K and Ono T 2012 *Appl. Phys. Lett.* **100** 122402
[354] Chiba D, Kawaguchi M, Fukami S, Ishiwata N, Shimamura K, Kobayashi K and Ono T 2012 *Nature Commun.* **3** 888
[355] Sugahara S and Tanaka M 2005 *J. Appl. Phys.* **97** 10D503
[356] Shibata T and Ohmi T 1992 *IEEE Trans. Electron. Devices* **39** 1444
[357] Hirohata A, Yang T, Kimura T and Otani Y 2006 *19th Int. Colloqium on Magnetic Films and Surfaces (Sendai, 17 August)*
[358] Dery H and Sham L J 2007 *Phys. Rev. Lett.* **98** 46602
[359] Chantis A N, Belashchenko K D, Smith D L, Tsymbal E Y, van Schilfgaarde M and Albers L C 2007 *Phys. Rev. Lett.* **99** 196603

[360] Honda S, Itoh H, Inoue J, Kurebayashi H, Trypiniotis T, Barnes C H W, Hirohata A and Bland J A C 2008 *Phys. Rev.* B **78** 245316
[361] Fleet L R, Yoshida K, Kobayashi H, Kaneko Y, Matsuzaka S, Ohno Y, Ohno H, Honda S, Inoue J and Hirohata A 2013 *Phys. Rev.* B **87** 024401
[362] Sugahara S and Tanaka M 2004 *Appl. Phys. Lett.* **84** 2307
[363] Dery H, Dalal P, Cywiński Ł and Sham L J 2007 *Nature* **447** 573
[364] Mizukami S, Ando Y and Miyazaki T 2002 *Phys. Rev.* B **66** 104413
[365] Staciu C D, Hansteen F, Kimel A V, Kirilyuk A, Tsukamoto A, Itoh A and Rasing T 2007 *Phys. Rev. Lett.* **99** 047601
[366] Kiselef S I, Sankey J C, Krivorotov I N, Emley N C, Schoelkopf R J, Buhrman R A and Ralph D C 2003 *Nature* **425** 380
[367] Boulle O, Cros V, Groller J, Pereira L G, Deranlot C, Petroff F, Faini G, Barnaś J and Fert A 2007 *Nature Phys.* **3** 492
[368] Kubota H *et al* 2008 *Nature Phys.* **4** 37
[369] Deac A M, Fukushima A, Kubota H, Maehara H, Suzuki Y, Yuasa S, Nagamine Y, Tsunekawa K, Djayaprawira D D and Watanabe N 2008 *Nature Phys.* **4** 803
[370] Sankey J C, Braganca P M, Garcia A G F, Krivorotov I N, Buhrman R A and Ralph D C 2006 *Phys. Rev. Lett.* **96** 227601
[371] Tulapurkar A A, Suzuki Y, Fukushima A, Kubota H, Maehara H, Tsunekawa K, Djayaprawira D D, Watanabe N and Yuasa S 2005 *Nature* **438** 339
[372] Stern N P, Steuerman D W, Mack S, Gossard A C and Awschalom D D 2008 *Nature Phys.* **4** 843
[373] Pribiag V S, Krivorotov I N, Fuchs G D, Braganca P M, Ozatay O, Sankey J C, Ralph D C and Buhrman R A 2007 *Nature Phys.* **3** 498
[374] Yamada K, Kasai S, Nakatani Y, Kobayashi K, Kohno H, Thiaville A and Ono T 2007 *Nature Mater.* **6** 269
[375] Silva T J and Rippard W H 2008 *J. Magn. Magn. Mater.* **320** 1260
[376] Parkin S S P 2003 Shiftable magnetic shift register and method of using the same *US Patent* 6834005
Parkin S S P 2003 System and method for writing to a magnetic shift register *US Patent* 6898132
Parkin S S P 2003 System and method for reading data stored on a magnetic shift register *US Patent* 6920062
Parkin S S P 2004 Magnetic shift register with shiftable magnetic domains between two regions, and method of using the same *US Patent* 7031178
Parkin S S P 2004 System and method for transfering data to an magnetic shift register with a shiftable data column *US patent* 7236386
[377] Yamada K, Kasai S, Nakatani Y, Kobayashi K and Ono T 2008 *Appl. Phys. Lett.* **93** 152502
[378] Kasai S, Nakano K, Kondou K, Ohshima N, Kobayashi K and Ono T 2008 *Appl. Phys. Exp.* **1** 091302
[379] Thomas L, Moriy R, Rettner C and Parkin S S P 2010 *Science* **330** 1810
[380] Thomas L, Hayashi M, Jiang X, Moriya R, Rettner C and Parkin S S P 2006 *Nature* **443** 197
[381] Thomas L, Hayashi M, Jiang X, Moriya R, Rettner C and Parkin S S P 2007 *Science* **315** 1553
[382] Hayashi M, Thomas L, Rettner C, Moriya R and Parkin S S P 2007 *Nature Phys.* **3** 21
[383] Lavrijsen R, Lee J H, Fernández-Pacheco A, Petit D C, Mansell R and Cowburn R P 2013 *Nature* **493** 647
[384] Gardner J (ed) 2011 *J. Phys. Condens. Matter* **23** 160301
[385] Rössler U 2009 *Spin Waves: Magnons* (Berlin: Springer)
[386] Kane C L and Mele E J 2005 *Phys. Rev. Lett.* **95** 146802
[387] Bernevig B A, Hughes T L and Zhang S C 2006 *Science* **314** 1757
[388] Fu L, Kane C L and Mele E J 2007 *Phys. Rev. Lett.* **98** 106803
[389] Checkelsky J G, Ye J T, Onose Y, Iwasa Y and Tokura Y 2012 *Nature Phys.* **8** 729
[390] Garcia N, Munoz M and Zhao Y W 1999 *Phys. Rev. Lett.* **82** 2923
[391] Agrait N, Rodrigo J G and Vieira S 1993 *Phys. Rev.* B **47** 12345
[392] Tatara G, Zhao Y W, Munoz M and Garcia N 1999 *Phys. Rev. Lett.* **83** 2030
[393] Bruno P 1999 *Phys. Rev. Lett.* **83** 2425
[394] Imamura H, Kobayashi N, Takahashi S and Maekawa S 2000 *Phys. Rev. Lett.* **84** 1003
[395] Egelhoff W F Jr *et al* 2004 *J. Appl. Phys.* **95** 7554
[396] Sekiguchi K, Yamaguchi A, Miyajima H, Hirohata A and Usui S 2008 *Phys. Rev.* B **78** 224418
[397] Craig N J, Taylor J M, Lester E A, Marcus C M, Hanson M P and Gossard A C 2004 *Science* **304** 565
[398] Sinova J and Žutić I 2012 *Nature Mater.* **11** 368
[399] Inokuchi T, Marukami T, Ishikawa M, Sugiyama H and Saito Y 2009 *Appl. Phys. Express* **2** 023006
[400] Ishikawa M, Sugiyama T, Inokuchi K, Hamaya K and Saito Y 2012 *Appl. Phys. Lett.* **100** 252404